# Context discovery in Cognitive Radio Networks

Liliana Bolea

Cover Design by Liliana Bolea

ISBN 978-84-695-8025-7

Departament de Teoria
del Senyal i Comunicacions

UNIVERSITAT POLITÈCNICA DE CATALUNYA

# Context discovery in Cognitive Radio Networks

By

Liliana Bolea

A thesis submitted to the
Department of Teoria del Senyal i Comunicacions
of the Universitat Politècnica de Catalunya
in partial fulfillment of the requirements for the degree of

DOCTOR OF PHILOSOPHY

Thesis Advisor: Prof. Ramon Agustí Comes

Thesis Co-Advisor: Dr. Jordi Pérez-Romero

Barcelona, May 2013

# Summary

The technological progress and the development of wireless communication market have experienced a spectacular growth over the last decades. They have been globally expanded to a competitive and mass market oriented environment. There is a consensus forecast that the wireless communication market will continue to be one of the most dynamical in industrial area and one of the fundamental pillars for the informational society progress.

The low utilization of the limited radio spectrum bands has motivated the research communities to focus on the concept of granting, use and management of radio spectrum, in particular, to achieve a dynamic management of spectrum. The ability to perform a secondary use of radio spectrum that ensures that no harmful interference occurs on primary users, who are licensed for a particular band, is something that in our days has already begun to be experimented and standardized, e.g. with IEEE 802.22 standard for the secondary use of TV bands. In this framework, the use of geo-location databases and the more general concept of Radio Environment Map (REM) that stores different characteristics of the radio environment are recognized as important pillars for bringing dynamic spectrum management and Cognitive Radio (CR) concepts to reality.

The topic of this Ph.D. dissertation had been written in the context of CR networks, which promise significantly improvements to enhance the utilization of radio spectrum. In this framework, the studies performed in this thesis are concentrated on techniques for estimating the context where the CR network operates, extracting the relevant parameters that can be stored in the REM to be further used to achieve an optimized CR network operation. This estimation will be done by means of properly combining a number of samples about the received power gathered by secondary sensors located at different positions. Then, methodologies for the primary transmitter detection making use of both omnidirectional and directive antennas will be proposed first.

Afterwards, with the goal of deeper characterization of CR context, this thesis proposes and evaluates techniques for propagation model estimation (which includes the estimations of propagation factor, received power at 1 m, and shadowing standard deviation), antennas orientation estimation, and antenna radiation pattern estimation. Knowledge about these parameters becomes an essential aspect for an efficient CR network deployment and operation.

In the field of proposed methodologies, this thesis also tackles a comparative study of different interpolation techniques for the measurement obtained from a limited number of sensors and the evaluation of the results in several frameworks, including correlated and non-correlated shadowing effects. Finally, this thesis examines a comparative study of the obtained results with a state-of-the-art Maximum Likelihood reference algorithm, with the aim of obtaining inferior complexity and less computation times, while keeping adequate performance.

# Acknowledgments

În primul rând țin sa-I mulțumesc Domnului pentru că mi-a călăuzit paşii spre această etapă a vieții şi m-a învrednicit să cercetez şi să descopăr cele expuse în această lucrare.

I wouldn't be here today if weren't for my advisors Prof. Ramon Agustí and Dr. Jordi Pérez-Romero, offering me continuous support, motivation and guidance for this PhD. dissertation. Foremost, I would sincerely like to thank Prof. Ramon Agustí for accepting me under his protected wings, guiding me through this wonderful field of research. His wise advices were a great help during the studies of this doctorate program. Gràcies Ramon per tot el que has fet per mi. I would also like to thank Dr. Jordi Pérez-Romero for his great support and immense patience, teaching me how to express my ideas on the paper. Estic molt agraïda per tota l'ajuda que em vas donar Jordi. I'm feeling bless for meeting you both.

Additionally, I wish to express my gratefulness to my colleagues from Grup de Recerca de Comunicacions Mòbils (GRCM) who make so easier and enjoyable the time spend here, giving me unforgettable moments. I learnt from them which are the meaning of gracias, obrigada, gràcies, hvala, shukriya, grazie, shukran, efharisto, xiexie. Thanks guys.

I could not forget all my friends who encourage me to keep going on this path. They supported me even in my impossible moments, being there for me. Thanks Cami, Vali, Cati, Cătă, Denisa, Marius, Răzvan, Mary, and Elvis. As well as Steluța, Costin, Bogdan, Eugenia, Irina, and Alexandra. Vă mulțumesc tuturor.

Furthermore, the work of this thesis has been developed under the FI-DGR (personal investigador novell) grand (2009FI-00321) of the Catalan Regional Government and the FPU (Formación de Profesorado Universitario) grant (AP2008-02291) of the Spanish Education Council whose financial support is hereby acknowledged.

Last but not least, I am deeply grateful to my family for the unconditional love, endless encouragement, and unwavering support. They were always close to me even being far. A special thank to Iustin and Antonia who embellish my days with there innocent smiles. I am indebted to my parents for their help, encouragement, and prayers, giving me fortitude to archive this goal. Vă mulțumesc din suflet.

# Contents

# List of Figures

# List of Tables

# List of Abbreviations

| | |
|---|---|
| **2D** | 2 Dimensional space |
| **3D** | 3 Dimensional space |
| **ARM** | Available Resource Map |
| **BS** | Base Station |
| **CR** | Cognitive Radio |
| **CRN** | Cognitive Radio Network |
| **DSA** | Dynamic Spectrum Access |
| **EIRP** | Equivalent Isotropic Radiated Power |
| **FCC** | Federal Communications Commission |
| **IC** | Interference Cartography |
| **ITU** | International Telecommunication Union |
| **LIvE** | LocatIon Estimation |

| | |
|---|---|
| **MCD** | Measurement Capable Device |
| **ML** | Maximum Likelihood |
| **MLACFE** | Maximum Likelihood Aided Context Feature Extraction |
| **PU** | Primary User |
| **RAT** | Radio Access Technology |
| **REM** | Radio Environment Map |
| **RF** | Radio Frequency |
| **RRM** | Radio Resource Management |
| **RSS** | Received Signal Strength |
| **SA** | Storage and Acquisition |
| **SDR** | Software-Defined Radio |
| **SU** | Secondary User |
| **TV** | TeleVision |
| **xG** | Next Generation |

# 1.
# Introduction

Wireless communications have facilitated our lives for more than one hundred years. It all started in 1893, in St. Louis, Missouri, when Nikola Tesla made his public demonstration of radio. That time he presented his demonstration of wireless radio communication in front of Franklin Institute in Philadelphia and the National Electric Light Association. From that time, communications and information technologies have spread so much into everyone's lives that their devices invaded our homes, workplaces, even our bodies.

The applications and consumers of wireless communication have highly developed and continue to expand. Accordingly, the demand for the radio spectrum is anticipated to rise even more quickly in the coming years. However, this radio spectrum is finite, and progressively crowded. All this indicates a coming soon crisis of radio spectrum.

Dr. Martin Cooper, a former vice-president of Motorola who helped to create the first cell phone, said that the only way to solve people's need to communicate wirelessly "is by new technology. You can't create new spectrum" [1]. And he is right. The problem is not about the lack of spectrum, but the way it is used.

Some preliminary field spectrum measurements have pointed out the scarcity and inefficient use of the radio spectrum in the environment [2]. Many studies have focused on improving spectrum efficiency by employing spectrum sharing techniques.

Cognitive radio (CR) techniques are proposed to solve these problems, by providing the capacity to use or share the spectrum in an opportunistic manner and smartly adjust radio parameters in conformity with the surrounding environment [3]. CR devices have the ability to sense, learn, and adapt to its surroundings by dynamically changing their parameters in conformity with the detected conditions of the environment. These devices can access and use the unutilized detected spectrum bands without causing harmful interference to other wireless devices.

A proper estimation of context where these devices operated is essential for the proper operation of CR networks (CRNs). This context includes features such as transmitter positions, transmission power, radiation pattern, path loss model, and shadowing characterization among others. Once obtained, this context information should be stored in a database system, usually denoted as Radio Environment Map (REM) [4], to be used during the optimization of the CR operation.

There are many challenges on this domain. Even that the first phone over CR was already made, in January 2010 [5], there is still long way to go before everyone can enjoy the benefices of CR devices.

## 1.1. Objectives of the thesis

The main purpose of this thesis is to contribute to the evolution and development of CR and in particular of the REM concept. It discusses the need for building REMs in cognitive radio and introduces different computing frameworks that discover the surrounding radio environment.

The objectives of this thesis rely in the identification, characterization, estimation and performance related issues for the calculation of the context components of CR, using to this end just the radiofrequency (RF) strength measurements performed by a number of mobile terminals or sensors lying in the CRN deployed area. Context would include at least the knowledge of the primary transmitter positions, primary antenna radiation patterns, transmitter power, estimates of the path loss and shadowing features of the local environments.

A key issue in this thesis will consist in envisaging scalable and simple enough procedures to be carried out without imposing hardware/software extra constraints on the terminals and sensors, keeping in mind a cost as low as possible in terms of incurred overhead. To this end, a realistic image-based methodology will be introduced that favors the simplicity at the expense of having sub-optimum but realistically attained performance.

## 1.2. Outline of the thesis

The organization of this Ph.D. dissertation is depicted in Figure 1.1. Chapter 2 presents the basic background of several concepts that are used in this thesis. Through the topics discussed in this chapter, concepts such as CR, CRNs, cooperative spectrum sensing, and REM will be reviewed.

The estimation of context features on CR starts in Chapter 3 where two methods of transmitter position estimation are presented. Chapter 4 continues with antenna orientation estimation, antenna radiation pattern estimation, and propagation model estimation.

In Chapter 5, different interpolation techniques used in context features estimation are presented, like natural neighbor interpolation, linear interpolation, and kriging interpolation. Chapter 6 contributes with a more complex and promising methodology, based on Maximum Likelihood (ML) estimation. Finally, the document is concluded in Chapter 7 with a detailed description of the most important aspects of the thesis and with some suggestions for future work.

## 1.3. Publications

The following publications have been derived from the work of this dissertation.

**Journal publications**

- Liliana Bolea, Jordi Pérez-Romero, Ramón Agustí, "ML aided context feature extraction for cognitive radio," submitted for publication to Computer Networks.

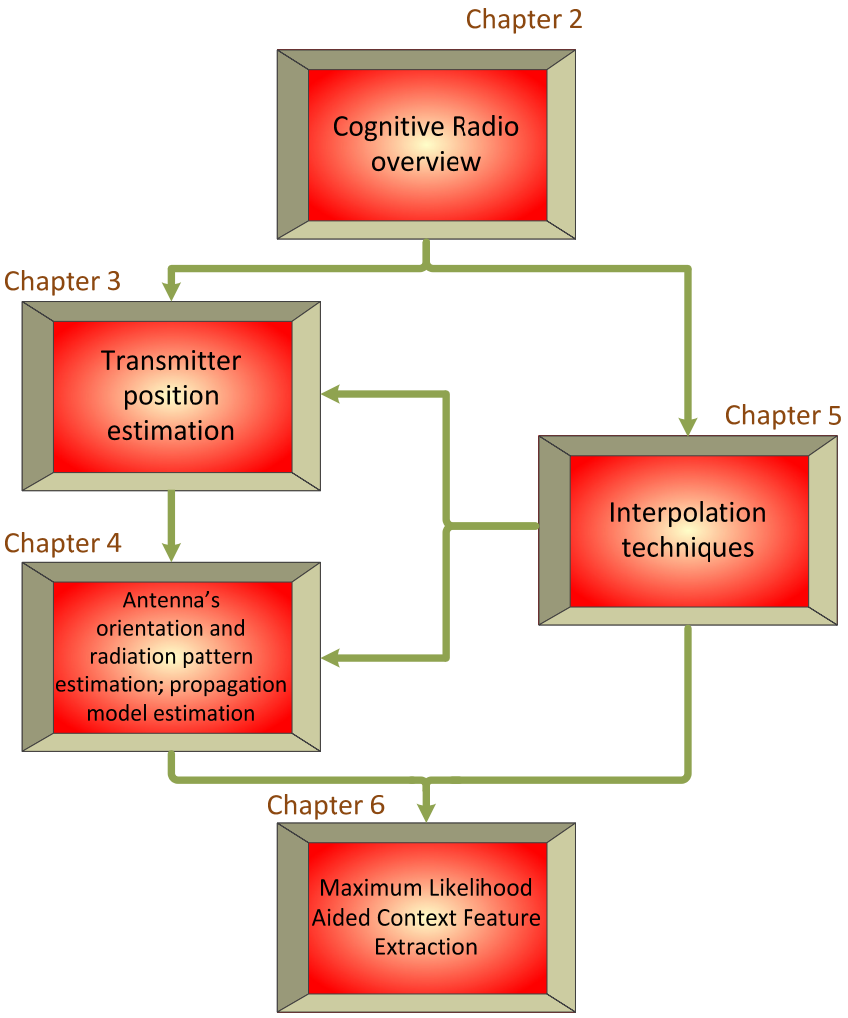


Figure 1.1: Structure of the thesis.

- Liliana Bolea, Jordi Pérez-Romero, Ramón Agustí, Oriol Sallent, "Primary transmitter discovery based on image processing in cognitive radio," Lecture Notes in computer science , Springer, vol. 5773, pp. 178 – 187, Oct. 2009, ISBN: 978 - 3 - 642 - 03699 - 6,

  http://www.springerlink.com/content/55u721983r802p53/.

**Conference publications**

- Liliana Bolea, Jordi Pérez-Romero, Ramón Agustí, "Received signal interpolation for context discovery in cognitive radio," International

Symposium on Wireless Personal Multimedia Communications (WPMC), pp. 1 – 5, Oct. 2011, ISBN: 978 - 1 - 4577 - 1786 - 4,

http://ieeexplore.ieee.org/stamp/stamp.jsp?tp=&arnumber=6081519.

- Liliana Bolea, Jordi Pérez-Romero, Ramón Agustí, Oriol Sallent, "Context discovery mechanisms for cognitive radio," IEEE Vehicular Technology Conference (VTC–Spring), pp. 1 – 5, May 2011, ISBN: 978 - 1 - 4244 - 8332 - 7,
  http://ieeexplore.ieee.org/stamp/stamp.jsp?tp=&arnumber=5956366.
- Liliana Bolea, Jordi Pérez-Romero, Ramón Agustí, Oriol Sallent, "Image processing techniques as a support to transmitter positioning determination in cognitive radio networks," Advanced International Conference on Telecommunications (AICT), pp. 112 – 117, May 2010, ISBN: 978 - 1 - 4244 - 6748 - 8;

  http://ieeexplore.ieee.org/stamp/stamp.jsp?tp=&arnumber=5489870.
- Liliana Bolea, Jordi Pérez-Romero, Ramón Agustí, Oriol Sallent, "Primary transmitter discovery based on image processing in cognitive radio," International Workshop on Eunice - The Internet of the Future, pp. 178 – 187, Sep. 2009, ISBN: 978 - 3 - 642 - 03699 - 6,

  http://www.springerlink.com/content/55u721983r802p53/
- Liliana Bolea, "Context discovery in cognitive radio networks," Proceedings of the 2012 Barcelona Forum on Ph.D. Research in Information and Communication Technologies, pp. 69 – 70, Oct. 2012, ISBN: 978 - 84 - 615 - 9915 - 8,
  http://phdbarcelonaforum.upc.edu/documents/proceedings-forum-phd-2012-final.

# 2. Overview of related works on Cognitive Radio

The goal of this Chapter is to present a general overview of the technical foundations of the work derived from this thesis. Therefore, this Chapter is organized into three parts. Section 2.1 presents an insight into CR, particularly different definitions in the literature and its structure architecture. In the second part, Section 2.2 examines in details the spectrum management functions. The Radio Environment Maps are described in Section 2.3, with a specific focus on context discovery.

## 2.1. Cognitive Radio survey

Lately we have been witness of an important increase in the demand for radio spectrum. With the emergence of new applications and the compelling need for mobile Internet access, demand for the spectrum is expected to grow even more rapidly in the coming years. Nevertheless, as it is nowadays widely recognized, the

licensed radio frequency spectrum is severely underutilized in most regions [2], [6], with temporal and geographical variations in the utilization of the assigned spectrum ranging from 15% to 85% [7], as shown in Figure 2.1. As a result, CR and Dynamic Spectrum Access (DSA) paradigms [3], [9] – [11] have emerged in the last decade as a promising solution to exploit the existence of the non used spectrum, the so-called white spaces, through opportunistic spectrum access. It consists in allowing secondary users (SUs) to access in an opportunistic and non-interfering manner some licensed bands temporarily unoccupied by primary users (PUs) holding a license.

### 2.1.1. Cognitive Radio definition

Different definitions have been given in the literature to the CR concept since it was originally proposed. In 1999, Joseph Mitola III defines a cognitive radio as [10]: "*A radio that employs model based reasoning to achieve a specified level of competence in radio-related domains*."

A formal definition of CR was given by Federal Communications Commission (FCC) in [7] as:

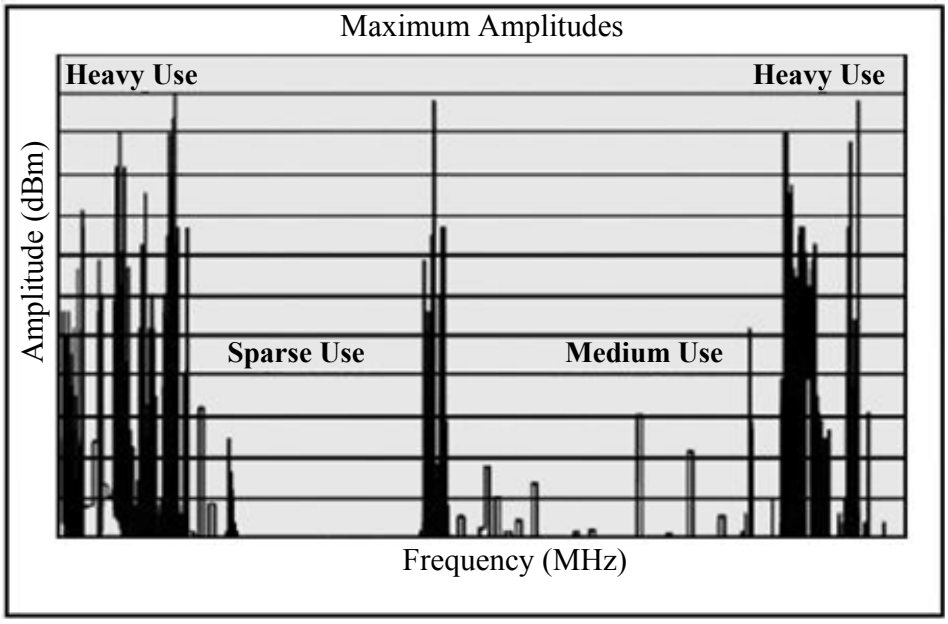


Figure 2.1: Spectrum utilization [8].

"*CR is a radio that can change its transmitter parameters based on interaction with the environment in which it operates*".

On the other hand, Haykin proposed a more detailed definition in [11]:

"*CR is an intelligent wireless communication system that is aware of its surrounding environment (i.e., its outside world), and uses the methodology of understanding-by-building to learn from the environment and adapt its internal states to statistical variations in the incoming RF stimuli by making corresponding changes in certain operating parameters (e.g., transmit power, carrier-frequency, and modulation strategy) in real-time, with two primary objectives in mind: highly reliable communications whenever and wherever needed and efficient utilization of the radio spectrum.*"

A definition of CR now adopted by most is given by International Telecommunication Union (ITU) in [12] as:

"*CR system is a radio system employing technology that allows the system to obtain knowledge of its operational and geographical environment, established policies and its internal state; to dynamically and autonomously adjust its operational parameters and protocols according to its obtained knowledge in order to achieve predefined objectives; and to learn from the results obtained.*"

From these definitions, some common characteristics of the cognitive radio can be extracted [7] – [12]:

• cognitive capability: the ability to acquire information from radio environment;

• reconfigurability capability: the ability to adapt to the changes from radio environment;

• learning capability: the capability to learn from the results obtained in order to improve its performance.

Thanks to the above characteristics, CR offers a great potential for implementing the DSA concept. The basic idea of DSA is to allow SUs (unlicensed users) to access some licensed bands temporarily unoccupied by PUs (licensed users) without causing harmful interference. The operating rule is to identify spatial and temporal spectrum gaps not occupied by PUs, place SU transmissions within such spaces and vacate the channel as soon as PUs return.

The term "spectrum holes" stands for those licensed subbands of the radio spectrum that are not actually utilized at a particular instant of time and specific geographic location [11], (see Figure 2.2). These spectrum holes could be used opportunistically by SUs provided that they are able to sense the spectrum, to detect the presence of either PU or SU transmissions, and to adapt to the varying spectrum conditions, ensuring that the primary rights are preserved [13].

### 2.1.2. Cognitive Radio Network Architecture

A typical architecture of a Cognitive Radio Network (CRN), also referred to as DSA network or Next Generation (xG) network ([8], [14]), is shown in Figure 2.3, where different possible scenarios are considered. The components of such network architecture can be classified in primary network and secondary/CR network.

*Primary network* is referred as an existing network infrastructure that has an exclusive right to access a certain spectrum band. Some examples are the mobile telephony networks and the broadcast TV networks. *Primary (licensed) users* (PUs) have a license to operate in a certain spectrum band and are controlled by *primary base station* (BS).

On the contrary, *CR (secondary or unlicensed) network* is defined as a network with fixed infrastructure or an ad hoc network, without license to operate

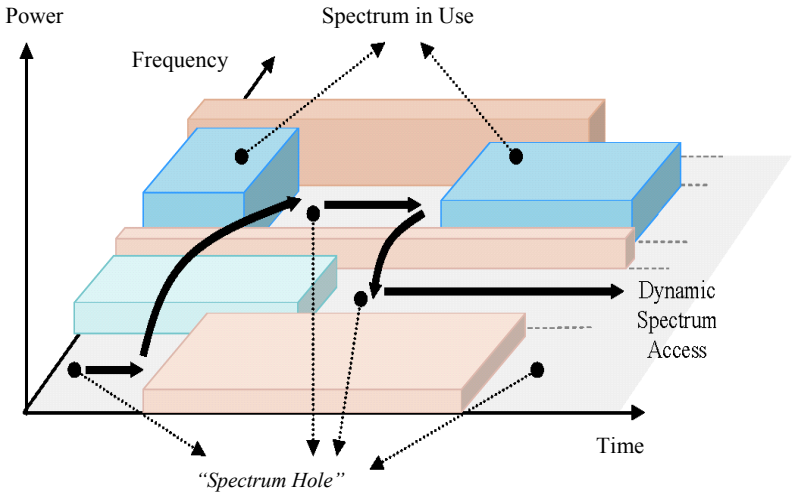


Figure 2.2: Spectrum hole concept [8].

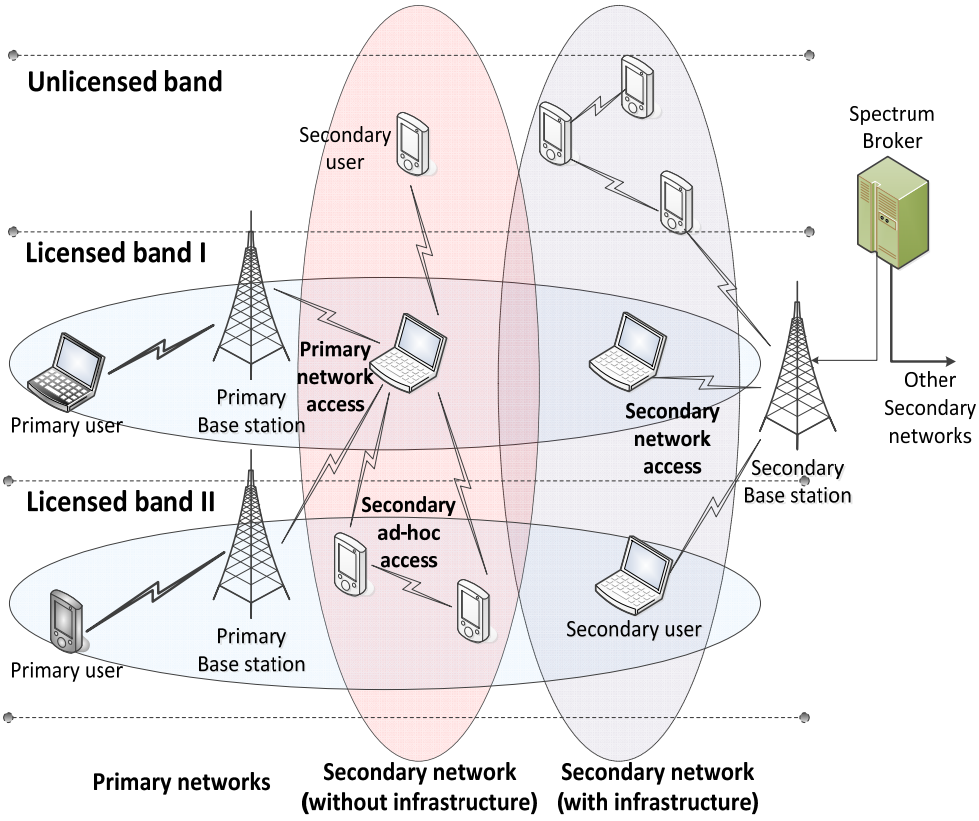


Figure 2.3: CR network architecture [8], [14].

in a specific band. The *secondary users* (SUs) are making use of the spectrum in an opportunistic manner without affecting the primary network transmission. That is, the SUs coexist with the primary ones geographically and temporally. *CR base station* provides single hop connection to SUs without spectrum access license [8]. An important element of these networks is the *spectrum broker*. This central network entity is in charge of managing the access and the usage of the spectrum between different CRNs [15] – [17].

## 2.2. Spectrum management functions

In order to access licensed bands without affecting the primary network and to guarantee efficient usage of the spectrum, a set of function are claimed by a CRN, which can be summarized as follows [8], [14]:

- *Spectrum sensing*: this function determines which portions of the spectrum are available and detect the presence of PUs when a user operates in a licensed band so as to avoid interference.

  Depending on information sheering on the CR network, spectrum sensing techniques can be performer in a non-cooperative detection approach or a cooperative detection approach. In the first case, SUs take decision based on there on local observation of the spectrum. However, in case of cooperative spectrum sensing, SUs rely also on the information shared by other nodes in the network [18] – [24]. The detection capability can improve significantly through cooperation spectrum sensing [19] – [21].

  Cooperative detection can be performed in a centralized ([25] – [27]) or distributed ([28] – [31]) mode. In centralized schemes, a central unit (that could be a CR BS or one of the SUs [21]) collects the information from SUs with the purposes of finding spectrum holes. In the distributed method, different SUs share sensing information and take the decision independently.

  To have knowledge about the spectrum and to avoid harmful interference with PUs, CR needs to detect not only the spectrum holes but also to detect PUs, by observing the radio environment. In case of primary transmitter detection, the sensing is effectuated over the weak signal received by the SUs from primary transmitter. Related work [32] – [35] have investigated techniques for detecting primary transmitters through three main schemes: matched filter detection, energy detection, and cyclostationary feature detection. Reference [36] presents a study that extensively evaluates the performance and limitations of these detection methods. A primary receiver detection method is based on detecting the local oscillator leakage power emitted by the RF front-end of the primary receiver [37]. Relative work has proposed detection of primary receivers based on the concept of interference temperature [38] – [39]. Primary transmitter detection techniques from network optimization perspective have bean investigated in [40].

  The work reporting in [41] – [44] demonstrates that cooperative spectrum sharing systems between primary and secondary networks regarding spectrum utilization would enable secondary systems to have perfect knowledge of the spectrum. Still, this approach implies modification of the existed primary network, which may not be feasible.

The concept of spectrum sensing can be generalized to the so-called *spectrum awareness* that incorporates all the means to acquire information about spectrum occupancy. This includes the use of geolocation databases that can provide different levels of information ranging from pure spectrum availability to more detailed elements of the radio environment characterization including transmitter characteristics, propagation models, etc., in what is usually called Radio Environment Map (REM). This concept, which constitutes a key element of this thesis, will be detailed in the next sub-section. A classification of the spectrum sensing forms is presented in Figure 2.4.

- *Spectrum decision*: by this function, CR analyzes the information from the spectrum sensing stage and selects the most appropriate channel for transmission. This decision is made at the beginning of the transmission, when the quality of the current transmission degrades, or when a PU appears.

- *Spectrum sharing*: by means of this function, CR coordinates access to the spectrum with other SUs. Spectrum sharing is based on cooperation or coexistence. In first case, there is clear communication and coordination

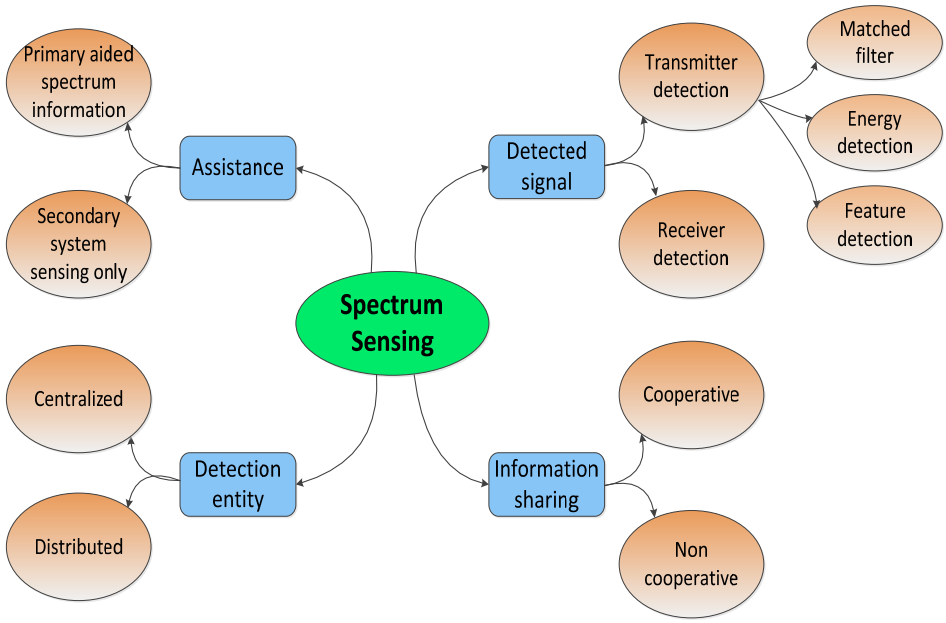


Figure 2.4: A taxonomy of spectrum sensing [45].

between primary networks and secondary networks meanwhile in second case there is none [46]. In case of coexistence, the primary network is not aware of the presence of CRN, practically CRN is invisible for it.

- *Spectrum mobility*: this function vacates the channel whenever a PU is detected and move to an alternative spectrum hole. This function has to be executed when the PU is detected, when, due to mobility, the SU loses its connection, or when the current spectrum band can not provide the desired quality of transmission.

## 2.3. Radio environment map

The difficult tasks of SUs to decide about the adequate spectrum band to transmit, modulation formats, power level, and so on, are highly affected by the radio environment and the PUs activity. Simply knowing about the presence or absence of the PUs in a specific spectrum band in the moment of decision is not enough information. The efficiency of spectrum decision can be significantly improved by having additional information of the radio environment. The concept of REM was introduced by the Virginia Tech team as information collection that can assist cognitive operation [4], [47]. REM has been proposed as a centralized or distributed database containing information on the radio environment such as device locations and their activities, policies and regulations, geographical features, available services, etc. (see Figure 2.5).

In 2010, the FCC set as a rule that, for the unlicensed operation in the TV broadcast bands, the SUs need to access a database for the list of the available channels [48]. This reflects the relevance of the use of databases, such as the REM, for implementing CRNs. The Available Resource Map (ARM) proposed by Krenik as a real time map of all radio activity in the network ([49] – [50]) can be seen as a precursor of REM.

The aim of REM is to allow CR to become situation-aware by simply referencing the REM [46]. Hence, it will considerably decrease the work of CRN. The observations of CR nodes can be used to update the global or/and local REM information (depending on the origin, extent and the purpose of the information stored [51]), which can be broadcasted throughout CRNs, providing the useful awareness of environmental status [52].

The CR central entity is responsible for collecting sensing data, constructing REM, and coordinating the Radio Resource Management (RRM) [53] (see Figure 2.6). It consists of two blocks: REM Manager and REM data Storage and Acquisition (SA) unit.

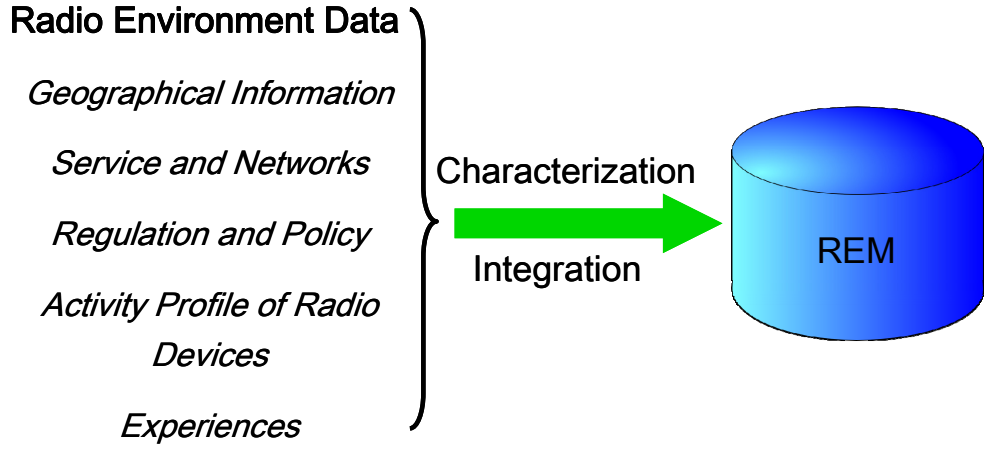


Figure 2.5: REM characterizes the radio scenario and offers network support and prior knowledge [4].

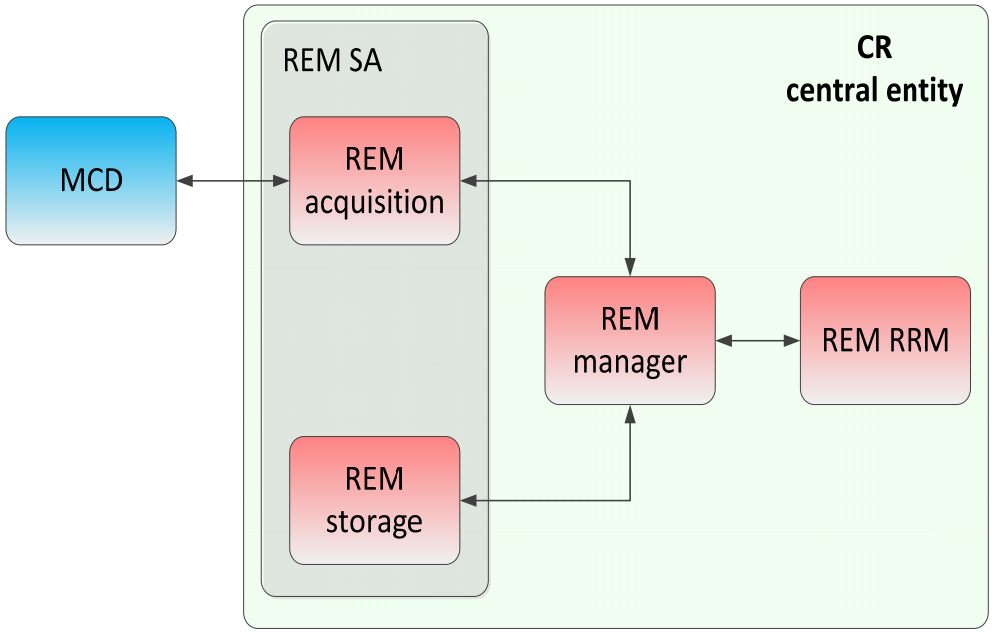


Figure 2.6: REM architecture [53].

Measurement Capable Devices (MCDs) are network entities in charge to provide local measurements from the environment and represent the SUs. REM SA acquires sensing data from MCDs (REM acquisition) and saves it as a local database (REM storage). The last unit preserves, besides this raw reported data by the MCDs, also processed data in form of maps [54].

REM Manager decides which measurements are performed, by which nodes, and when they should be performed. It sends measurement instructions to the REM SA, and it processes raw data to generate REMs [55]. The resulting REM database can be accessed and controlled by different entities of the network in charge of making decisions about the management of the available spectrum resources. This thesis is focused on REM manager, more precisely in processing data from MCDs.

REMs could store different relevant data. According to [56], the information contained in REM can be grouped in three categories, described as following:

- *Radio elements* which represent static information, data that do not change frequently; this includes location and mobility of each radio device, transmitters and receivers operations, etc.

- *Radio environment* which represent volatile information, data that is highly dynamic; this include geographical information and propagation model, both used to estimate the radio interference field, etc.

- *Radio scene* includes both static and dynamic information (derived); this category covers policy derivation, socio-economic information, security and access rights, etc.

There is a large amount of existing work on REM that has been investigated on how to improve its accuracy and decrease the number of measurement required. A trade-off exists between the accuracy of REM and the number of measurements needed to achieve it. This relationship was considered in [57] where it was demonstrated by computer simulations that the REM accuracy increases by increasing the density of sensors. However, a too high density of sensors would not lead to any meaningful improvement.

The main function of REM is to store information of the surrounding radio environment, based on the local measurements. Many studies on localization use

the Received Signal Strength (RSS) measurements [58] – [59]. RSS is a measure of how strong a signal is when it arrives at a sensor. It is commonly taken as a voltage measurement, or equivalently calculated as a signal power (e.g., the magnitude squared). In [60], a Maximum Likelihood (ML) estimator was derived for self-localization of a network of omnidirectional sensors, in which small subsets of the sensors were "anchor nodes" at known locations. In [61], the Cramer Rao Lower Bounds for such location estimation techniques were derived.

The construction of REM was investigated by many researchers in the last years. An iterative process based on kriging interpolation technique in order to obtain the REM was proposed in [62]. Reference [63] proposed a REM obtained by combining measurements performed by heterogeneous sources that can assist in detecting, identifying and using spectrum opportunities. In [64], Yilmaz and Tugcu proposed an active transmitter LIvE (LocatIon Estimation) based REM construction technique in fading channels. They used the least squares method to estimate channel parameters that can help building the REM.

As was mention before, the main function of REM is storage. Apart from storing, REM also process data, one of the methods being spatial interpolation. A brief overview of the interpolation methods in the literature in context of REM is presented in Chapter 5.

### 2.3.1. Context discovery

Besides the determination of the presence or absence of PUs in RF environment, not so many published works have made an attempt to describe and determine the context where a CR network operates [65] – [69]. L. Husheng proposed the concept of geographical-spectral pattern of interruptions from primary users within an area [65]. This pattern can be considered as hyperspectral images for multi-channel case and can be recovered form reports of SUs.

A detection and RF characterization algorithm, collecting signal data from multiple points in the network, using a network of Software-Defined Radios (SDRs) as an experimental test bed was implemented in [66]. The authors implement a ML RSS scheme on a cheap for exploring transmitter characterization.

In [67], a ML based approach is used to estimate transmitted power and transmitter positioning relying on a low number of sensors. The authors assume a

scenario with independent lognormal shadowing and consider omnidirectional antennas in a well known propagation environment.

In [68], RSS data is used to jointly estimate the locations and radiation patterns of multiple transmitters. These estimates are used to create an RF footprint of each transmitter, and the collection of footprints can be used to estimate which nodes are communicating with other nodes.

The 5.1 dimensional RF topography developed by Martin and Thomas [69] uses simulation results to demonstrate their transmitter characterization algorithm which identifies the presence, positions, and additional transmitter parameters such as power, path loss, transmitter directionality and beamwidth of PUs within a search space populated by SUs cooperating in a noisy environment. Using the RSS obtained at each receiving sensor and known receiver positions, they have demonstrated how their algorithm can be used to improve decisions on spectrum availability in a dynamic spectrum access system. However, authors investigate only the case of Gaussian antenna pattern. Moreover, the 3D or 2D search space over a set of different parameters involves great complexity of the algorithm.

In this context, the goal of this thesis is to explore the characterization of the relevant PUs context features through the use of a simple methodology but still retaining satisfactory performance and without making any a priori considerations regarding the radiation patterns of the PUs or RF environment. Thus, transmitter position estimation and other context features estimation will be presented in Chapter 3, respectively Chapter 4, while Chapter 6 describes a more complex methodology that will be explained there.

## 2.4. Conclusions

This Chapter has reviewed the technical concepts where this Ph.D. dissertation develops its work. At start, an introduction into CR has been presented, providing details as relevant definitions in the literature or explaining concepts as “spectrum holes”. Then, the components of a typical CRN architecture were presented. The second section of this Chapter has explained the spectrum management functions where a special emphasis has been placed on sensors sensing function. This chapter has also reviewed, in the third part, the basic concepts of REM, covering details about its meaning, structure architecture,

contained elements, and construction. It has also been illustrated the concepts and most relevant approaches found in the literature on context discovery.

# 3. Estimation of transmitter position

The fundamental problems of context discovery were described in subsection 2.3.1 of Chapter 2. It was concluded that knowing about primary network can be an important input for secondary users to determine the frequencies available for secondary use at different points. This Chapter focuses on estimating the transmitter position. The two methods presented here, the binary method and the multi-level method, are based on image processing techniques, aimed at combining a number of sensed samples at different geographical positions collected by secondary sensors, in order to estimate the positions of the different primary transmitters and to have an insight about their coverage area. In the following, Section 3.1 presents in more detail the system model and problems that are considered in this thesis. The two proposed methodologies for estimating transmitter position are described in Section 3.2. Afterwards, simulation environments and simulation results are presented in Section 3.3, respectively Section 3.4. Finally, the conclusions are summarized in Section 3.5.

## 3.1. Problem statement and assumptions

Let assume a generic scenario such as the one depicted in Figure 3.1 It is characterized by a number of transmitters corresponding to different Radio Access Technologies (RATs) which operate at different frequencies and having very different coverage areas (e.g., the central transmitter operating in a broadcast-like RAT with an extensive coverage area at frequency $f_5$, or the transmitters operating at RATs 1 and 2 with frequencies $f_1$, $f_2$, $f_3$ and $f_4$ that could correspond to some cellular-like RATs). The $k$-th transmitter is located at geographical position $(x_k, y_k)$. Its horizontal antenna pattern is $G_k(\varphi - \varphi_k)$ (dB) where $\varphi_k$ is the pointing direction. The maximum of the antenna pattern is $G_k(0) = 0$ dB, for the pointing direction $\varphi = \varphi_k$.

The secondary network can rely on the information measured by a number of sensors randomly scattered in the scenario and that could be built-in e.g., mobile terminals, and the appropriate post-processing of this information. This corresponds to the concept of "Sensor Network aided Cognitive Radio" [70] in order to assist in the detection of primary networks. Then, this elaborated information could be stored in a REM, for further assistance in future decisions of

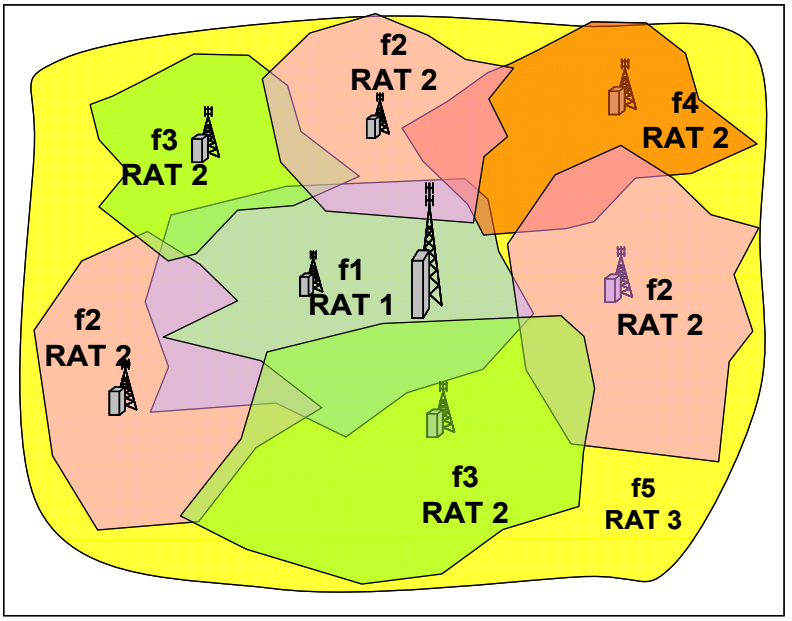


Figure 3.1: Generic scenario with different RATs and frequencies.

the secondary network operation (the utility of REM was presented in Chapter 2, Section 2.3). It is supposed that the sensors cooperate with each other in a centralized manner, where a central entity plays the role to gather all sensing information from the sensors and to estimate the different context parameters.

A sensor measures the received power in a number of $N$ specific frequencies in its geographical position. It is considered that frequency $f_i$ ($i$ = 1, 2, …, $N$) is detected by the sensor at position $(x_s, y_s)$ when the received power is above a given threshold $P_{th}(f_i)$. It is assumed that in a given sensor position, only one transmitter is received above the threshold $P_{th}(f_i)$ in a given frequency $f_i$. This could be a reasonable assumption in case that the threshold $P_{th}(f_i)$ is set in accordance to typical sensitivity levels of specific primary systems. Nevertheless, multiple transmitters can be detected at different frequencies in the same sensor position.

Received power will be affected by the distance-dependant propagation and by the long-term shadowing effects. It is assumed that fast fading effects are averaged. Then, a sensor located at position $(x_s, y_s)$ will measure a power $P_{R,k}(x_s, y_s)$ from the $k$-th transmitter given by (in dBm):

$$P_{R,k}\left(x_s, y_s\right) = P_{0,k} + G_k\left(\varphi_{s,k} - \varphi_k\right) - 10\alpha_k \log_{10} d_{s,k} + \xi_{s,k}, \tag{3.1}$$

where $P_{0,k}$ (dBm) is the received power at reference distance 1 m, $\alpha_k$ is the path loss exponent (ranging, in practice, between approximately 2 in free space propagation model and 5 in dense urban environments [61]), and $\xi_{s,k}$ is a Gaussian random variable with 0 mean and standard deviation $\sigma_k$ (dB) representing the shadowing losses, ranging in practice from 4 dB (corresponding to uncluttered environment, e.g., open area) to 12 dB (corresponding to environments rich in shadowing and multipath, e.g., urban canyons) [71]. $d_{s,k}$ and $\varphi_{s,k}$ are, respectively, the distance between the sensor and the transmitter and the angle of the sensor with respect to the transmitter, given by:

$$d_{s,k} = \sqrt{\left(x_s - x_k\right)^2 + \left(y_s - y_k\right)^2} \tag{3.2}$$

and

$$\varphi_{s,k} = \arctan\frac{y_s - y_k}{x_s - x_k}. \tag{3.3}$$

For simplicity in the notation, the explicit dependency with the frequency $f_i$ in the above parameters of the propagation model has been removed, assuming that in the sensor location each transmitter $k$ is received at a different frequency.

Different RSS measurements at random positions associated to the sensors represent a partial vision of the scenario. The problem considered in this thesis consists in defining a methodology to smartly combine these measurements in order to get a full vision in which the primary transmitters' parameters are estimated. This Chapter focuses on determining, for each transmitter, its geographical position $(x_k, y_k)$ while Chapter 4 focuses on determining, for each transmitter, its antenna direction $\varphi_k$, its antenna radiation pattern $G_k(\varphi - \varphi_k)$, and parameters of propagation model, $P_{0,k}$ and $\alpha_k$.

Two different methods are presented in this Chapter, denoted as binary and multi-level methods. In the binary method, each sensor sends just one bit, for each frequency $f_i$, to a central entity, in charge of combining the measurements of every sensor. Instead, in the multi-level method, the value detected by a given sensor for each frequency is quantified to a set of $2^n - 1$ values. Then, the sensor will send to the central entity this value encoded as a word of $n$ bits. The binary method is build to be used in case of omnidirectional antennas only, instead the multilevel method can be used also in case of directive antennas.

It is worth mentioning that this thesis focuses mainly on the combination of the sensing results to extract the context features, assuming these sensing results are available at the central entity. Both the considerations on the sensing process itself (such as errors in the process or the determination on which frequencies has to sense every sensor) and the means to report the sensing results are out of the scope of the thesis and are left for future work.

## 3.2. Proposed techniques for transmitter position estimation

It is assume that the radio environment can be characterized by an image [72], where each pixel (i.e., a rectangular area of dimensions $\Delta x \times \Delta y$) contains the information of the RSS levels associated to the frequencies measured in this area. It is assumed that a pixel can only have the result of one sensor. This information can be encoded either with the binary or the multi-level methods. Then, given that

only the values of the pixels where a sensor is located are known, these values need to be combined using image processing techniques in order to reconstruct the overall image and to estimate primary network, as it is illustrated in Figure 3.2. In the following, the proposed methods, that have the purpose to discover the transmitter positions, are presented.

### 3.2.1. Binary method

As previously mentioned, in binary method each sensor measures the received power in a number of specific frequencies in its position and sends just one bit, for each frequency $f_i$, which takes the value 1 if the received power is above a given threshold $P_{th}(f_i)$ and 0 otherwise. Considering that transmitter $k$ uses frequency $f_i$, it can be obtained the following binary representation for each frequency at each sensor position:

$$M(f_i,x_s,y_s)=\begin{cases}1 & \text{if } f_i \text{ detected in} (x_s,y_s) \Leftrightarrow \text{if } P_{R,k}(x_s,y_s)\geq P_{th}(f_i)\\ 0 & \text{if } f_i \text{ not detected in} (x_s,y_s) \Leftrightarrow \text{if } P_{R,k}(x_s,y_s)< P_{th}(f_i)\end{cases}. \quad (3.4)$$

From this binary representation, it is possible to characterize the measurement at all frequencies given by the sensor at coordinate $(x_s, y_s)$ by a value corresponding to the sum of the binary representations of the entire $N$ considered frequencies:

$$I(x_s,y_s)=\sum_{i=1}^{N} M(f_i,x_s,y_s)2^{i-1}. \quad (3.5)$$

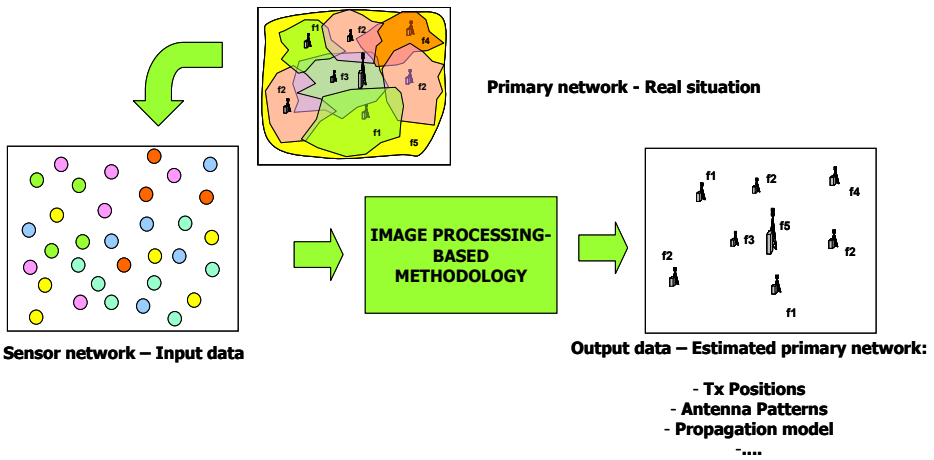


Figure 3.2: Inputs and outputs of the considered problem.

It is assumed that the coverage area of a transmitter to be discovered will be approximately circular, which would be valid in terms of average received power according to the distance-dependent path loss whenever omnidirectional antennas are used. Then, the proposed methodology aims at identifying in the image the existing circular regions, using an object-based reconstruction technique.

The steps of this method are illustrated in Figure 3.3 and explained in the following.

- First, from the information received from the secondary sensors an image is build by interpolating the intermediate pixels for those positions where no sensor was available. It is done through the nearest neighbor interpolation technique, by attributing to each unknown pixel the value of the nearest known pixel. More about other interpolation techniques are presented in Chapter 5.
- From the resulting image, a set of $N$ binary images are built, each one corresponding to one frequency. The pixels of the binary image corresponding to frequency $f_i$ take the binary values $M(f_i, x_s, y_s)$. These images will be used as the basis to identify the different "objects" (i.e., an object is a region where a certain frequency $f_i$ is detected, or correspondingly where the pixels of the binary image take the value 1).
- It is possible that in some cases, some objects are not properly detected, because they are not clearly separated from each other. In order to eliminate this drawback, before of object-based reconstruction technique, an image processing technique called *erosion* is applied to the binary images resulting from the interpolated image. In the erosion, the value of the output pixel is the minimum value of all the pixels in the input pixel's neighborhood. It is considered that a pixel's neighborhood corresponds to a circular structuring element [73], defined by a circular area of radius 5 pixels around the input pixel. Note that in the particular case of a binary image, if any of the pixels of the neighborhood is set to the value 0, the output pixel after the erosion will be set to 0, which will tend to decrease the size of the objects and thus to separate them.
- Then, for each binary image (i.e., for each frequency $f_i$), an object-based reconstruction technique is applied in order to detect the objects and measure their properties. Object detection is done following the so-called

connected-component labeling technique [74] that consists in scanning the image and making groups of adjacent pixels having the same value (it is assumed that pixels are adjacent if their edges touch). For each detected object, the measured properties are the centroid and the radius, which correspond, respectively, to the centre and radius of a circle with the same area than the object. With these properties, the object-based reconstruction process regenerates a new image replacing each object by a circle with the corresponding radius and centered in the corresponding centroid.

- Because of the prior erosion process, the resulting object area after object-based reconstruction technique has become smaller than in the binary images, which would lead to more reduced coverage areas than in the real situation. To compensate this effect, the *dilation* technique is applied to the binary images resulting from the object-based reconstruction technique. A simple example of erosion and dilation is shown in Figure 3.5. The dilation is the image processing technique opposite to the erosion process, and in this case the value of the output pixel is the maximum value of all the pixels in the input pixel's neighborhood [73]. In particular, in a binary image, if any of the pixels of the neighborhood is set to the value 1, the output pixel is set to 1, which will tend to increase the size of the objects. The same neighborhood shape (i.e., circular structuring element) as in the erosion is considered. After dilation, a second object based reconstruction process is carried out, to obtain the final centroids and radii of the detected objects. Note that the computed centroids will correspond to the final estimated transmitter positions. In addition, the radii will provide a first insight of the coverage ranges.

- Due to the shadowing effects in the propagation, after the reconstruction process, it may happen that certain objects are detected with an area significantly smaller than that of the rest of objects, so they cannot be considered as transmitters. To cope with this, in the last step, the resulting images are filtered out by eliminating those objects that have an area below a fraction $\beta$ of the average area of all the detected objects.

- Finally, after this filtering, the binary images are combined to obtain a new image including information of all the frequencies. This image includes the transmitter estimated positions, coverage areas assumed to be circular and frequencies of the different primary transmitters.

### 3.2.2. Multilevel method

In the multi-level method, each sensor measures the received power in a number of specific frequencies in its position and quantifies this value in a set of $2^n - 1$ levels within the range $[P_{th}(f_i), P_{max}(f_i)]$ (note that the value 0 is reserved for the case that the received power is below the threshold $P_{th}(f_i)$) and with quantification step $\Delta$ given by:

$$\Delta = \frac{P_{\max}(f_i) - P_{th}(f_i)}{2^n - 1}. \tag{3.6}$$

This value is sent to the CR central entity encoded as a word of $n$ bits, for each frequency.

From the information of each sensor, an image is built in which each pixel is characterized not only by the frequencies detected, like in the binary method, but also by the values of received powers at each frequency. In particular, the value of one pixel will be a set of quantified values, one per frequency. The steps of multi-level method are shown in Figure 3.4 and explained in the following.

- From the results of the sensors an image is built by interpolating the intermediate pixels for those positions where no sensor was available. The process is equivalent to the interpolation of the binary method, aiming to fill the empty spaces by attributing to each unknown pixel the value of the nearest known pixel.
- From the resulting interpolated image, like in the binary method, a set of $N$ binary images is built, one per frequency $f_i$, whose pixels take the value 1 when frequency $f_i$ is detected (i.e., it is above $P_{th}(f_i)$) and 0 otherwise. These images will be used as the basis to identify the different "objects".
- Then, for each binary image (i.e., for each frequency $f_i$), an object identification technique following the same connected component labeling technique (explained in the description of the binary method) is applied. Each group of pixels will be then an "object" associated to the coverage area of a certain transmitter using frequency $f_i$.
- The pixels belonging to each of the identified objects at frequency $f_i$ are colored again using the quantified values from the received power after the interpolation process. Then, as a result of the object identification process,

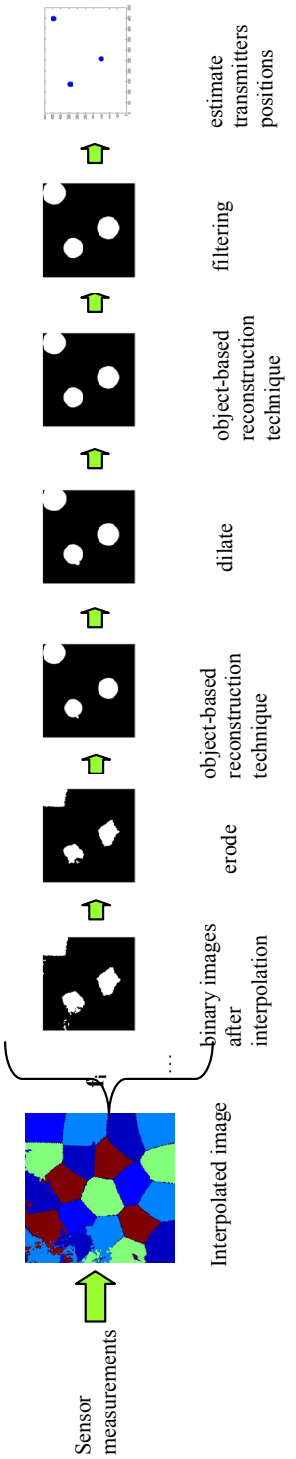


Figure 3.3: Steps of binary method.

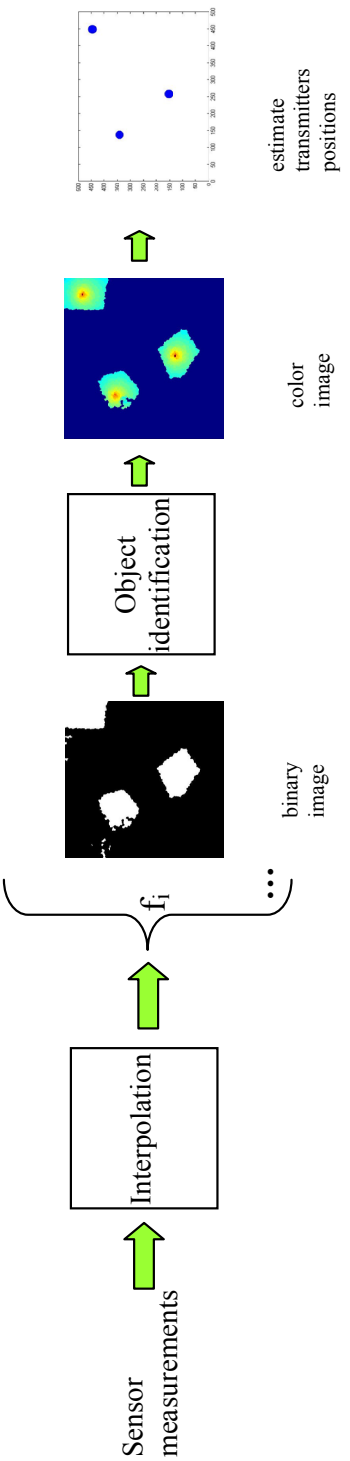


Figure 3.4: Steps of multi-level method.

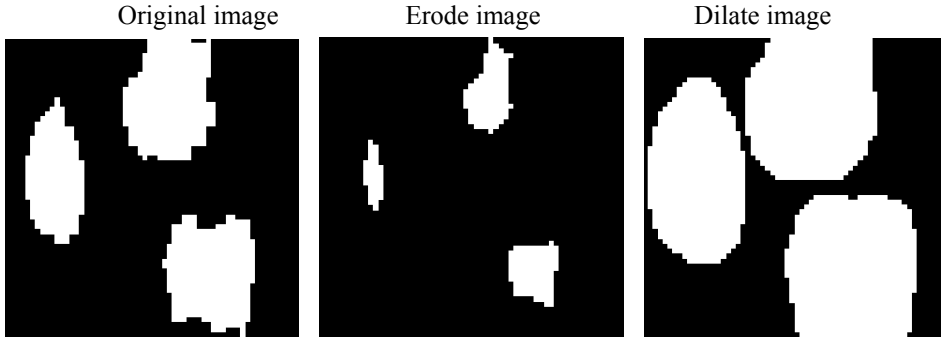


Figure 3.5: Exemple of erosion and dilation for a simple image.

the algorithm will provide a color image per object (i.e., transmitter) and frequency composed by all the pixels where the corresponding transmitter was detected and the associated power levels (see Figure 3.4).

- Then, each object is individually analyzed to determine the transmitter positions. In particular, given that the highest received power will be measured in the pixels where the primary transmitter is located, for each object the pixels with the highest received power are identified and the centroid of these pixels is calculated. The value of the centroid will be the estimated transmitter position.

On the other hand, in addition to the transmitters' positions it can also be obtained an estimate of the coverage range for each transmitter by applying to the binary images the same object-based reconstruction technique that was used in the binary method.

#### 3.2.2.1. Particular case of directive antennas

In case of having a directional antenna, the estimated position is biased as the quantified and retained maximum received power extends in a greater extent the pixels' laying in the direction of the radiation pattern. In this situation, and once it is observed that the antenna is directive (will be explained in Chapter 4), the estimation can be further refined as follows.

1.- Take as an intermediate estimation of the transmitter position the extreme point of the object formed with the pixels of maximum received power in the opposite direction of the maximum radiation pattern (point B in Figure 3.6).

2.- Assuming point B as the transmitter position, estimate antenna pattern and propagation model coefficient as will be explained in Chapter 4.

3.- Estimate transmitter position by shifting the previous intermediate estimation (point B in Figure 3.6) in the direction of the antenna by distance $d_1$. This distance is computed considering that the received power in points A and B of the figure, respectively, is equal, meaning that the following relationship holds:

$$\frac{G_k(\pi)}{d_1^{\alpha_k}} = \frac{G_k(0)}{(d_2 - d_1)^{\alpha_k}} = \frac{1}{(d_2 - d_1)^{\alpha_k}}, \tag{3.7}$$

where $G(\pi)$ is the value of the antenna radiation pattern in the back direction, $\alpha$ is the propagation coefficient and $d_2$ is the distance between the extreme points A and B in Figure 3.6. From previous expression $d_1$ is easily obtained as:

$$d_1 = \frac{d_2 \cdot G_k(\pi)^{1/\alpha_k}}{1 + G_k(\pi)^{1/\alpha_k}}, \tag{3.8}$$

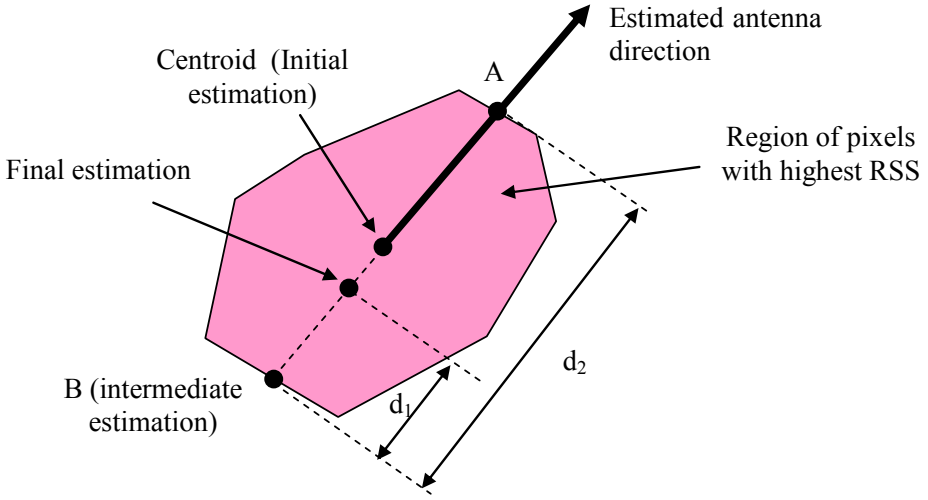


Figure 3.6: Position estimation for directive antennas.

## 3.3. Simulation environment

The proposed methods have been evaluated by means of computer simulations in different scenarios. In the following basic simulation elements and parameters are presented.

### 3.3.1. Scenario A: Omnidirectional antennas placed homogeneously in a field

First scenario consists in 42 cell radius of 1 km placed uniformly in a field, following a hexagonal layout, with a 3 frequency reuse pattern ($f_1, f_2, f_3$). The total scenario size is $10 \times 10$ km$^2$, and the pixel size is $\Delta x = \Delta y = 10$ m. The transmitter power is 30 dBm, propagation losses as a function of distance $d$ (km) are given by:

$$L = 128.1 + 37.6 \log_{10} d \,, \tag{3.9}$$

and the shadowing standard deviation is 3 dB. Power threshold $P_{th}(f_i)$ is set at –99.6 dBm for all frequencies.

Figure 3.7 shows the original image corresponding to the digitalization (i.e., the image if all the pixels were known). Having just $N = 3$ frequencies, pixels are encoded according to (3.5) with $8 = 2^N$ different intensity levels (i.e., colours) where the value $7 = 111_2$ corresponds to the areas where three cells are overlapped, the values $3 = 011_2$, $5 = 101_2$, and $6 = 110_2$ corresponds to the areas where two

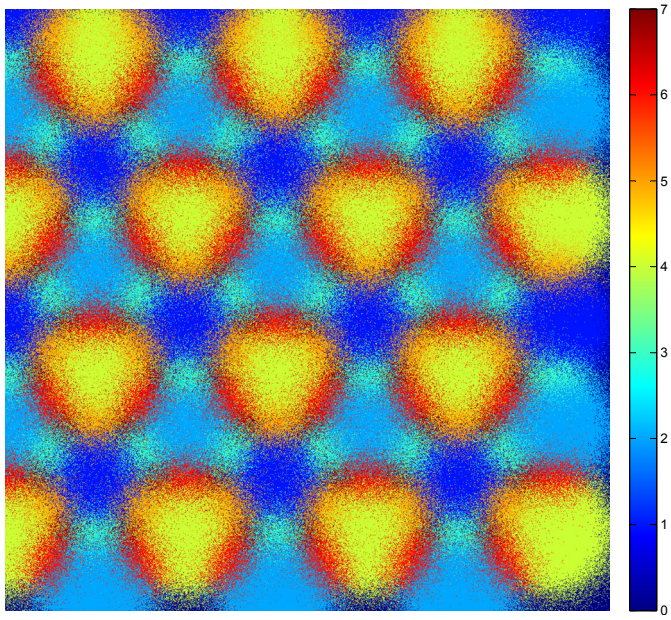


Figure 3.7: Image corresponding to scenario A with 3dB shadowing standard deviation. In the right part, the color scale corresponding to each pixel intensity between 0 and 7 is plot.

cells overlap, and finally the values $1 = 001_2$, $2 = 010_2$, and $4 = 100_2$ correspond to the central areas of each cell.

### 3.3.2. Scenario B: Omnidirectional antennas irregularly distributed in a field

Scenario B has 5 frequency reuse pattern ($f_1, f_2, f_3, f_4, f_5$) in a field of 10 × 10 km$^2$. Pixel size is $\Delta x = \Delta y = 20$ m. There are 21 primary transmitters, each one having EIRP (Equivalent Isotropic Radiated Power) of 40 dBm. Simulated cellular network deployment should represent a realistic network deployment. For that, in this scenario, propagation losses are computed using a planning tool in a realistic environment (ATOLL – one of the most famous tools in radio network planning and optimization domain), given by (distance $d$ in km):

$$\begin{aligned} L = {} & 46.3 + 33.9\log_{10} f - 13.82\log_{10} Hb + \left(44.9 - 6.55\log_{10} Hb\right)\log_{10} d - \\ & -\left(1.1\log_{10} f - 0.7\right)Hr + \left(1.56\log_{10} f - 0.8\right) - 4.78\left(\log_{10} f\right)^2 + 18.33\log_{10} f - 40.94 \end{aligned}, \quad (3.10)$$

where frequency $f$ is 900 MHz, transmitter's height, $Hb$, is 30 m, receiver's height, $Hr$, is 1.5 m. Relation (3.10) does not apply to small path lengths. After calculations and transforming distance $d$ in meters, propagation losses are:

$$L = -8.16 + 35.22\log_{10} d, \quad (3.11)$$

Power threshold $P_{th}(f_i)$ is set to –85 dBm for all frequencies. Furthermore, the number of bits used to encode the RSS measurements is $n = 5$ and the quantization step is $\Delta = 3.6$ dB. In turn, the value of $\beta$ in the object detection process is 0.3. Figure 3.8 presents the original image representing the scenario with the position of transmitters, corresponding to a terrain in the surroundings of Barcelona, and Figure 3.9 presents the transmitters' coverage area where each color represents a different frequency.

### 3.3.3. Scenario C: Directive antennas

The third scenario has a tri-sector antenna system that uses 3 frequency reuse pattern ($f_1, f_2, f_3$). The total scenario size is 3780 × 3780 m$^2$ and pixel size is $\Delta x = \Delta y = 20$ m. The EIRP is 57.15 dBm, propagation losses as a function of distance $d$ (km) are computed using the same planning tool as the previous scenario in a realistic environment and are given by:

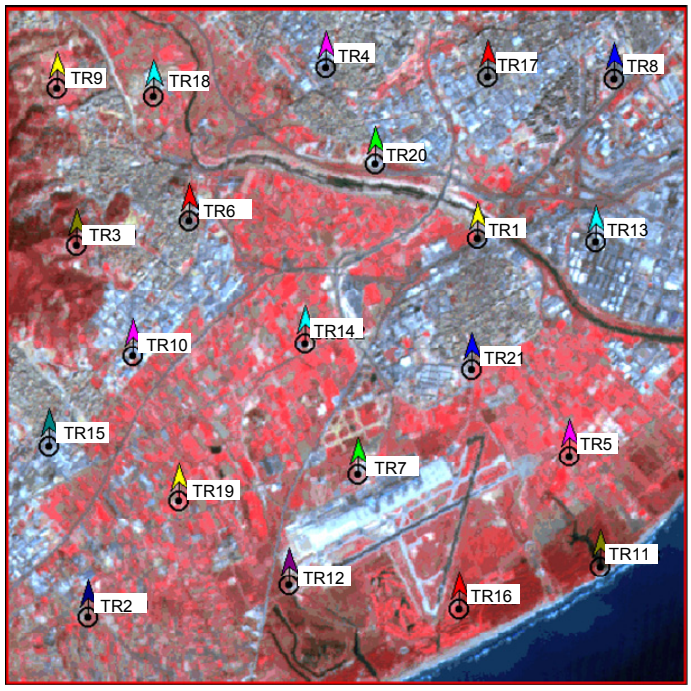


Figure 3.8: Image corresponding to scenario B and its transmitter positions.

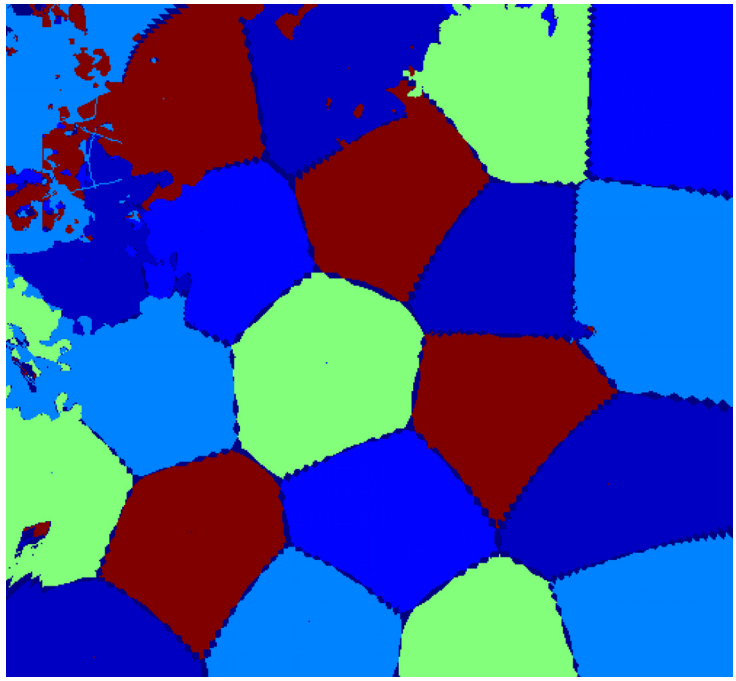

Figure 3.9: The coverage area of primary transmitters in scenario B.

$$L = 69.55 + 26.16\log_{10} f - 13.82\log_{10} Hb + \left(44.9 - 6.55\log_{10} Hb\right)\log_{10} d - \\ -3.2\left(\log_{10}\left(11.75Hr\right)\right)^2 + 4.97 - 4.78\left(\log_{10} f\right)^2 + 18.33\log_{10} f - 40.94 \quad , \qquad (3.12)$$

where frequency $f$ is 1800 MHz, transmitter's height, $Hb$, is 30 m, receiver's height, $Hr$, is 1.5 m. After the calculations and transforming distance $d$ in meters, the propagation losses are:

$$L = -3.3 + 35.22\log_{10} d \qquad (3.13)$$

Power threshold $P_{th}(f_i)$ is set to –85 dBm for all frequencies. In addition, in multi-level method, the number of bits is $n$ = 5 and the quantization step is $\Delta$ = 2 dB. Figure 3.10 shows the original image representing the new scenario with the position of transmitters, corresponding to a terrain in the surroundings of Barcelona, and Figure 3.11 presents the radiation pattern of the transmitter antenna, the same for all 3 transmitters.

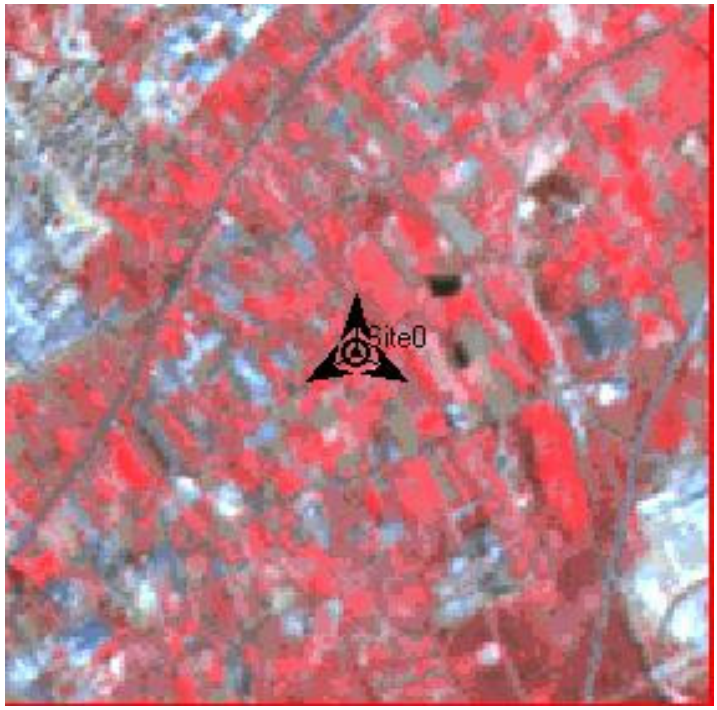


Figure 3.10: Image corresponding to scenario C and its transmitter positions.

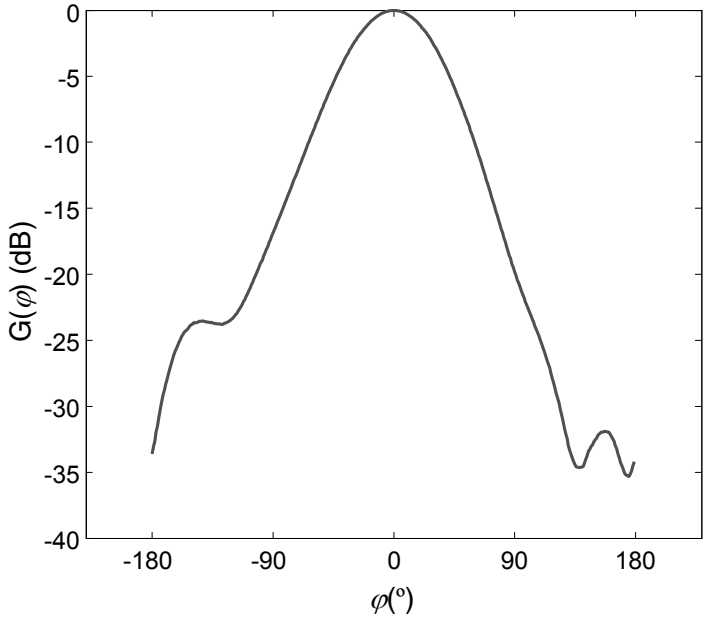


Figure 3.11: Horizontal radiation pattern of the transmitter antenna on scenario C.

## 3.4. Simulation results

In this Section some results are provided to illustrate the performance of the two proposed methods.

### 3.4.1. Binary method

The original image of the scenario A (3.3.1) with omnidirectional antennas uniformly distributed in a field is sensed with a random sensor distribution with average density $D$ and then the binary method is applied. In Figure 3.12 it can be observed the difference between the original image with shadowing effects, the sensed and interpolated image, and the reconstructed image, in case that density of sensors $D$ = 100 sensors/km$^2$. Visually it can be remarked an important improvement of the original image as the shadowing effects are no longer included in the reconstructed image, so that the positions and coverage areas of the different transmitters can be more clearly identified.

Figure 3.13 plots the resulting images for different values of the sensor density $D$. Note that for a low density of sensors such as $D$ = 4 sensors/km$^2$ the transmitters can not be properly identified.

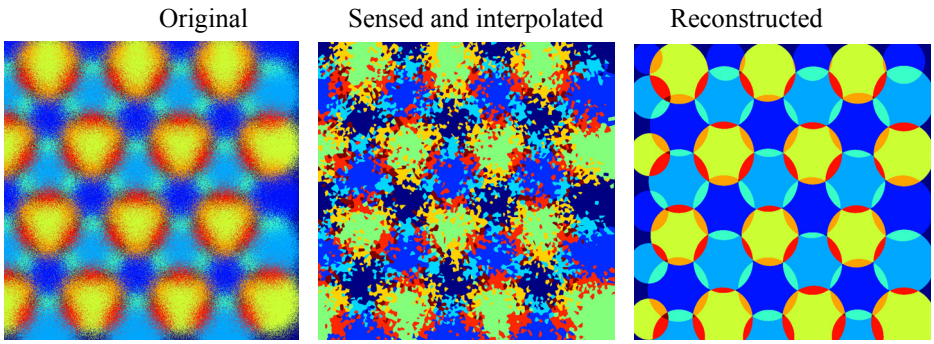


Figure 3.12: Comparation between the original image, the sensed and interpolated image, and the reconstructed image for the case $D$ = 100 sensors/km$^2$, binary method applied on scenario A.

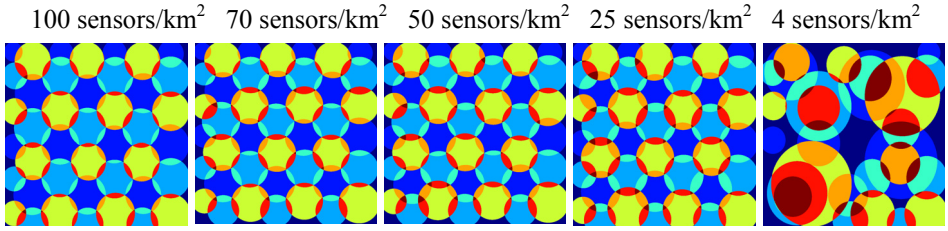


Figure 3.13: Images resulted after binary method for different sensor densities on scenario A.

Every centroid of the detected objects represents the estimation of the position of each transmitter. In order to measure the accuracy in this estimation, the relative error in the position estimation is computed as the difference between the real transmitter position and the detected position, divided by the estimated transmitter coverage radius. For this computation, the transmitters that are located in the borders of the image are not taken in account, since they do not form a complete circle in the original image and consequently they lead to larger errors due to border effects.

Figure 3.14 presents the relative error for each transmitter in the considered scenario in case that density of sensors $D$ = 100 sensors/km$^2$. It can be observed that, in all the cases, the values of the relative errors are below 8%.

The mean error and the standard deviation error (represented as vertical lines) for different density of sensors are shown in Figure 3.15. In addition, Figure 3.16 plots the rate of transmitter detection representing the ratio between the

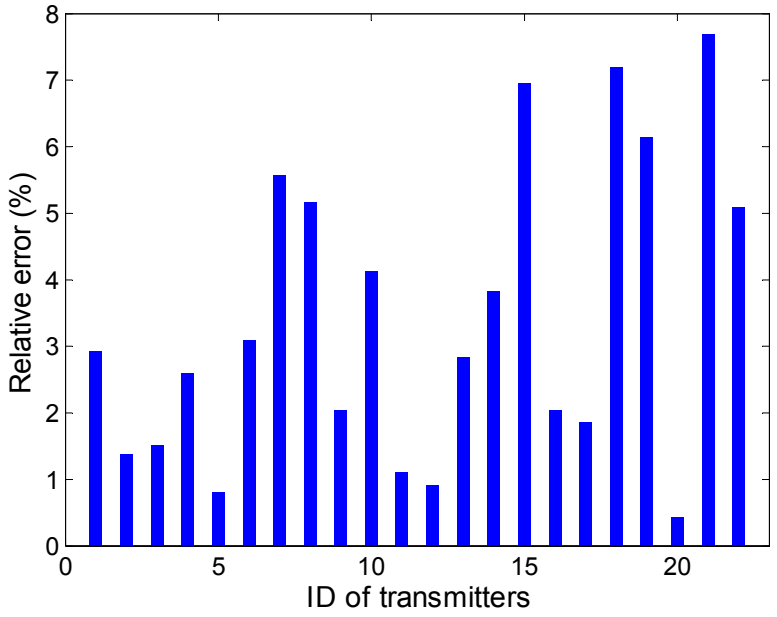


Figure 3.14: Relative error in the transmitter positions for $D$ = 100 sensors/km$^2$, binary method applied on scenario A.

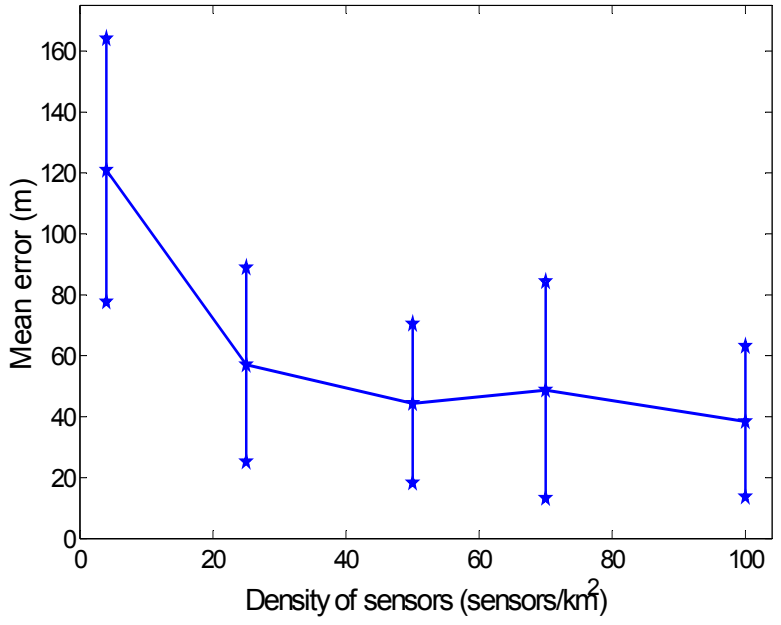


Figure 3.15: Mean error and standard deviation error, binary method applied on scenario A.

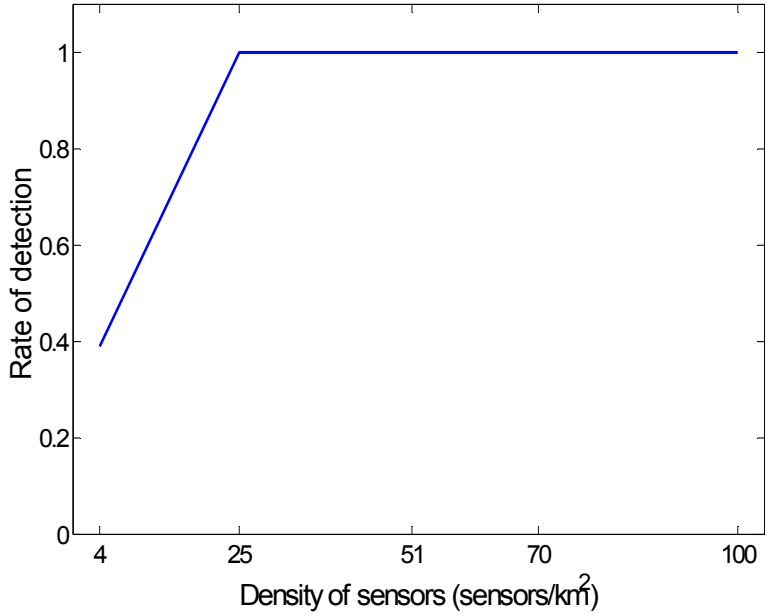


Figure 3.16: Rate of transmitter detection, binary method applied on scenario A.

number of transmitters properly detected and the exact number of transmitters. In case $D$ = 4 sensors/km$^2$, only 40% of the transmitters are detected, and the mean error is high, as well as the standard deviation error. As the density of sensors grows, the rate of detection is 100%, and the mean error is smaller. Gathering more than about 25 sensors per km$^2$ (i.e., on average 1 sensor every 200 × 200 m$^2$ or equivalently about 80 sensors per transmitter coverage area) leads to minor marginal gains to the mean error of about 5% (or 50 m in the base station position) and to a detection probability of 100% in the analysis performed.

Figure 3.17 and Figure 3.18 show the obtained results for different values of cell radius. As expected, in case that the cell radius is small (e.g., 500m), fewer sensors are inside the cell coverage area, the errors are bigger, and the rate of detection smaller. Instead, if the cell radius is large (e.g., 1500m), the number of sensors inside the cell coverage area is also large, the errors are smaller, and the rate of detection is higher.

Accepting an error below 5% and a rate of transmitter detection above 95%, from the results it can obtained the minimum density of sensors necessary in order to make a proper estimation of the transmitters' position. This is indicated in Table 3.1.

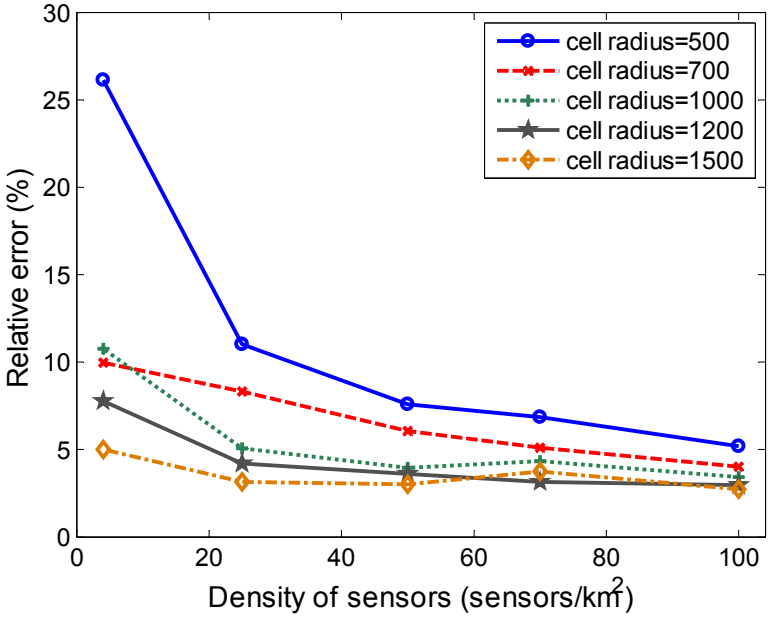


Figure 3.17: Relative error for different values of cell radius, binary method applied on scenario A.

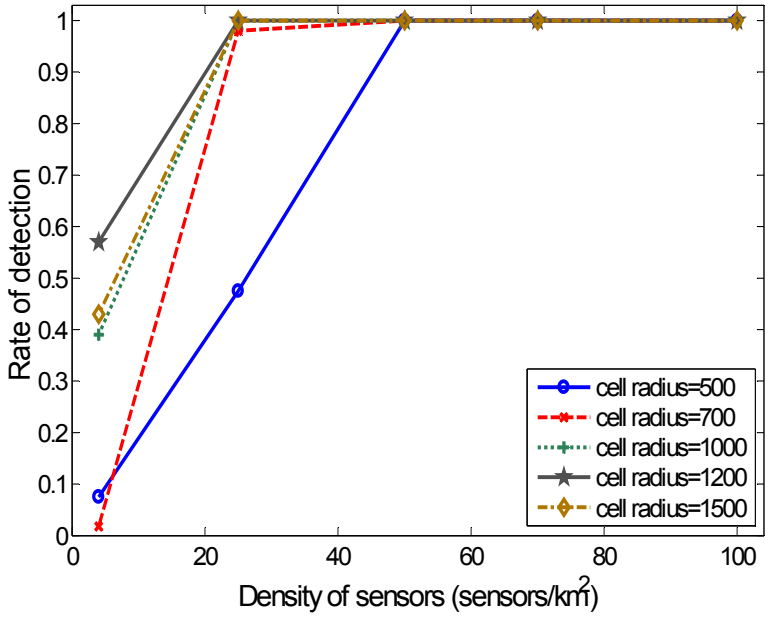


Figure 3.18: Rate of transmitter detection for different values of cell radius, binary method applied on scenario A.

Table 3.1: Minimum density of sensors necessary for different cell radius, binary method applied on scenario A.

| | cell radius 500 m | cell radius 700 m | cell radius 1000 m | cell radius 1200 m | cell radius 1500 m |
|---|---|---|---|---|---|
| density of sensors per km$^2$ | 110 | 73 | 28 | 22 | 10 |

### 3.4.2. Multi-level method for omnidirectional antennas

A random sensor deployment with average density $D$ is retained and multi-level method is applied on scenario B (3.3.2) with omnidirectinal antennas randomly distributed in the field. In Figure 3.19 one can observe the reconstructed images for different values of the sensor density $D$ – this will represent the estimate coverage area of the primary transmitters. It can be noticed that as the density of sensors grows the performance improves, providing a better estimation of the reference image (Figure 3.9).

100 sensors/km$^2$ 70 sensors/km$^2$ 50 sensors/km$^2$ 25 sensors/km$^2$ 4 sensors/km$^2$

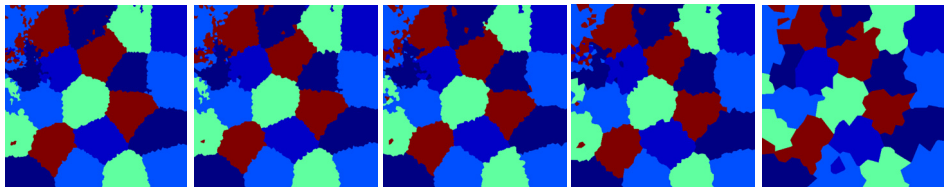

Figure 3.19: Images resulted after multi-level method for different sensor densities on scenario B.

Figure 3.20 plots the comparison between the real primary transmitter positions and the corresponding positions estimated with both methods, binary and multi-level, on scenario B. It can be observed that, although the two methods are able to identify quite accurately the positions, the estimation is more precise with the multi-level method.

As it was mentioned in previous subsection, the relative error is computed as the difference between the real transmitter position and the estimated position, divided by the estimated transmitter coverage radius. Figure 3.21 shows the relative error for each of the 21 transmitters in scenario B for $D$ = 100 sensors/km$^2$, together with the estimated radii with the two methods. One can remark that, with the binary method, the values of the relative errors have a wide variation for the

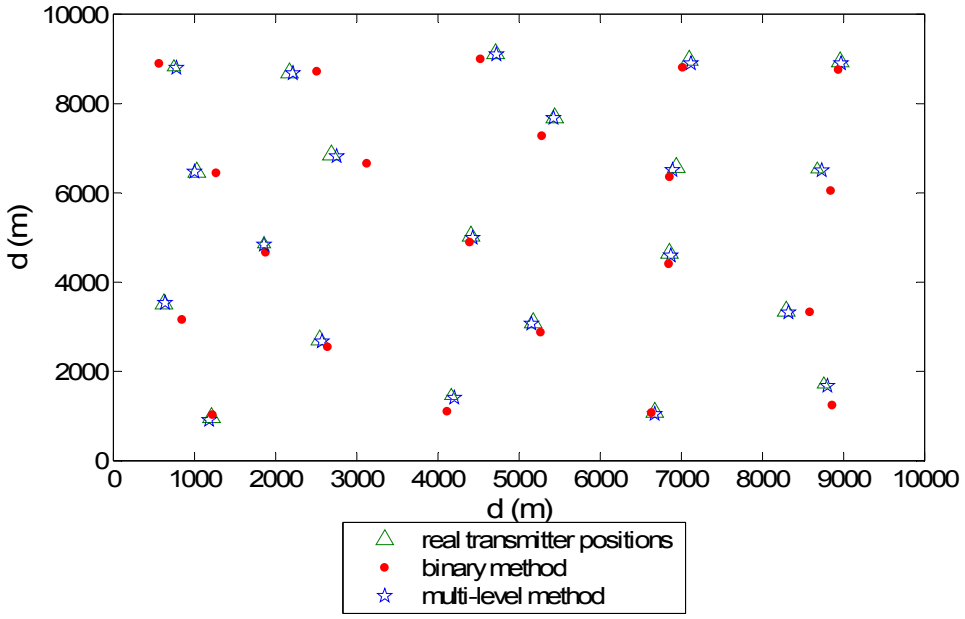


Figure 3.20: Real and estimated primary transmitter positions for $D$ = 100 sensors/km$^2$, compare between binary and multi-level methods on scenario B.

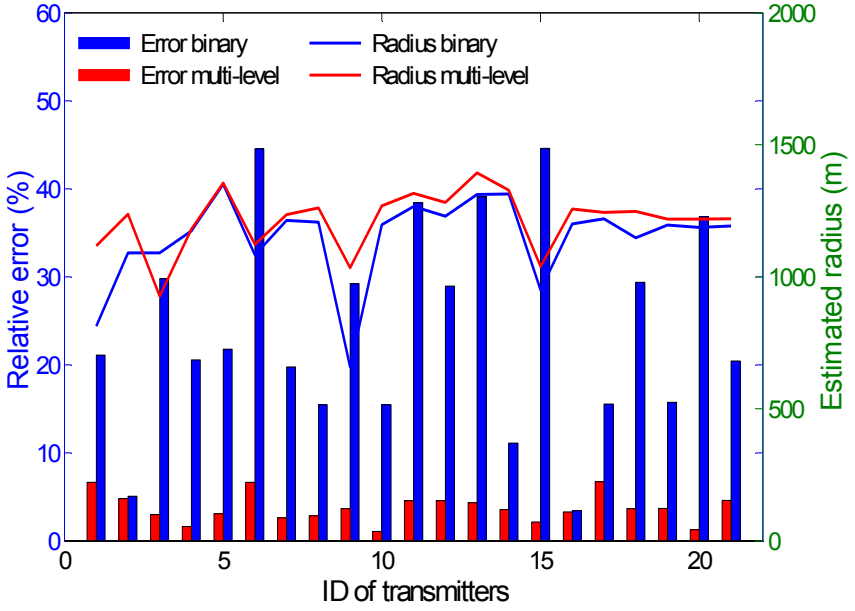


Figure 3.21: Relative error in transmitter positions and estimated radius for $D$ = 100 sensors/km$^2$, compare between binary and multi-level methods on scenario B.

different transmitters and can be in some cases as high as 45%. Instead, with the multi-level method, in all the cases the values of the relative errors are below 7%. It can also be observed that the estimated radius for the different transmitters is quite similar for the two methods.

Figure 3.22 shows the mean relative error and the standard deviation error for different values of sensor density $D$ with the two considered methods. For the binary method, notice that the mean error improves very slowly when increasing the sensor density. In particular, the mean relative errors are still above 24%, for sensor densities as high as $D$ = 100 sensors/ km$^2$. On the contrary, for the multi-level method, it can be observed a more significant reduction in both the average error and the standard deviation error as the density of sensors grows. Notice in this case that only for a rather low sensor density (e.g., $D$ = 4 sensors/km$^2$) the mean error as well as the standard deviation error are high. These results allow establishing the minimum required density of sensors for a desired accuracy. For example, in order to achieve an error below 5%, the required density of sensors will be $D$ = 50 sensors/km$^2$ with multi-level method.

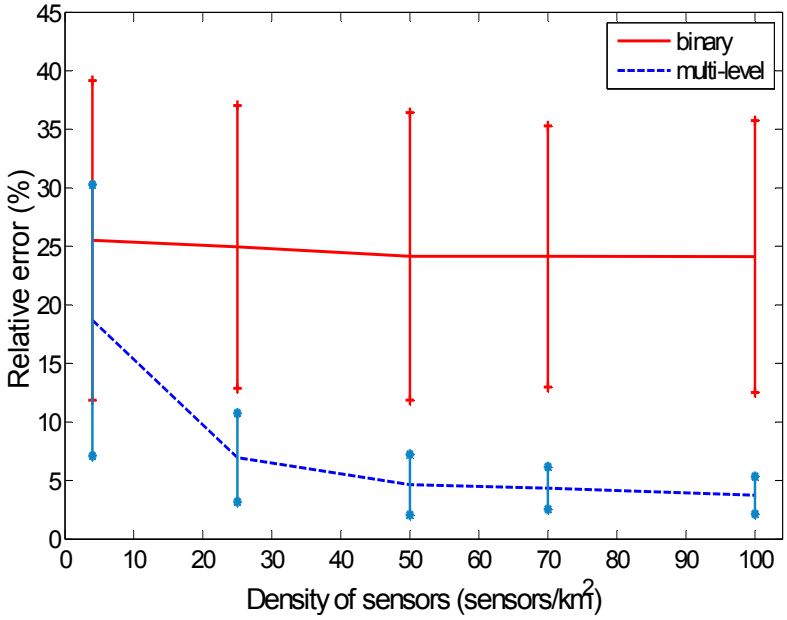


Figure 3.22: Mean relative error and standard deviation error in the transmitter position estimation, compare between binary and multi-level methods on scenario B.

### 3.4.3. Multi-level method for directive antennas

Figure 3.23 presents the mean error and standard deviation error of the final position estimation and initial position estimation based on Figure 3.6, for different values of sensor density *D*, in a scenario C with directive antennas (3.3.3). Results were averaged for the three transmitters over 10 realizations of sensors distribution. Errors are reduced as the density of sensors increases in both average error and standard deviation error. It can be noticed a remarkable improvement in the final position estimation compare with the initial position estimation.

## 3.5. Conclusions

In this Chapter two frameworks have been proposed, binary and multi-level methods, built on image processing techniques, targeted to estimate positions and coverage areas of different primary transmitters. The information obtained can be store in databases (e.g., REM) which can be used by secondary networks in order to discover the presence of primary network transmitters and to use spectrum

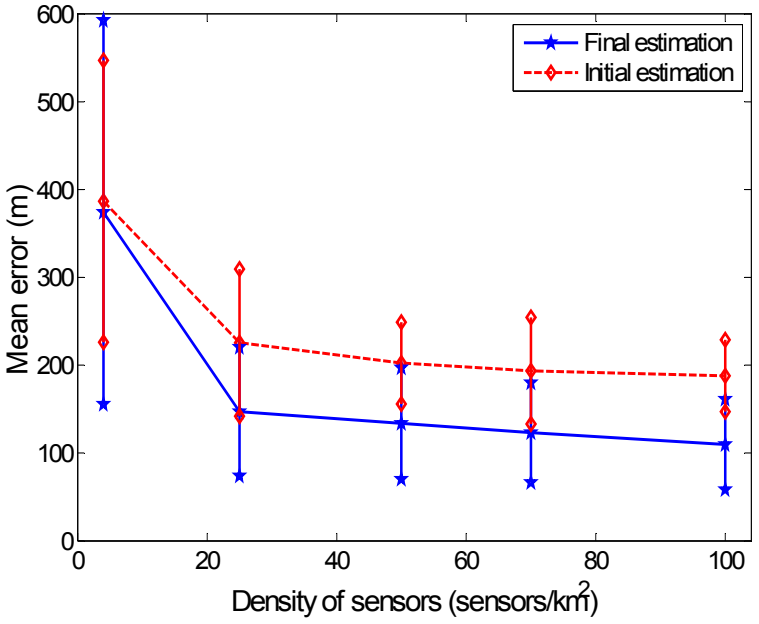


Figure 3.23: Mean error and standard deviation error in initial and final transmitter position estimation for different sensor densities, multi-level method on scenario C.

opportunities without disturbing the primaries. The results obtained with binary method in a scenario with omnidirectional antennas uniformly distributed reveal the utility and efficacy of this method, with relative errors below 5% in the transmitter position. Instead, in more complex scenarios, under data obtained from a planning tool, the results with multi-level method for omnidirectional antennas and directive antennas reveal the advantages of the proposed framework, with relative errors below 7%, respectively 150 m in the transmitter position estimation.

# 4. Extraction of other context features

Some of the most relevant primary context features that a secondary system would require to be properly deployed are: the transmitter positions, orientations of their directional antennas, radiation pattern, and propagation model. Chapter 3 starts the estimation of primary networks by presenting two positioning estimation methods. This Chapter extends prior work by including in multi-level method other context features like antenna pattern, antenna orientation, and propagation model.

The structure of this Chapter is as follows. Section 4.1 and Section 4.2 presents a methodology that estimates antennas orientation and antenna radiation pattern of primary networks. Then, in Section 4.3 a propagation model estimation is proposed. Simulation results of the considered estimation methods are discussed in Section 4.4. Finally, the conclusions of the work are drawn in Section 4.5.

## 4.1. Antenna orientation estimation

One important context component relies in the radiation pattern of the primary transmitter's antenna. In practice, omnidirectional antennas can not be necessarily assumed. Usually, directional antennas are used, and even this radiation pattern can vary with smart antennas. So, in order to plan the deployment of a secondary network, it is a key issue to be aware of the actual radiation features of the primary system. In this respect, the proposed methodology considers two steps, the first one to estimate the antenna orientation, explained in this Section, and the second one to estimate the radiation pattern, explained in Section 4.2.

First, it is determined whether a transmitter $k$ corresponds to an omni-directional or a directive antenna and which is the orientation. Using the methodology of Chapter 3 (see Figure 3.3), for each identified object (i.e., transmitter), the values of the pixels corresponding to the quantified received power after interpolation are analyzed. This is done by analyzing the values of the pixels corresponding to the quantified received power after interpolation for each identified object. In particular, the procedure computes the difference between the maximum and minimum power of all the pixels located at a given distance $d_{p,k}$ from the initial estimation of transmitter position in subsection 3.2.2.1 (centroid in Figure 3.4) for different azimuth angles $\varphi$, and averages this difference over the set of distances $d_{p,k}$:

$$\delta_k = \frac{1}{M}\sum_{p=1}^{M}\left(\max_{\varphi} P_{R,k}^{I}\left(d_{p,k},\varphi\right) - \min_{\varphi} P_{R,k}^{I}\left(d_{p,k},\varphi\right)\right), \tag{4.1}$$

where $M$ is the number of distances $d_{1,k}$, ..., $d_{M,k}$ considered in the computation (with a granularity of 1 pixel) and $P_{R,k}^{I}\left(d_{p,k},\varphi\right)$ is the quantified received power of object $k$ after interpolation at distance $d_{p,k}$ and angle $\varphi$ from the estimated transmitter position. In case $\delta_k$ is below a given threshold $\delta_{th}$ it is assumed that the antenna is omnidirectional, while on the contrary the antenna is assumed to be directive. In the latter case, the estimation of the antenna direction $\varphi_k$ is given by the angle with maximum received power averaged over the different distances, which is:

$$\varphi_k = \frac{1}{M}\sum_{p=1}^{M}\arg\max_{\varphi} P_{R,k}^{I}\left(d_{p,k},\varphi\right). \tag{4.2}$$

As previously mentioned, in case that the antenna is found to be directive after the first execution of this step, the position estimation process is further refined following the procedure explained in subsection 3.2.2.1.

## 4.2. Antenna radiation pattern estimation

In this step, once transmitter position ($x_k$, $y_k$) and direction $\varphi_k$ have been obtained, antenna's radiation pattern can be estimated for directional antennas based on the average over the distances of the received power for each azimuth angle $\varphi$ relative to the average power at the antenna direction $\varphi_k$, that is:

$$G_k(\varphi-\varphi_k)=\frac{1}{M}\sum_{p=1}^{M}\left(P_{R,k}^{I}\left(d_{p,k},\varphi\right)-P_{R,k}^{I}\left(d_{p,k},\varphi_k\right)\right). \tag{4.3}$$

## 4.3. Propagation model estimation

The knowledge of the key propagation parameters can make more efficient the planning and deployment for a secondary system. Following the radio signal propagation model expressed in (3.1) and based on the prior estimation of the transmitter position, in this step a linear regression analysis with the available sensors is carried out to obtain the estimate of parameters $\alpha_k$ and $P_{0,k}$ (see Figure 4.1 (a). A differentiation has to be done between the case of directive and omnidirectional antennas. Specifically, for directive antennas, to remove the effect of antenna radiation pattern in the propagation model estimation, the power values used in the regression analysis, $P_{R,k}^{*}\left(x_s,y_s\right)$, are obtained by subtracting the value of the estimated radiation pattern from the measured power at each sensor, that is:

$$P_{R,k}^{*}\left(x_s,y_s\right)=P_{R,k}\left(x_s,y_s\right)-G_k\left(\varphi_{s,k}-\varphi_k\right). \tag{4.4}$$

It should be noted that, in addition to providing $\alpha_k$ and $P_{0,k}$ as the slope and the constant term of the regression analysis, respectively, an estimation of the shadowing standard deviation $\sigma_k$ as the standard deviation error of the regression is also obtained.

The regression analysis can also be used to discard those objects identified in subsection 3.2.2 that do not actually correspond to transmitters but are due to

effects such as shadowing or detection noise. In particular, the regression analysis should reveal a clear correlation between distance (to the estimated transmitter position) and received power for all the identified objects, translating into reasonable values of correlation coefficient $r_{d,P,k}$ (a measure of the strength of the linear relationship between two variables) [75], defined as:

$$r_{d,P,k} = \frac{S\sum_{s=1}^{S} d_{s,k} P_{R,k}(x_s, y_s) - \sum_{s=1}^{S} d_{s,k} \sum_{s=1}^{S} P_{R,k}(x_s, y_s)}{\sqrt{S\sum_{s=1}^{S} d_{s,k}^2 - \left(\sum_{s=1}^{S} d_{s,k}\right)^2} \sqrt{S\sum_{s=1}^{S} P_{R,k}^2(x_s, y_s) - \left(\sum_{s=1}^{S} P_{R,k}(x_s, y_s)\right)^2}}. \quad (4.5)$$

Correlation coefficient $r_{d,P,k}$ can range from +1 to –1; the value of –1 indicates a perfect negative correlation, a value of +1 indicates a perfect positive correlation while a value of 0 indicates that the two variables are not linearly correlated. Values between 0.7 and 1.0 (–0.7 and –1.0) indicate a strong positive (negative) linear relationship via a firm linear rule. In this situation, when no clear correlation of power with the distance is found (a value of $r_{d,P,k}$ between –0.7 and 0.7) this will correspond to an object that is not actually a transmitter. In Figure 4.1 (b), what the process has detected and identified as an object is not actually a transmitter but an error of the process due to shadowing effects. This allows identifying and filtering "spurious" objects. The pseudocode of discarding "spurious" objects algorithm is presented in Figure 4.2.

## 4.4. Simulation results

The two scenarios, scenario B that include omnidirectional antennas and scenario C that include directive antennas, presented in 3.3.2, respectively 3.3.3, are used in order to evaluate the proposed methodology. This Section presents the performance evaluation results through these scenarios. Threshold $\delta_{th}$, that determine if the transmitter has a directive or omnidirectional antenna, was set to 10 dB after various calculation of $\delta_k$ (4.1) for different objects (corresponding to omnidirectional or directive antennas), for distance between 0.5 km and 1.1 km. Figure 4.3 presents two examples of calculating $\delta_k$ for an omnidirectional antenna (a), respective a directive antenna (b).

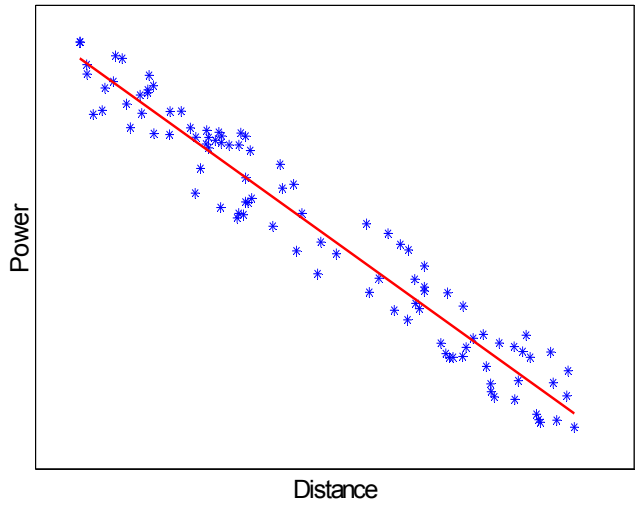


(a)

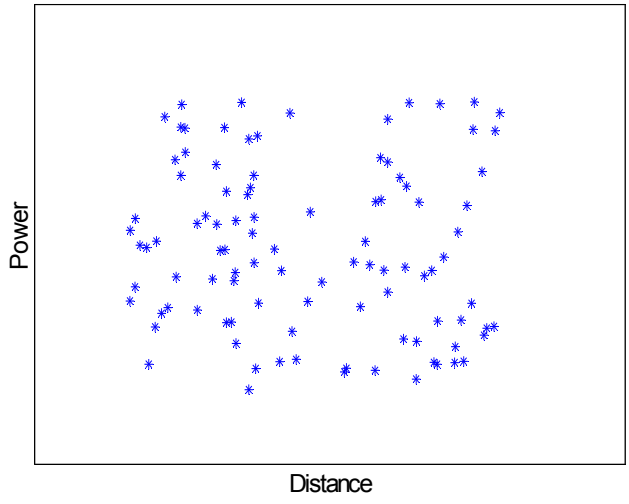


(b)

Figure 4.1: (a) Clear correlation with distance; (b) No correlation with the distance.

### 4.4.1. Scenario with omnidirectional antennas

Based on the propagation model used by the planning tool on scenario B (3.11), and knowing that:

$$P(dBm) = EIRP(dBm) - L(dB), \tag{4.6}$$

```
1. for every object k do
2.     calculate r_{d,P,k} from (4.5):
3.     if |r_{d,P,k}| ≤ 0.7 then
4.           object k is not a transmitter;
5.           eliminate object k;
6.     else
7.           object k is a transmitter;
8.           calculate α_k and P_{0,k} by regression analysis;
9.     end if;
10. end for;
Output (α_k, P_{0,k})
```

Figure 4.2: Pseudocode of discarding "spurious" objects algorithm.

the expected received power should be:

$$P(dBm) = 48.16 - 35.22 \log_{10} d(m), \tag{4.7}$$

which should be taken only as a reference, since there can be additional losses due to diffraction (considered by the planning tool depending on the terrain) and also there is some heterogeneity in the scenario so that different propagation expressions depend on each region type.

The correlation between distance and received power for the available sensors was examined for each transmitter detected. As an example, Table 1 presents 10 values of correlation coefficient $r_{d,P}$ for 10 different identified objects that are plotted in Figure 4.4, for the case $D$ = 25 sensors/km$^2$. According to the algorithm presented in Figure 4.2, objects 1, 2, 3, 4, 5, 6, and 9 are considered "spurious" objects and they are discarded while the rest of the objects indicate a strong negative relationship of power and distance and are considered real transmitters.

With respect to the propagation model estimation, Figure 4.5 plots the average received power (corresponding to one transmitter) measured by sensors according to the distance between each of the sensors and the transmitter, for $D$ = 100 sensors/km$^2$. The estimated received power as a function of the distance

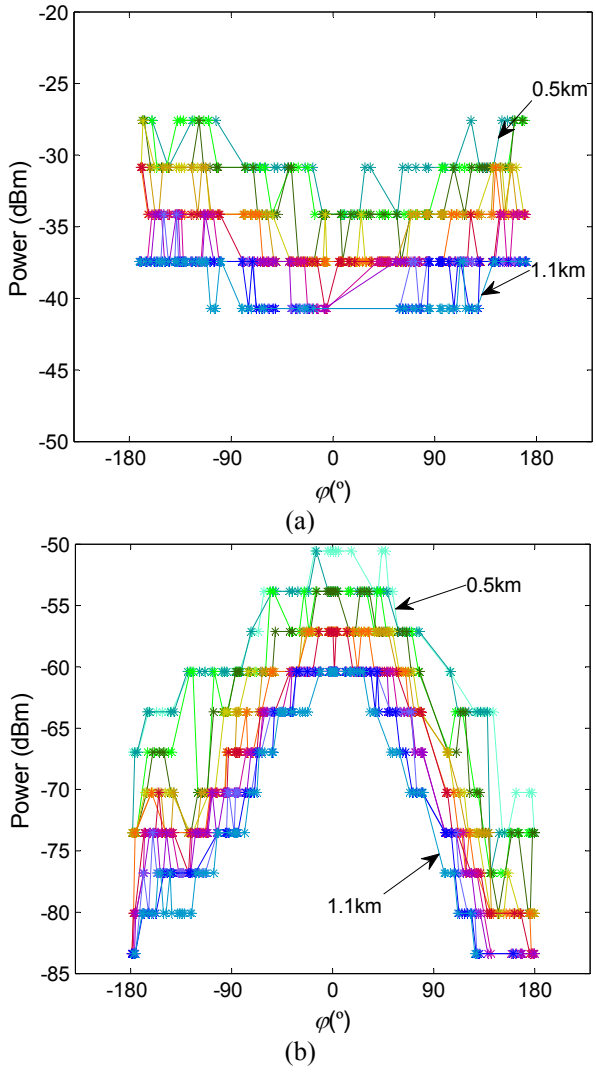


Figure 4.3: Exemple of calculating $\delta_k$ for an omnidirectional antenna (a), respective a directive antenna (b).

obtained from linear regression is given by:

$$P(dBm) = 53.65 - 30.62 \lg d(m). \tag{4.8}$$

In turn, in a scenario with sensor density $D$ = 50 sensors/km$^2$, the estimated received power as a function of the distance obtained from linear regression leads to:

Table 4.1: 10 values of correlation coefficient for 10 different identified objects for the case $D$ = 25 sensors/km$^2$, on scenario B.

| Identified objects | $r_{d,P}$ | Decision |
|---|---|---|
| **1** | 0.3521 | "spurious" object |
| **2** | -0.3606 | "spurious" object |
| **3** | 0 | "spurious" object |
| **4** | 0 | "spurious" object |
| **5** | 0 | "spurious" object |
| **6** | 0 | "spurious" object |
| **7** | -0.7108 | real transmitter |
| **8** | -0.8971 | real transmitter |
| **9** | 0 | "spurious" object |
| **10** | -0.9214 | real transmitter |

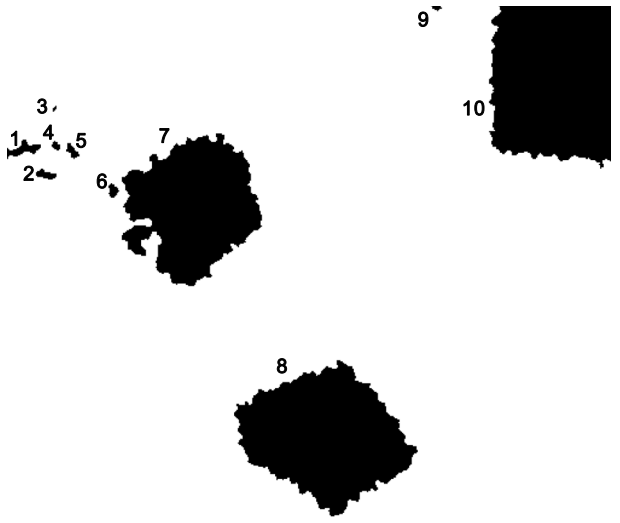


Figure 4.4: 10 different identified objects for the case $D$ = 25 sensors/km$^2$, on scenario B.

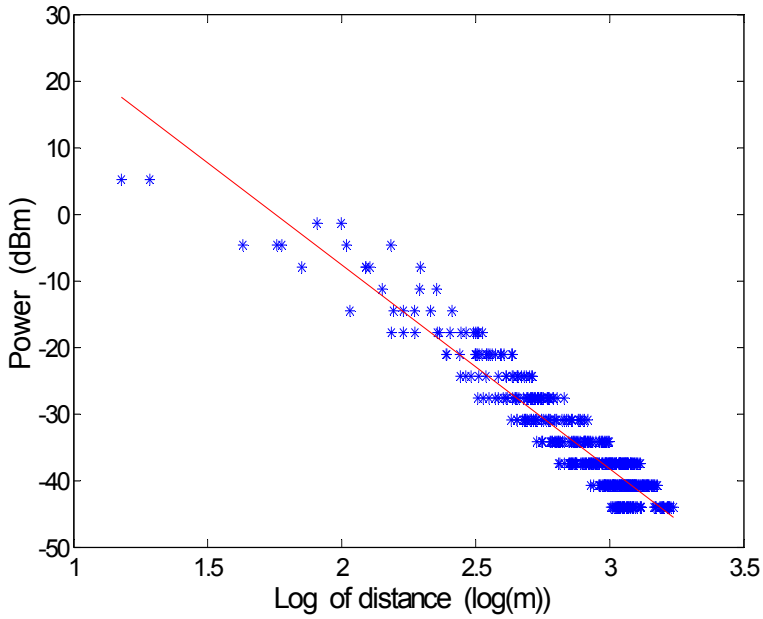


Figure 4.5: Linear regression of the received power as a function of distance in case of $D$ = 100 sensors/km$^2$, for one transmitter on scenario B.

$$P(dBm) = 54.34 - 30.87 \lg d(m). \tag{4.9}$$

As it can be observed, the relative error in the propagation factor $\alpha$ is around 13.06% for $D$ = 100 sensors/km$^2$, and around 12.35% for $D$ = 50 sensors/km$^2$, while the relative error in the received power, $P_0$, is 11.39% for $D$ = 100 sensors/km$^2$, and increases up to 12.83% for $D$ = 50 sensors/km$^2$.

The mean estimated values and standard deviation errors of propagation factor $\alpha$ and power $P_0$ are presented in Figure 4.6 (a), respectively Figure 4.6 (b) as function of sensor density for all the transmitters on scenario B (named "Estimate" in figures). The theoretical values according to (4.7) are also plotted, named "Real" in figures. As it is expected, in both of the parameters, the errors reduce when increasing the sensor density. It is worth pointing out that there is an insignificant gain of the parameters above 20 sensors/km$^2$.

### 4.4.2. Scenario with directive antennas

In scenario C, the expected received power at distance $d$ should be approximately:

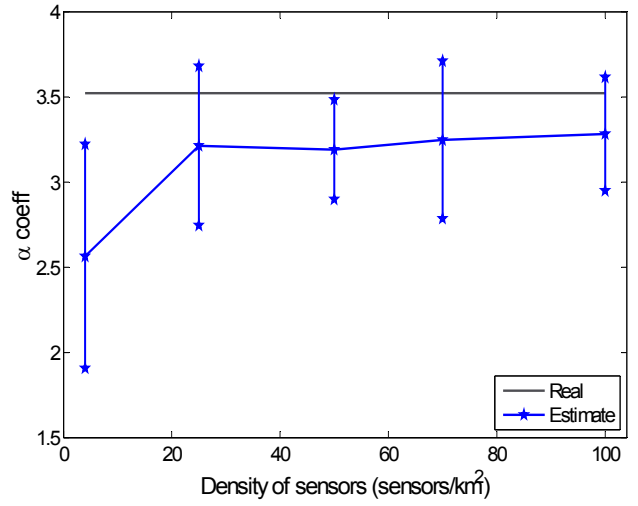


(a)

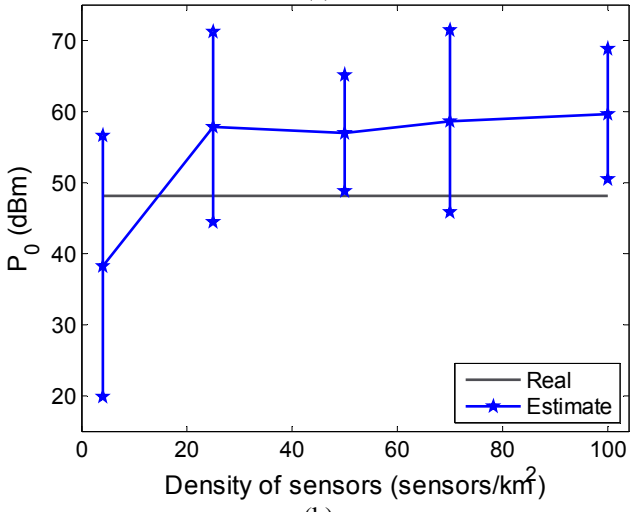


(b)

Figure 4.6: Estimated propagation factor $\alpha$ (a), estimated power $P_0$ (b), and their standard deviation error as a function of sensor density, on scenario B.

$$P(dBm) = 53.85 - 35.22 \lg d(m). \tag{4.10}$$

When considering a sensor density $D$ = 100 sensors/km$^2$ the estimated propagation model based on regression analysis of one transmitter leads to:

$$P(dBm) = 47.8 - 35.68 \lg d(m). \tag{4.11}$$

Instead, in case of a scenario with sensor density $D$ = 50 sensors/km$^2$, the estimated received power as a function of the distance obtained from linear regression is given by:

$$P(dBm) = 49.04 - 35.93 \lg d(m). \tag{4.12}$$

Notice that the error in the propagation factor $\alpha$ is only 1.3% for $D$ = 100 sensors/km$^2$, and 2% for $D$ = 50 sensors/km$^2$, while the error in power $P_0$ is around 11.2% for $D$ = 100 sensors/km$^2$, respectively 9% for $D$ = 50 sensors/km$^2$, similar to the previous scenario with omnidirectional antennas. The higher accuracy of the directive antenna case compared with the omnidirectional situation could be justified by the lower terrain heterogeneity associated to the area covered by a narrower antenna beam.

Figure 4.7 presents the mean error and standard deviation error in antenna's direction estimation, for different values of sensor density $D$. Results were averaged for the three transmitters over 10 realizations of sensors distribution. It should be noted that the average error in the estimation of the

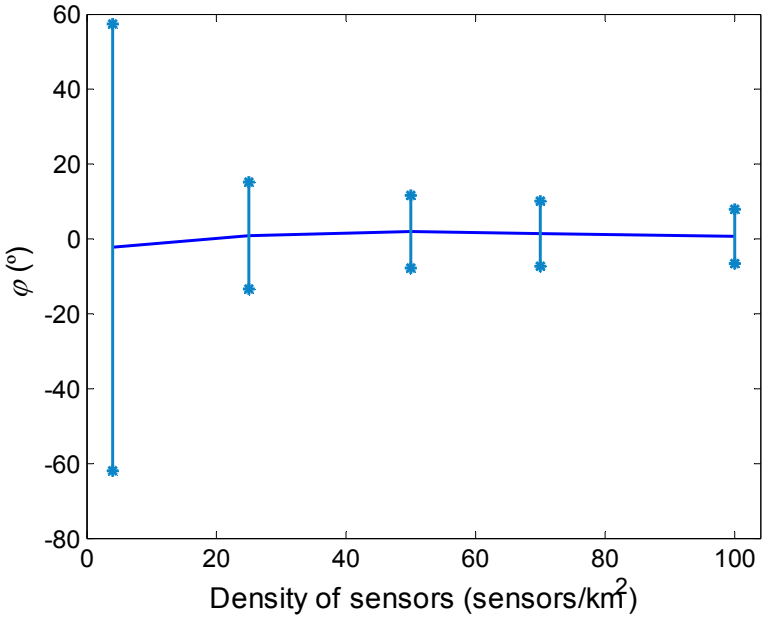


Figure 4.7: Mean error and standard deviation error in antenna's direction estimation for different sensor densities, on scenario C.

antenna direction is very close to zero and the standard deviation of the error decreases when increasing the sensor density.

The estimated radiation pattern of the primary transmitter antenna is presented in Figure 4.8 for the case $D$ = 50 sensors/km$^2$. It can be observed how the estimated radiation pattern follows quite adequately the original radiation pattern, particularly in the main lobe, and differences with respect to the real pattern mainly appear in the back side of the antenna. For the case $D$ = 50 sensors/km$^2$, the beam width at –3 dB is detected to be 75.04º, a value 10.3º higher than the beam width of the considered antenna.

## 4.5. Conclusions

This Chapter has introduced a methodology that continues the estimation of primary networks started in Chapter 3 by providing an acceptable accuracy in context features such as antenna pattern, antennas orientation, and propagation

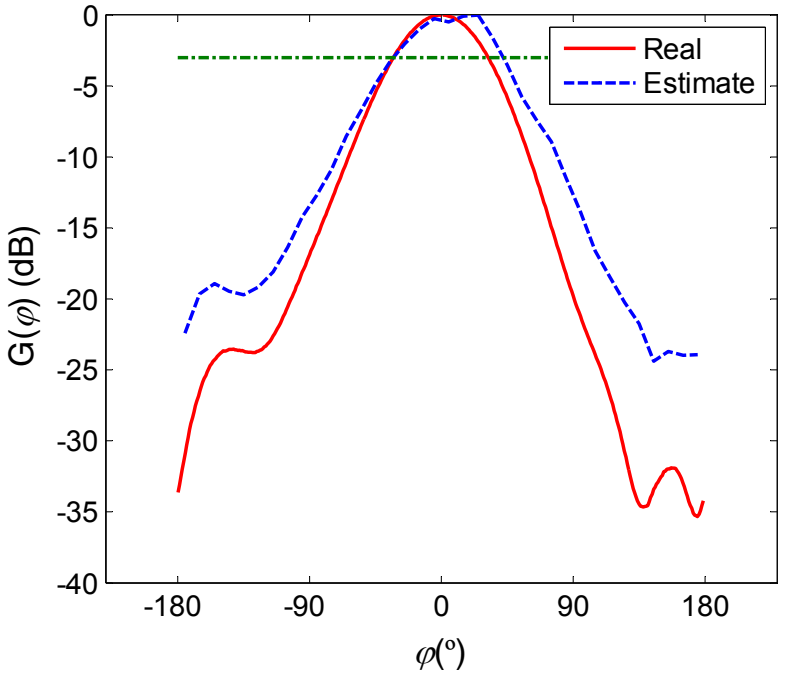


Figure 4.8: Horizontal radiation pattern of the primary transmitter's antenna for the case $D$ = 50 sensors/km$^2$, on scenario C.

model, particularly in the case of directive antennas. Methodology has been tested in different scenarios with both omnidirectional and directive antennas under data obtained from a planning tool. The results have reveled that an acceptable accuracy can be obtained, with errors in order of 12 % for propagation model estimation.

# 5.

# Analysis of interpolation techniques

This Chapter expands the prior work that used nearest neighbor interpolation in the multi-level method by considering three other interpolation techniques, namely linear, natural neighbor, and kriging interpolation. These three methods, in spite of not retaining the great simplicity of the nearest neighbor interpolation, are still non-involved methodologies that can offer a better characterization of the RF environment. The rest of this Chapter is structured as follows. Section 5.1 presents a summary of interpolation in cognitive context. Then Section 5.2, Section 5.3, Section 5.4, and Section 5.5 describe in details the four interpolation techniques: nearest neighbor, linear, natural neighbor, and kriging interpolation. The simulation environment is shown in Section 5.6 while the results are presented in Section 5.7. A summary of the main conclusions of this Chapter is finally given in Section 5.8.

## 5.1. Interpolation in cognitive context

Interpolation is the process of approximating the values of a given function by using the known values at a discrete set of points. In this way, from the measurements of the sensors at a given frequency an image will be created by interpolating the intermediate pixels for those positions where no sensor was available. This is the first step intended to determine the RSS associated to those pixels without any sensor based on the pixels available.

The concept of sensor network aided cognitive radio with cooperative sensing has been envisaged to characterize the whole area where a primary transmitter is detected [76]. By combining (with appropriate fusion rules) the signals measured by a number of sensors deployed it is possible to estimate the received power in any position. As shown in Figure 5.1, the power measurements (on a given frequency) taken by a number of neighboring sensors at different positions can be used to estimate the power at a given position (x, y).

From a general perspective, the interpolation can be done as:

$$P(x,y) = f\left(P_1(x_1,y_1), P_2(x_2,y_2), ..., P_N(x_N,y_N)\right), \tag{5.1}$$

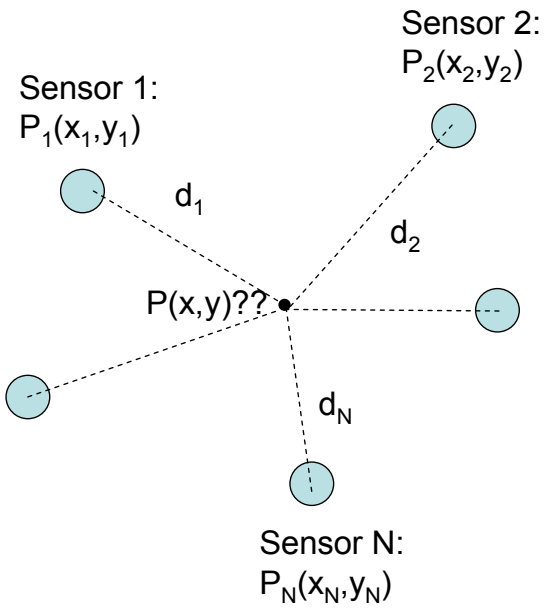


Figure 5.1: Interpolation of the sensors power measurements at different position.

where $p = 1,..., N$ would be the closest sensors to position (x, y).

From the information received from the secondary sensors an image is built by interpolating the intermediate pixels for those positions where no sensor was available.

The need for interpolation from irregularly spaced data occurs in many different fields, such as earth science and geographic [77] medical imaging, meteorological or geological modeling, cartography, and computer aided geometric design. In [78], the author presents a survey of scattered data interpolation methods in image processing. The linear interpolation of intensity was first introduced in [79] and is known as Gouraud Shading. The use of various linear and non-linear interpolation schemes has been constantly suggested to improve the speed and visual quality of the results, as these are two thrust areas in the improvement of rendering algorithms [80].

Natural neighbor interpolation was suggested by Sibson in [81] and [82] for data approximation and smoothing. It has been shown that natural neighbor interpolation avoids most of the problems of conventional methods and therefore performs well for irregularly distributed data [76].

First introduce by a South-African mining engineer Krige [83], kriging interpolation is a spatial interpolation method used to estimate the value of a property at un-sampled location by referring to neighboring locations. In case data is sparse, kriging is the best interpolation technique available for applications in geosciences [84].

Kriging is not a new concept in cognitive context. In [85], authors introduce the concept of Interference Cartography (IC) that correspond to a geo-localized combination and exploitation of radio measurements. IC is defined as a map of the measured quantity (e.g., the total RSS values on a specific frequency band) on the whole area of interest and kriging interpolation is used to build it. In [86], a possible implementation of IC in a hierarchical access context is given.

Among the existing interpolation methods, the ones considered in this thesis are nearest neighbor, linear, natural neighbor, and kriging interpolation, explained in the following.

## 5.2. Nearest neighbor interpolation

It is the simplest method of multivariate interpolation. The nearest neighbor algorithm selects for each position the value of the nearest sampling point. The value of the $P^I_{R,k}(x_p, y_p)$ in all positions without sensor can be interpolated simply as:

$$P^I_{R,k}(x_p, y_p) = \min_{d_k} P_{R,k}(x_k, y_k), \tag{5.2}$$

that is, the value of $P^I_{R,k}(x_p, y_p)$ is simply obtained as the value measured by the closest sensor (i.e., the one with minimum distance $d_k$). This algorithm is very simple to implement.

## 5.3. Linear interpolation

It involves estimating a new value by connecting two adjacent known values with a straight line. If the two known values are $P_{R,k}(x_1, y_1)$ and $P_{R,k}(x_2, y_2)$, then the interpolated value at position $(x_p, y_p)$ is:

$$P^I_{R,k}(x_p, y_p) = P_{R,k}(x_1, y_1) + u\left(P_{R,k}(x_2, y_2) - P_{R,k}(x_1, y_1)\right), \tag{5.3}$$

where $u$ is a number between 0 and 1 representing the fraction of the distance between $(x_1, y_1)$ and $(x_2, y_2)$ at which $(x_p, y_p)$ lies, defined as:

$$u = \frac{d_{p,1}}{d_{2,1}}. \tag{5.4}$$

This method works best when the function is not changing quickly between known values.

## 5.4. Natural neighbor interpolation

Natural neighbor interpolation is a weighted average method that constructs the interpolant by using natural neighbor coordinates based on Voronoi tessellation of a set of positions. This has the advantage over simpler methods in

that it provides a smoother approximation to the underlying "true" function. Interpolation is given by the following expression:

$$P_{R,k}^{I}\left(x_p, y_p\right) = \sum_{j=1}^{J} h_j\left(x_p, y_p\right) P_{R,k}\left(x_j, y_j\right), \tag{5.5}$$

where $(x_p, y_p)$ is the query pixel to be interpolated, and $P_{R,k}^{I}\left(x_p, y_p\right)$ is the corresponding interpolated function value at this query pixel, [81] [82]. The points $(x_j, y_j)$ $j = 1, ..., J$ are the $J$ natural neighbors of the query pixel $(x_p, y_p)$ in the Voronoi diagram of the original data sites, with known function values $P_{R,k}(x_j, y_j)$. The values $h_j(x_p, y_p)$ are the coefficients referred to as natural neighbor coordinates for each natural neighbor. Figure 5.2 shows an example, where query pixel $(x_p, y_p)$ has $J = 5$ natural neighbors $(x_1, y_1), \ldots, (x_5, y_5)$.

For a given query pixel $(x_p, y_p)$ to be interpolated, the process builds first the Voronoi polygons of its $J$ natural neighbours. The Voronoi polygon of the $j$-th neighbour $(x_j, y_j)$, denoted as $V_j$, consists of all pixels which are closer to $(x_j, y_j)$ than to any other neighbour. Then, the Voronoi polygon of the query pixel $(x_p, y_p)$, denoted as $V_{P(x_p,y_p)}$, is also built with the pixels that are closer to $(x_p, y_p)$ than to any of its neighbours (in the example of Figure 5.2 $V_{P(x_p,y_p)}$ is represented in dotted lines and grey color while the Voronoi polygon of neighbour 1, $V_1$, is represented in solid line and sky blue). Based on these 2 polygons, the coefficient for the $j$-th neighbour is computed as the ratio between the area of the intersection between $V_{P(x_p,y_p)}$ and $V_j$ (for the case of $V_1$ this intersection is represented in Figure 5.2 as the highlighted blue area labeled $h_1$) and the area of $V_{P(x_p,y_p)}$, that is:

$$h_j\left(x_p, y_p\right) = \frac{Area\left(V_{P\left(x_p, y_p\right)} \cap V_j\right)}{Area\left(V_{P\left(x_p, y_p\right)}\right)}. \tag{5.6}$$

## 5.5. Kriging interpolation

Kriging is a statistical process that estimates a value at a point using the spatially dependent values in a neighborhood zone near the point. The kriging process is based upon the concept of using regionalized variables to model spatially dependent data. Kriging makes the common assumption that there is a

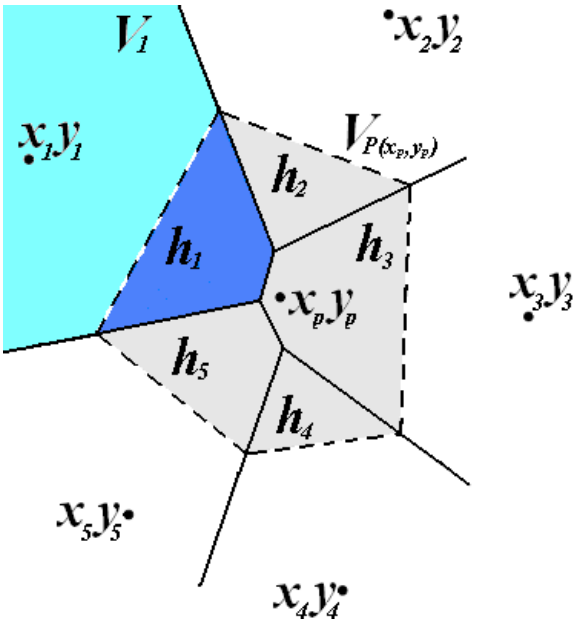


Figure 5.2: Illustration of the computation of natural neighbor coordinates.

spatial, linear relationship between the unknown value at a point and the known values of neighboring points. Kriging computes the value for the unknown data point using a weighted linear sum of known data values.

As explained in [87], the aim of kriging is to estimate the unknown value of a function $P^I_{R,k}\left(x_p, y_p\right)$ at the location $(x_p, y_p)$ based on the available values of this function in the neighboring locations $\{P_{R,k}(x_j, y_j)\}_{j=1}^{J}$. This is expressed through a weighted linear combination:

$$P^I_{R,k}\left(x_p, y_p\right) = \sum_{j=1}^{J} w_j P_{R,k}\left(x_j, y_j\right), \tag{5.7}$$

$w_j$ corresponds to the kriging weights and depends on the spatial correlation between the considered data samples. To calculate the kriging weights a new function is necessary, called semi variogram, defined as:

$$\gamma\left(d_k\right) = \frac{1}{2} Var\left[P_{R,k}\left(x_1, y_1\right) - P_{R,k}\left(x_2, y_2\right)\right], \tag{5.8}$$

where $d_k$ is the distance between $(x_2, y_2)$ and $(x_1, y_1)$. The kriging interpolation includes the number of available neighboring observations $J$ in the calculation of the missing values at the unobserved locations. Due to practical considerations, an

ordinary kriging version developed by Sidler [87] is considered in this work. In [87], kriging interpolation is proposed with Von Karman covariance model [88], which is:

$$C(d_k) = \frac{\chi^2}{2^{\upsilon-1}\Gamma(\upsilon)}\left(\frac{d_k}{a}\right)^{\upsilon} K_{\upsilon}\left(\frac{d_k}{a}\right), \tag{5.9}$$

where $d_k$ is the distance separating two locations, $\chi^2$ is the variance, $a$ is the correlation length, $\Gamma$ is the gamma function, and $K_\upsilon$ is a modified Bessel function of the second kind of order $0 \le \upsilon \le 1$. The relation between semi variogram and covariance, for a first and second order stationary function, is given by [89]:

$$\gamma(d_k) = C(0) - C(d_k). \tag{5.10}$$

## 5.6. Simulation environment

To test the interpolated data accuracy, a framework was built to perform the proposed methodology, namely scenario D. This scenario has a total size of 3780 m x 3780 m with pixel size Δx = Δy = 20 m. There is one transmitter located in the center with EIRP 55 dBm. Propagation losses as a function of distance $d$ (m) are given by:

$$L = 30.5 + 35.22 \lg d \tag{5.11}$$

Based on the propagation model, the considered transmitted power, and according to (4.6) the received power at 1 m is $P_0$ = 24.5 dBm and the path loss exponent $\alpha$ = 3.522. Sensors are randomly scattered in the whole scenario, with a sensor density varied in the different simulations. The antenna direction is 0º. The same non-parameterized radiation pattern antenna used in scenario C, shown in Figure 3.11, is considered.

## 5.7. Simulation results

At start, the influence of the quantification parameters is analyzed by investigating the impact of threshold power $P_{th}$ and quantification step Δ on scenario D. Then, three different situations are analyzed in the following,

considering first the case where no shadowing exists, and then the cases with non-correlated and spatially correlated shadowing. For kriging interpolation method, parameter $J$ (available neighboring observation) is set at 12, variance, $\chi^2$, is 1, correlation length, $a$, is 100, and the order of modified Bessel function, $\upsilon$, is 0.98, based on [87].

## 5.7.1. Impact of quantification parameters

As was mentioned in Section 3.1, it is assumed that a sensor detects a given frequency $f_i$ if the received power is above $P_{th}(f_i)$. In this subection, the influence of $P_{th}$ on the multi-level method is analyzed first, while the value of quantification step Δ is determined afterwards.

### 5.7.1.1. Minimum received threshold $P_{th}$

Because the threshold value highly impacts the results in measuring the presence or absence of PUs, the decision threshold is a critical parameter in data post-processing. A high value of threshold power may conduct to underestimation of the actual spectrum occupancy. Nevertheless, a low threshold may conduct in overestimation caused by noise samples above the threshold. A set of empirical data was post-processed, in order to establish the value of threshold power.

To perform this analysis it is assumed that position and antenna direction are known a priori. A shadowing with 6 dB standard deviation is taken into account. No quantification is considered and all the pixels are assumed to be known. The impact of $P_{th}$ on the non-parameterized radiation pattern antenna is shown in Figure 5.3 where the estimated values of path loss coefficient $\alpha$, power $P_0$, and beam width are named "Estimate," while the expected values of this parameters are named "Real" in figure.

It is clear from the figure that a high value of $P_{th}$ leads to higher errors. Generally the optimal threshold setting is as low as possible to have optimal sensitivity, but well above noise level to prevent overestimation of spectrum occupancy [90]. In the following, the threshold power $P_{th}$ is chosen to be –120 dBm.

### 5.7.1.2. Quantification step Δ

In this subsection, the influence of the quantification step Δ on the

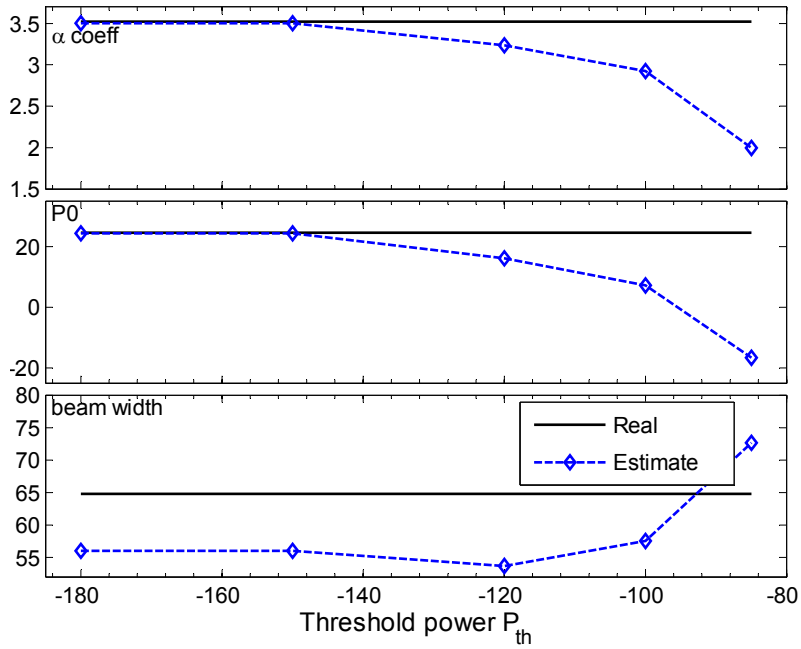


Figure 5.3: The impact of $P_{th}$ on the antenna.

proposed multi-level method is analyzed, using nearest neighbor and natural neighbor interpolation. In order to determine the value of quantification step Δ, various cases are analyzed. In scenario D with 6 dB shadowing standard deviation, the non-parameterized radiation pattern antenna is used as a transmitter, under the condition of unknown position and direction of the transmitter, power threshold $P_{th}$ being set to –120 dBm. From (3.6), $P_{max}$ is defined as:

$$P_{\max} = P_{th} + \left(2^n - 1\right)\Delta \tag{5.12}$$

It is consider that the number of bits $n$ used to encode the RSS measurements is fixed to 6 and the quantification step Δ is varied between 1 dB and 1.5 dB, meaning that $P_{max}$ varies between –56 dBm and –24 dBm. The results are averaged over 150 realizations of sensor distributions for each sensor density. Figure 5.4 plots the comparison of the cases when Δ = 1 dB and Δ = 1.5 dB, where it may be noticed that lower errors are given by Δ = 1.5 dB, respectively $P_{max}$ = –24 dBm for both of the interpolation methods.

In the following it is consider that $P_{max}$ is fixed to –24 dBm, $n$ varies between [4, 5, 6, 7], meaning that the quantification step Δ takes the values [6.0,

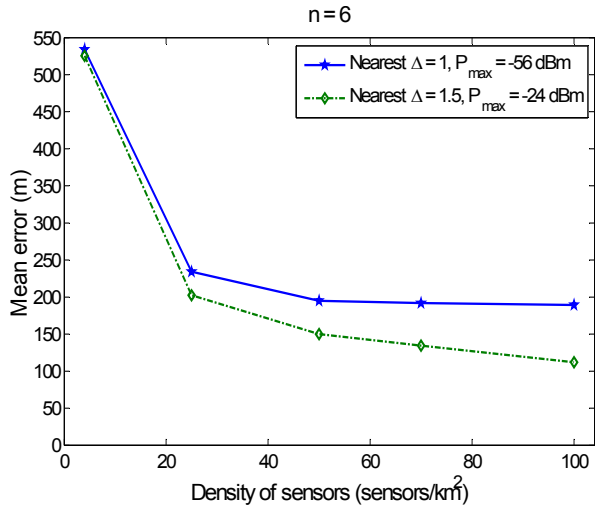


(a)

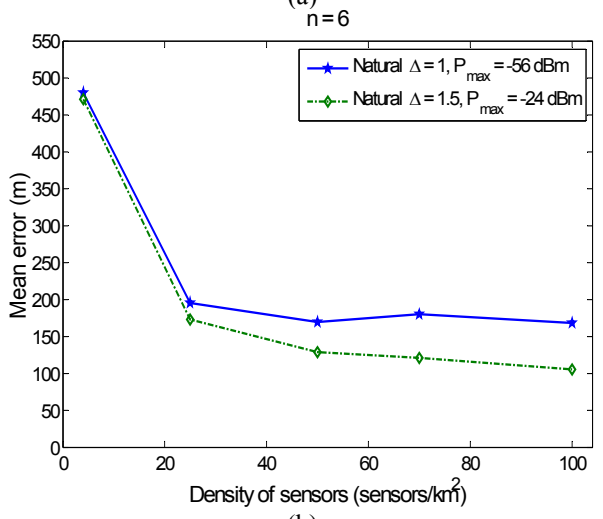


(b)

Figure 5.4: The impact of quantification step Δ and power $P_{max}$ in transmitter position estimation, for different sensor densities.

3.0, 1.5, 0.75] dB. Figure 5.5 plots the mean error in the transmitter position estimation as a function of the sensor density for different values of n. The results presented in Figure 5.5 show that the largest errors in transmitter position estimation are given by the case with $n = 4$ bits while the cases of $n = 5$, $n = 6$, and $n = 7$ bits present very similar results, so the proposed methodology is not very sensitive to the number of bits as long it is above a minimum. This facilitates the minimization of the signaling requirements for transmitting the sensing results

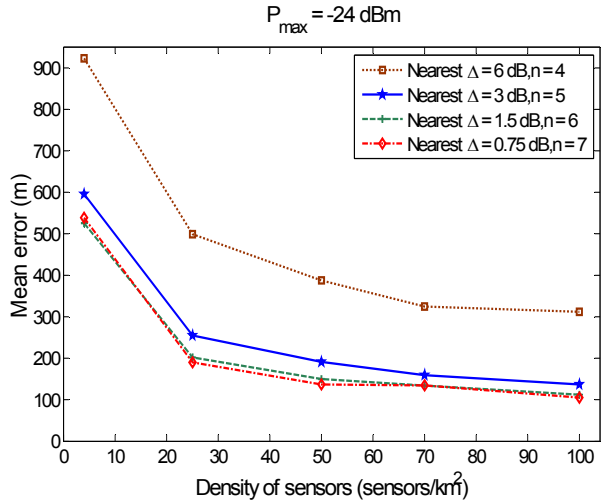


(a)

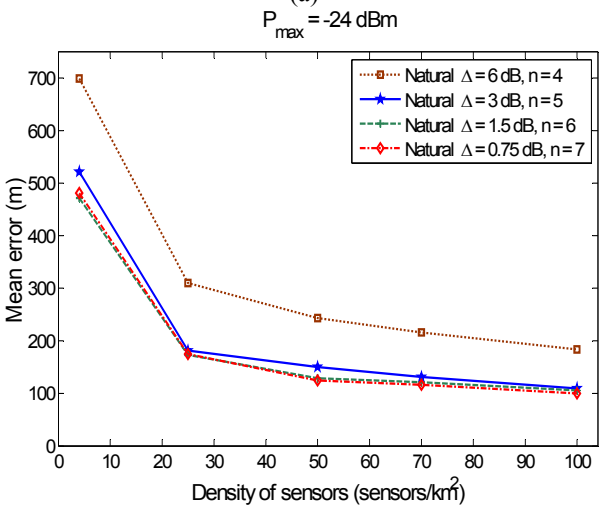


(b)

Figure 5.5: The impact of quantification step Δ and *n* in transmitter position estimation, for different sensor densities.

needed to execute the proposed methodology. In the following, the case of $n$ = 6 bits is analyzed, meaning that the quantification step Δ = 1.5 dB.

## 5.7.2. Impact of interpolation without shadowing

In this part, it is evaluated scenario D where received power threshold $P_{th}$ is –120 dBm, the quantification is made with $P_{max}$ = –24 dBm, $n$ = 6 bits, and the quantization step is Δ = 1.5 dB, no shadowing being added. Figure 5.6 presents the mean error and standard deviation error of the transmitter position estimation (a)

and antenna direction estimation (b), respectively, for different values of sensor density $D$, for all four methods of interpolation. Results were averaged over 150 realizations of the sensors distribution. For a low sensor density such as $D$ = 4 sensors/km$^2$ the mean error as well as the standard deviation error in both position estimation and antenna direction estimation are high for all four interpolation

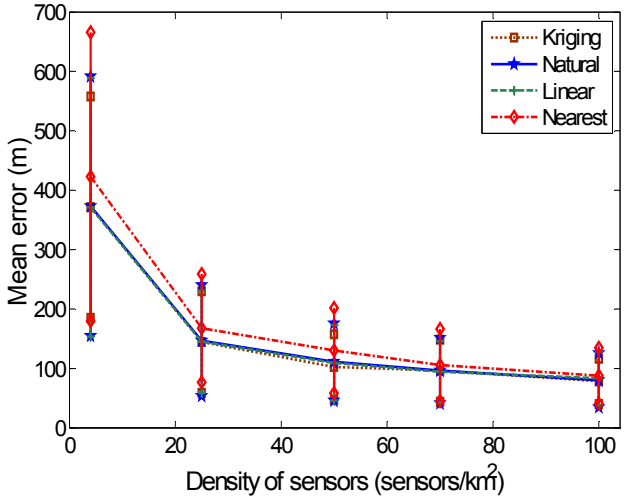


(a)

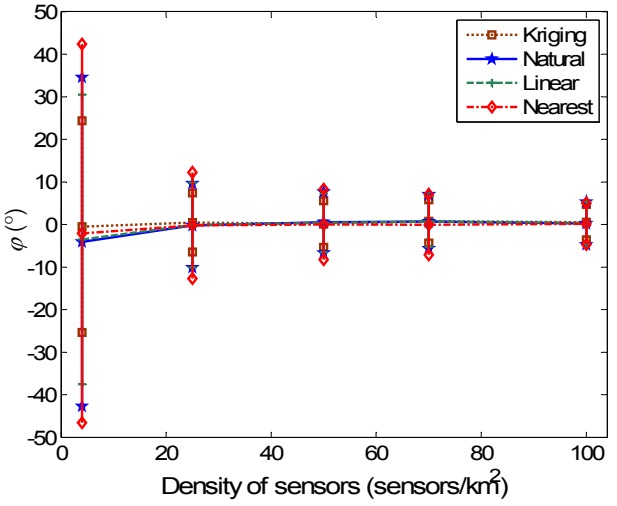


(b)

Figure 5.6: Mean error and standard deviation error in transmitter position estimation (a) and in antenna direction estimation (b) for different sensor densities, on scenario D without shadowing.

methods. As the density of sensors grows, errors are reduced. For example, with 50 sensors/km$^2$ the error is roughly 100 m that corresponds to 5 pixels. As a reference, this is approximately 5% of the transmitter coverage radius in the direction of the maximum antenna gain. Slightly higher errors are given by nearest neighbor interpolation method.

Concerning the estimation of the propagation model, Figure 5.7 plots the mean estimated value and standard deviation error of propagation factor $\alpha$ in

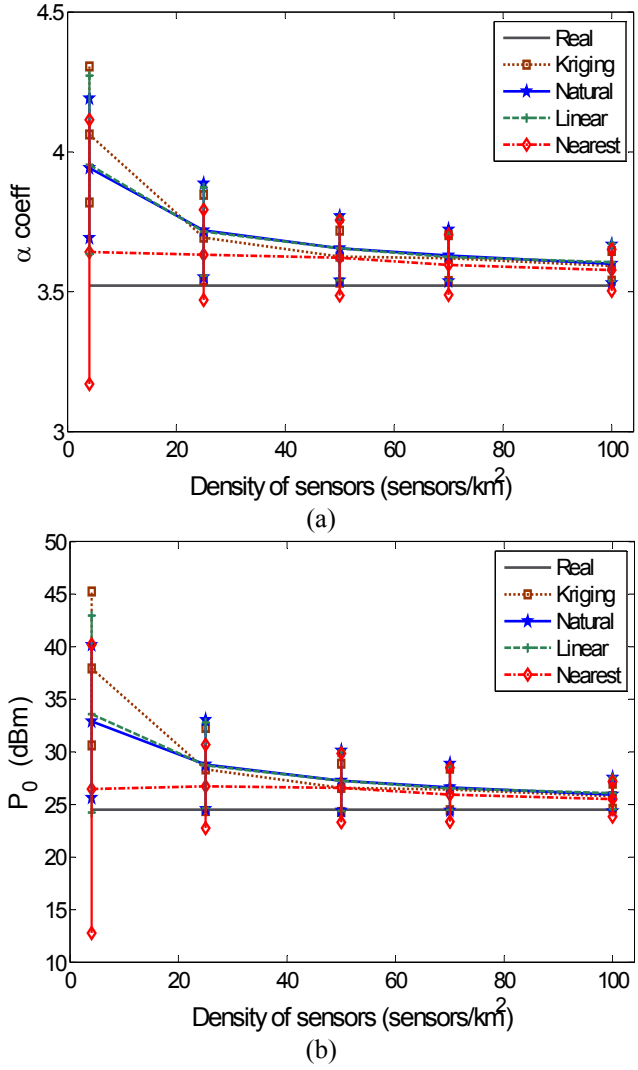


Figure 5.7: Estimated propagation factor $\alpha$ (a) and estimated $P_0$ (b) as a function of sensor density, on scenario D without shadowing.

Figure 5.7 (a), respectively power $P_0$ in Figure 5.7 (b), as functions of sensor density $D$. Also the theoretical values according to (3.1) are showed. Errors with respect to these theoretical values are reducing when increasing the sensor density. For both parameters, nearest neighbor interpolation gives a bit less errors while kriging interpolation gives a lower standard deviation than the other interpolation methods. It can be noted that neither in the estimation of the position nor of the propagation model parameters there exists a significant gain when the sensor density increases above 50 sensors/km$^2$, approximately.

The estimated radiation pattern of the primary transmitter antenna is presented in Figure 5.8 for the case $D$ = 50 sensors/km$^2$, for all four methods of interpolation, and their standard deviation error is presented in Table 5.1. Observe the similarity of the original radiation pattern and the estimated radiation patterns, especially in the main lobe. As it can be seen in Figure 5.8, the estimated radiation patterns are less accurate when looking at the back directions for all four interpolation methods. All four interpolation methods present a very similar behavior. The lowest standard deviation error is given by kriging interpolation as seen in Table 5.1.

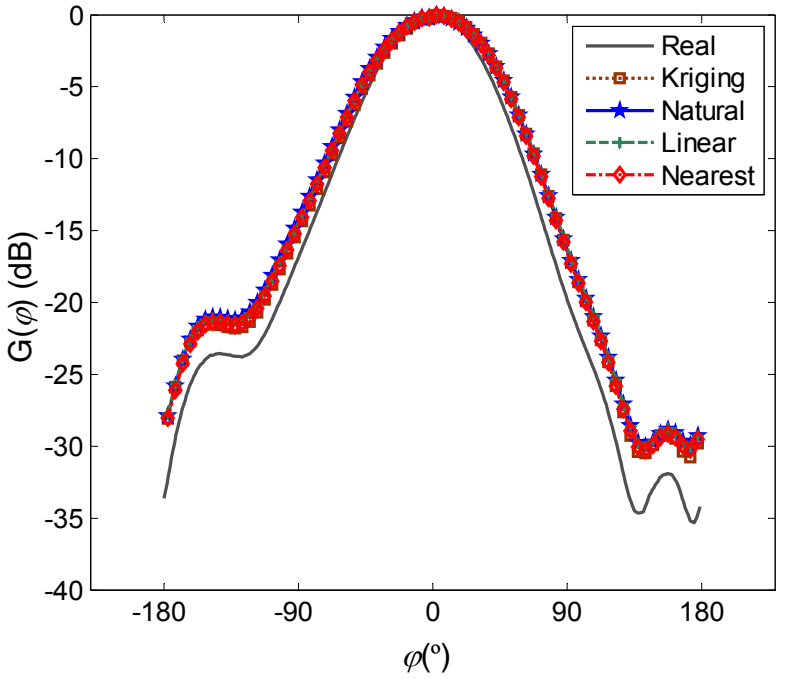


Figure 5.8: Horizontal radiation pattern of primary transmitter's antenna for the case $D$ = 50 sensors/km$^2$, on scenario D without shadowing.

Table 5.1: Standard deviation of the error in horizontal antenna radiation pattern for the case $D$ = 50 sensors/km$^2$, on scenario D without shadowing.

| | Kriging | Natural | Linear | Nearest |
|---|---|---|---|---|
| Standard deviation error (dB) | 1.3513 | 1.5534 | 1.4843 | 2.2453 |

### 5.7.3. Scenario with non-correlated shadowing

In this subsection, random shadowing losses are added to scenario D with a standard deviation $\sigma$ = 6 dB. Non-correlated shadowing is considered first, meaning that the shadowing losses are independent in all the pixels of the scenario. $P_{th}$ is –120 dBm, $P_{max}$ = –24 dBm, $n$ = 6 bits, and $\Delta$ = 1.5 dB. Figure 5.9 (a) presents the mean error and standard deviation error of position estimation, for different values of sensor density $D$, for all four methods of interpolation. Similarly, Figure 5.9 (b) presents the mean error and standard deviation error in antenna's direction estimation. Like in the previous sub-section, results were averaged over 150 realizations of sensors distribution. As expected, errors are reduced as the density of sensors increases. The performance is approximately the same with all four considered methods. When comparing with the case without shadowing in Figure 5.6 it can be observed how the introduction of shadowing causes an increase in average estimation errors and standard deviations errors.

Figure 5.10 shows the corresponding results for the mean estimation value and standard deviation error of the propagation factor $\alpha$ and power $P_0$ for different values of sensor density $D$. Errors are decreased as the density of sensors grows. In this case, it can be observed how nearest neighbor case offers the worst performance among the considered interpolation methods, while the differences between kriging, natural neighbor, and linear cases are small. Table 5.2 presents standard deviation error of the estimated antenna radiation pattern for the case $D$ = 50 sensors/km$^2$. In this situation, kriging exhibits the largest deviation in error, while natural neighbor provides a slightly better result than linear.

### 5.7.4. Scenario with correlated shadowing

In this part, correlated shadowing losses with 6 dB shadowing standard deviation are added to the original scenario. Shadowing is spatially correlated

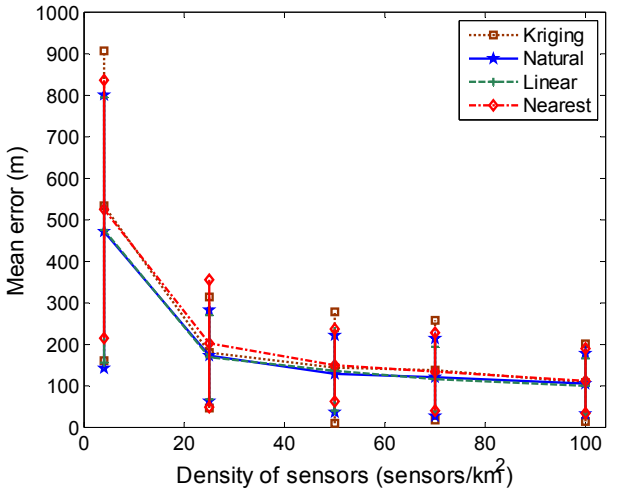


(a)

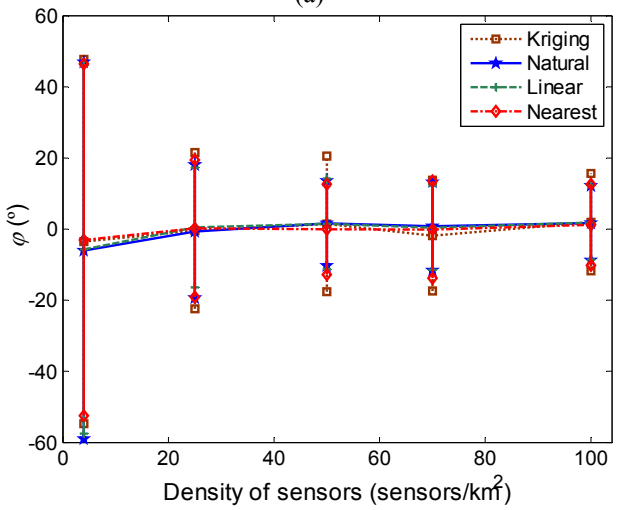


(b)

Figure 5.9: Mean error and standard deviation in transmitter position estimation (a) and in antenna direction estimation (b) for different sensor densities, on scenario D with non-correlated shadowing.

Table 5.2: Standard deviation of the error in horizontal antenna radiation pattern for the case $D$ = 50 sensors/km$^2$, on scenario D with non-correlated shadowing.

| | Kriging | Natural | Linear | Nearest |
|---|---|---|---|---|
| Standard Deviation (dB) | 4.2434 | 3.0019 | 3.1533 | 3.6904 |

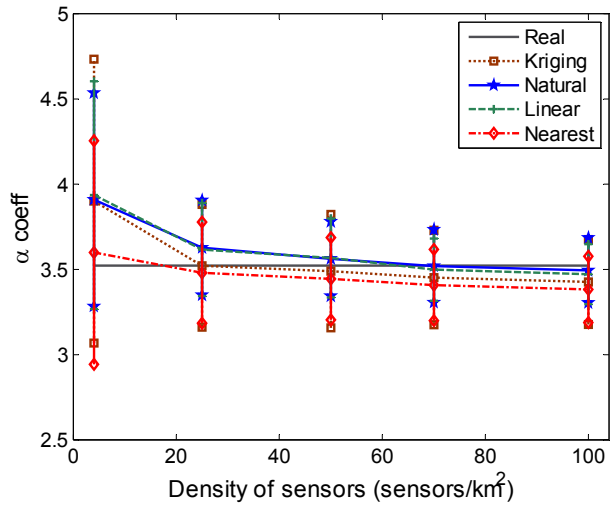


(a)

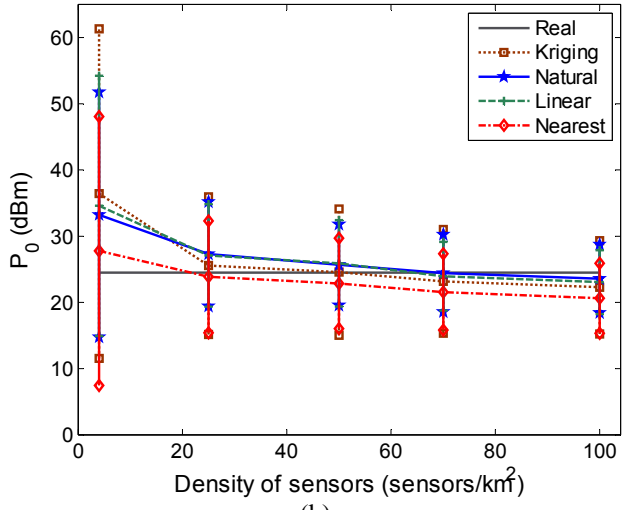


(b)

Figure 5.10: Estimated propagation factor $\alpha$ (a) and estimated $P_0$ (b) as a function of sensor density, on scenario D with non-correlated shadowing.

following an exponential autocorrelation function with decorrelation distance *dcorr* = 400 m. The generation of 2D spatially correlated shadowing is done using the methodology of [91] based on filtering a set of independent shadowing samples using a 2D filter defined from the Fourier transform of the exponential autocorrelation function. Results are obtained by averaging a total of 10 different shadowing realizations of the scenario, each of them consisting in turn in 150 realizations of the sensor distribution.

Table 5.3 shows the simulation results, for the case $D$ = 50 sensors/km$^2$, for all four methods of interpolation, and comparing them with the cases without shadowing and non-correlated shadowing. Results are presented in terms of average and standard deviation values of the error in position, antenna direction, and propagation model parameters. It can be observed how the case of correlated shadowing in general exhibits better estimation errors than the case of non-correlated shadowing for all parameters with the only exception of power $P_0$. In general, kriging interpolation presents better results than the rest of the

Table 5.3: Simulation results for case $D$ = 50 sensors/km$^2$, on scenario D without shadowing, with non-correlated shadowing, and with shadowing correlated.

| | Pos. error - Avg (m) | Pos. error – Std. dev (m) | Dir. error- Avg (º) | Dir. error – Std. dev (º) | α (avg) | α (Std. dev) | $P_0$ -Avg (dBm) | $P_0$ – Std. dev (dB) |
|---|---|---|---|---|---|---|---|---|
| | Kriging | | | | | | | |
| No sdw | 102.361 | 55.277 | 0.086 | 5.452 | 3.625 | 0.092 | 26.580 | 2.291 |
| Non corr. sdw | 144.159 | 134.521 | 1.452 | 19.053 | 3.489 | 0.332 | 24.592 | 9.545 |
| Corr sdw | 123.040 | 71.471 | -0.146 | 7.050 | 3.551 | 0.151 | 29.092 | 4.186 |
| | Natural neighbor | | | | | | | |
| No sdw | 110.794 | 65.075 | 0.490 | 7.168 | 3.655 | 0.114 | 27.258 | 2.859 |
| Non corr. sdw | 128.962 | 92.654 | 1.646 | 11.957 | 3.561 | 0.218 | 25.690 | 6.107 |
| Corr sdw | 129.016 | 81.432 | -0.537 | 8.392 | 3.605 | 0.171 | 30.206 | 4.655 |
| | Linear | | | | | | | |
| No sdw | 109.404 | 63.718 | 0.374 | 6.870 | 3.654 | 0.113 | 27.252 | 2.868 |
| Non corr.sdw | 136.329 | 95.608 | 1.505 | 12.700 | 3.566 | 0.231 | 25.921 | 6.520 |
| Corr sdw | 129.81 | 79.453 | -0.391 | 8.150 | 3.604 | 0.171 | 30.212 | 4.693 |
| | Nearest neighbor | | | | | | | |
| No sdw | 130.049 | 71.698 | 0.009 | 8.265 | 3.621 | 0.134 | 26.577 | 3.270 |
| Non corr.sdw | 149.891 | 87.390 | -0.092 | 12.717 | 3.444 | 0.241 | 22.867 | 6.836 |
| Corr sdw | 147.066 | 90.712 | 0.226 | 9.361 | 3.530 | 0.189 | 28.484 | 5.127 |

interpolation methods. Differences are particularly significant from the perspective of standard deviation, which is larger with the nearest neighbor interpolation.

## 5.8. Conclusions

This Chapter has presented a comparative study of kriging, natural neighbor, linear, and nearest neighbor interpolation techniques used to combine a set of RSS measurements obtained by a sensor network having the target of estimation and characterization of different context features such as transmitter position, antenna orientation estimation, antenna pattern estimation, and propagation model characterization. The results had been analyzed in different situations depending on the type of shadowing losses in the environment, either correlated or non-correlated.

It had been inferred that, in absence of shadowing, the proposed methodology is able to extract the transmitter position, the antenna orientation, the antenna pattern, and propagation model features adequately regardless the considered interpolation technique. On the other hand, when shadowing is present, either spatially correlated or non-correlated, the errors increase. In this case, kriging interpolation provides slightly better results while nearest neighbor interpolation provides similar performance from an average perspective but exhibits a larger dispersion than kriging, natural neighbor, and linear interpolation depending on how sensors are located in the different realizations.

# 6.

# ML aided context features extraction for Cognitive Radio

Few published works have tried to characterize the context where a secondary network operates. In this respect, [69] is so far one of the most relevant references in terms of a wide context acquisition. As it was mentioned in Chapter 2, it proposes a context characterization algorithm based on ML estimation which identifies the presence, positions, and antenna patterns of PUs in a scenario populated by CR nodes acting as sensors and cooperating in a noisy environment.

This Chapter proposes a new methodology, so called Maximum Likelihood Aided Context Feature Extraction (MLACFE), that combines the multi-level methodology, previous introduced in Chapter 3, Chapter 4, and Chapter 5 together with the ML approach. This enables to keep the benefits of the optimality of ML performance but yet reducing dramatically the computational complexity. As a significant difference from the work in [69], no prior knowledge about the antenna pattern is required under the MLACFE approach. Similarly, this methodology does not require knowing in advance the propagation model

parameters. The MLACFE methodology is compared against the optimal ML procedure of [69] in terms of both obtained accuracy and computation time.

In this context, Section 6.1 describes in detail the proposed hybrid algorithm, MLACFE, which is a combination of multi-level methodology and ML estimation algorithm. Afterwards, Section 6.2 presents the simulation environment and Section 6.3 presents, analyzes and discusses the obtained experimental results. Finally, Section 6.4 summarizes the main conclusions derived from the study presented in this chapter.

# 6.1. MLACFE method description

The main steps of the proposed MLACFE methodology are presented in Figure 6.1 and consist in interpolation, object identification, intermediate extraction of context features, and final extraction of context features with local ML estimation. The first three steps are identical as the ones from multi-level methodology, described in subsection 3.2.2 of Chapter 3, in Chapter 4, and in Chapter 5, and will provide transmitter position estimation $(x_{k,in}, y_{k,in})$, antenna orientation estimation $(\varphi_{k,in})$, antenna radiation pattern estimation $(G_{k,in}(\varphi - \varphi_{k,in}))$, propagation model estimation $(\alpha_{k,in}, P_{0,k,in})$, and shadowing standard deviation estimation $\sigma_k$. In the following, a detailed description of the operations performed in the last step of the proposed methodology is presented.

## 6.1.1. Final extraction of context features with local ML estimation

In this final stage of the MLACFE methodology the intermediate estimations of the different context features in the previous steps are used in a ML estimation process to obtain the final values of the estimated features.

Focusing on the $k$-th transmitter, let define $p_k = (P_{R,k}(x_1, y_1), P_{R,k}(x_2, y_2), \ldots, P_{R,k}(x_S, y_S))^T$ as the sensor power vector, whose components correspond to the quantified power (in dBm) measured in each one of the deployed sensors. The $s$-th component $P_{R,k}(x_s, y_s)$ of vector $p_k$ is assumed to be Gaussian of mean:

$$m_{s,k} = P_{0,k} + G_k\left(\varphi_{s,k} - \varphi_k\right) - 10\alpha_k \log_{10} d_{s,k}, \tag{6.1}$$

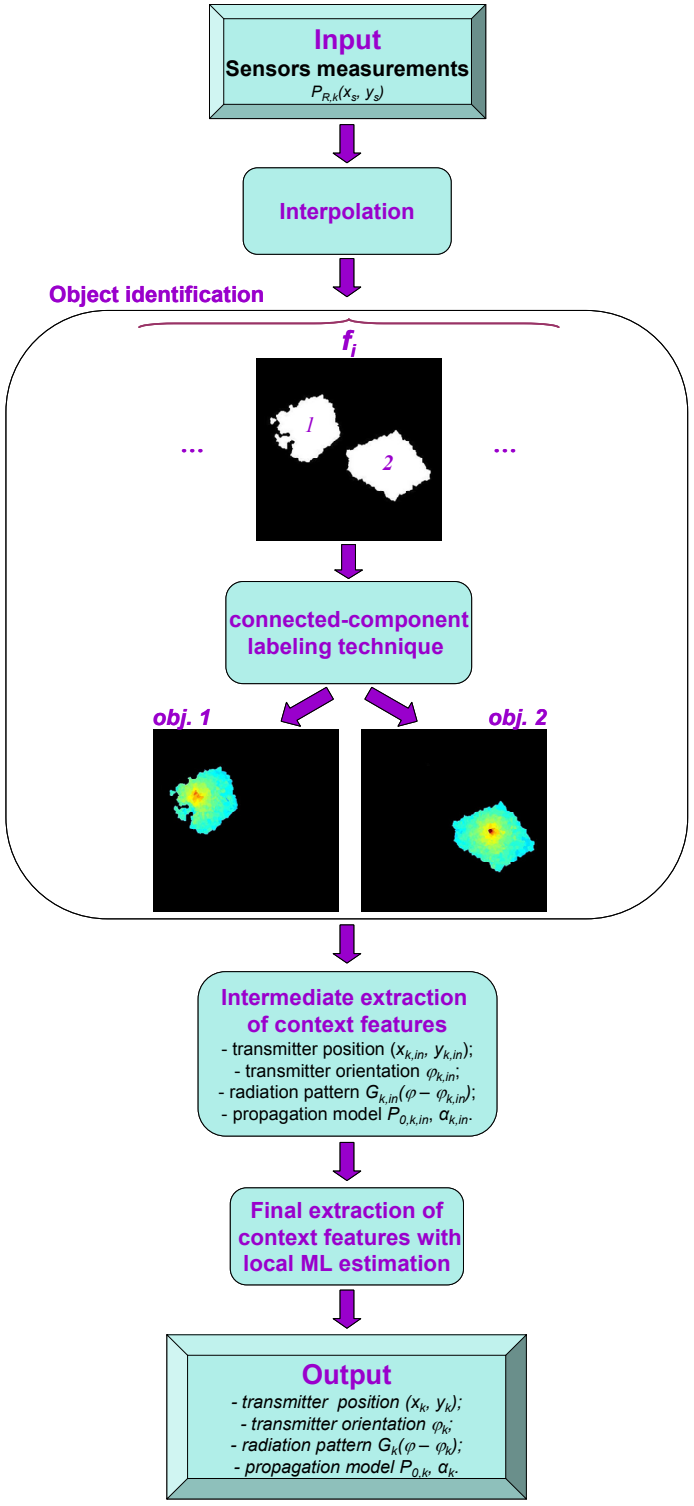


Figure 6.1: Overall steps of the MLACFE methodology.

The covariance matrix of the additive Gaussian random variable accounting for the shadowing fading in the different components of vector $p_k$ is:

$$C_k = \sigma_k^2 I\,, \tag{6.2}$$

being $\sigma_k$ the standard deviation of the uncorrelated shadowing fading, which has also been obtained in the previous step (see Section 4.3), and $I$ the Identity matrix.

The vector $p_k$ is affected by the unknown context features to be estimated, namely $P_{0,k}$, $\alpha_k$, $\sigma_k$, transmitter location $(x_k, y_k)$, antenna pattern radiation $G_k(\varphi - \varphi_k)$ and orientation of the antenna main beam $\varphi_k$.

Let define as $z_k$ the vector with all the above unknowns except the antenna radiation pattern $G_k(\varphi - \varphi_k)$ which is assumed to be obtained from the estimation carried out in previous step, i.e., $G_k(\varphi - \varphi_k) = G_{k,in}(\varphi - \varphi_k)$. Then, $z_k = [P_{0,k}, \alpha_k, x_k, y_k, \varphi_k]^{\mathrm{T}}$. By adopting the ML estimation strategy, the estimation $Z_{ML,k}$ of vector $z_k$ is given by:

$$Z_{ML,k} = \arg\max_{z_k} \ln f\left(p_k \mid z_k\right), \tag{6.3}$$

where $f(p_k|z_k)$ is the joint probability density function of $p_k$ conditioned to each one of the possible combinations of values of the context parameters in $z_k$ and $\ln f(p_k|z_k)$ is the so called log-likelihood function that can be formulated as:

$$L_k = \ln f\left(p_k \mid z_k\right) = \frac{1}{2}\left(p_k - m_k\right)^T C_k^{-1}\left(p_k - m_k\right), \tag{6.4}$$

where $m_k = (m_{1,k}, m_{2,k}, \ldots, m_{S,k})$.

Typically, this expression is solved by setting the gradient of the log-likelihood function to zero and solving the resulting set of equations. This formulation is feasible for all the above context parameters in case the antenna pattern is a priori known or parameterized to a specific pattern.

In that respect, this Chapter proposes to use the previous estimation of the antenna pattern that has been performed in multi-level methodology (detailed in Section 4.2) as an input to the ML estimation. Then, the proposed methodology does not require any a priori knowledge about the antenna pattern.

Unfortunately, the equations resulting from considering all 5 unknown parameters $z_k = [x_k, y_k, \varphi_k, P_{0,k}, \alpha_k]$ are highly nonlinear. Therefore, an approach, as considered in [69], is to solve the equations to obtain $[P_{0,k}, \alpha_k]$ for a given combination $[x_k, y_k, \varphi_k]$ and then to perform an exhaustive search in a 3D grid for all possible values of $[x_k, y_k, \varphi_k]$. In particular, if the position and direction of the transmitter were given by combination $[x_k, y_k, \varphi_k]$, $P_{0,k}$ and $\alpha_k$ can simultaneously be solved by simple linear algebra by setting the log-likelihood gradient with respect to the unknown parameters to zero, that is:

$$\frac{\delta L_k}{\delta z_k} = 0, \tag{6.5}$$

Then, the following equations are obtained:

$$P_{0,k} = \frac{\left\langle \overline{d_{s,k}}^2 \right\rangle \left\langle P_{R,k}(x_s, y_s) \right\rangle - \left\langle \overline{d_{s,k}} \right\rangle \left\langle \overline{d_{s,k}} P_{R,k}(x_s, y_s) \right\rangle - \left\langle \overline{d_{s,k}}^2 \right\rangle \left\langle G_k(\varphi_{s,k} - \varphi_k) \right\rangle + \left\langle \overline{d_{s,k}} \right\rangle \left\langle \overline{d_{s,k}} G_k(\varphi_{s,k} - \varphi_k) \right\rangle}{\left\langle \overline{d_{s,k}}^2 \right\rangle - \left\langle \overline{d_{s,k}} \right\rangle^2}, \tag{6.6}$$

$$\alpha_k = \frac{\left\langle \overline{d_{s,k}} \right\rangle \left\langle P_{R,k}(x_s, y_s) \right\rangle - \left\langle \overline{d_{s,k}} P_{R,k}(x_s, y_s) \right\rangle - \left\langle \overline{d_{s,k}} \right\rangle \left\langle G_k(\varphi_{s,k} - \varphi_k) \right\rangle + \left\langle \overline{d_{s,k}} G_k(\varphi_{s,k} - \varphi_k) \right\rangle}{\left\langle \overline{d_{s,k}}^2 \right\rangle - \left\langle \overline{d_{s,k}} \right\rangle^2}, \tag{6.7}$$

where $\langle \cdot \rangle$ represents a sample average, and

$$\overline{d_{s,k}} = 10 \log_{10} d_{s,k}, \tag{6.8}$$

Next, the whole 3D grid search for all possible values of $[x_k, y_k, \varphi_k]$ would ultimately be necessary to determine the combination of parameters for which $L_k$ is maximized. Yet, in practice, this approach is computationally too cumbersome as stated in [69].

To overcome this limitation, this thesis proposes an approach that takes advantage of the previous intermediate estimation that has been performed in the previous Chapters. In particular, just a local ML search is performed over the pixels falling in intervals $\Delta x_e$, $\Delta y_e$ and $\Delta \varphi_e$ around the intermediate estimations $(x_{k,in}, y_{k,in}, \varphi_{k,in})$ obtained with the procedure introduced in subsection 3.2.2.1 and Section 4.1, to refine their estimates. In this context, the ML estimation is applied over a much smaller search space, instead of the whole 3D space. The detailed pseudocode of the proposed procedure is presented in Figure 6.2.

While one of the focuses of this thesis is on unknown generic radiation patterns, for comparison purposes this Chapter will also consider the Gaussian shaped radiation pattern. Radiation pattern has the following parametric expression:

$$G_k(\varphi-\varphi_k)=10\log_{10}\left[\exp\left(-\frac{4(\varphi-\varphi_k)^2}{BW_k^2}\ln 2\right)\right], \quad -\pi<\varphi-\varphi_k\le\pi \tag{6.9}$$

Thereby, the antenna radiation pattern estimation is reduced to the estimation of the two parameters, namely the orientation angle $\varphi_k$ and 3 dB beam width $BW_k$.

In this particular case, the local ML estimation algorithm is presented in Figure 6.3.

```
Input (x_{k,in}, y_{k,in}, φ_{k,in})
1. for x_k ∈ (x_{k,in} - Δx_e, x_{k,in} + Δx_e) in steps of Δx do
2.           for y_k ∈ (y_{k,in} - Δy_e, y_{k,in} + Δy_e) in steps of Δy do
3.                         for φ_k ∈ (φ_{k,in} - Δφ_e, φ_{k,in} + Δφ_e) in
steps of Δφ do
4.                                   calculate P_{0,k} and α_k by
solving (6.6) and (6.7);
5.                                   calculate L_k from (6.4);
6.                         end for
7.           end for
8. end for;
9. estimate(x_k, y_k, φ_k) = argmax(L_k);
10. retain P_{0,k} and α_k corresponding to (x_k, y_k, φ_k)
Output (x_k, y_k, φ_k, P_{0,k} , α_k)
```

Figure 6.2: Pseudocode of the local ML algorithm for performing the final estimation of context.

**Input** ($x_{k,in}$, $y_{k,in}$, $\varphi_{k,in}$)

**1. for** $x_k \in (x_{k,in} - \Delta x_e,\ x_{k,in} + \Delta x_e)$ in steps of $\Delta x$ **do**

**2.** **for** $y_k \in (y_{k,in} - \Delta y_e,\ y_{k,in} + \Delta y_e)$ in steps of $\Delta y$ **do**

**3.** **for** $\varphi_k \in (\varphi_{k,in} - \Delta\varphi_e,\ \varphi_{k,in} + \Delta\varphi_e)$ in steps of $\Delta\varphi$ **do**

**4.** calculate $P_{0,k}$, $b_k$, and $\alpha_k$ by solving

$$\begin{bmatrix} P_{0,k} \\ b_k \\ \alpha_k \end{bmatrix} = \begin{bmatrix} 1 & \frac{-1}{2}\left\langle(\varphi-\varphi_k)^2\right\rangle & -\left\langle\overline{d_{s,k}}\right\rangle \\ \left\langle(\varphi-\varphi_k)^2\right\rangle & \frac{-1}{2}\left\langle(\varphi-\varphi_k)^4\right\rangle & -\left\langle\overline{d_{s,k}}(\varphi-\varphi_k)^2\right\rangle \\ \left\langle\overline{d_{s,k}}\right\rangle & \frac{-1}{2}\left\langle(\varphi-\varphi_k)^2\,\overline{d_{s,k}}\right\rangle & -\left\langle\overline{d_{s,k}}^2\right\rangle \end{bmatrix}^{-1} \begin{bmatrix} \left\langle P_{R,k}(x_s,y_s)\right\rangle \\ \left\langle P_{R,k}(x_s,y_s)(\varphi-\varphi_k)^2\right\rangle \\ \left\langle P_{R,k}(x_s,y_s)\overline{d_{s,k}}\right\rangle \end{bmatrix}$$

**5.** calculate $L_k$ from (6.4);

**6.** **end for**

**7.** **end for**

**8. end for;**

**9.** estimate $(x_k, y_k, \varphi_k) = \mathrm{argmax}(L_k)$;

**10.** retain $P_{0,k}$, $b_k$, and $\alpha_k$ corresponding to $(x_k, y_k, \varphi_k)$.

**11.** $BW_k = 2\sqrt{\dfrac{20\ln 2 \cdot \log_{10}(e)}{b_k}}$

**Output** ($x_k$, $y_k$, $\varphi_k$, $\alpha_k$, $P_{0,k}$, $BW_k$)

Figure 6.3: Pseudocode of the local ML algorithm for a Gaussian shaped antenna pattern.

## 6.2. Simulation environment

Two scenarios are used to evaluate MLACFE methodology. One is Scenario D, described in Section 5.6, and the second one is Scenario E, a copy of Scenario D, with the difference that a Gaussian shaped radiation antenna pattern is used in the transmitter. The beam width at 3 dB of this antenna is 70.52º. As

before, the quantization step is $\Delta$ = 1.5 dB and the number of bits used to encode the RSS measurements is $n$ = 6 bits. The local 3D grid is $\Delta x_e = \Delta y_e$ = 200 m, $\Delta\varphi_e$ = 10º. Moreover, $\Delta x = \Delta y$ = 20 m and $\Delta\varphi$ = 1º are used in the algorithms of Figure 6.2 and Figure 6.3.

## 6.3. Simulation results

This Section presents a comparison of multi-level methodology, described in Chapter 3, Chapter 4, and Chapter 5, with the proposed MLACFE methodology, using natural neighbor interpolation. The following results are shown for two cases, namely the non-parameterized radiation antenna pattern and the Gaussian antenna pattern, corresponding to the two Scenarios, D and E.

### 6.3.1. Scenario with Gaussian shaped radiation antenna pattern

Figure 6.4 presents the mean error and standard deviation error in transmitter position estimation (a), antenna direction estimation (b), and estimated beam width (c), for different values of sensor density $D$, for both of the methodologies, the multi-level methodology (named "multi-level" in figures) and the proposed MLACFE methodology (named "MLACFE" in figures). The theoretical value of beam width is also shown (named "Real" in figure). The results were averaged over 150 random realizations for each sensor density.

As it may be seen from Figure 6.4, MLACFE methodology reduces the mean error of the transmitter position estimation almost by half, presents a similar behavior in antenna direction estimation (very close to the expected value), and also reduces the error of beam width. As an example, with 50 sensors/km$^2$, the error of position is about 60 m that corresponds to 3 pixels, reflecting a very good performance. For all three parameters, MLACFE methodology gives a lower standard deviation error than the multi-level methodology.

Regarding the estimation of the propagation model, Figure 6.5 plots the mean estimated value and standard deviation error of the propagation factor $\alpha$ (a) and power $P_0$ (b), as function of sensor density $D$, for multi-level and MLACFE methodologies. Also the theoretical values are plot. It can be observed how the two methodologies offer very similar performance in terms of average error while

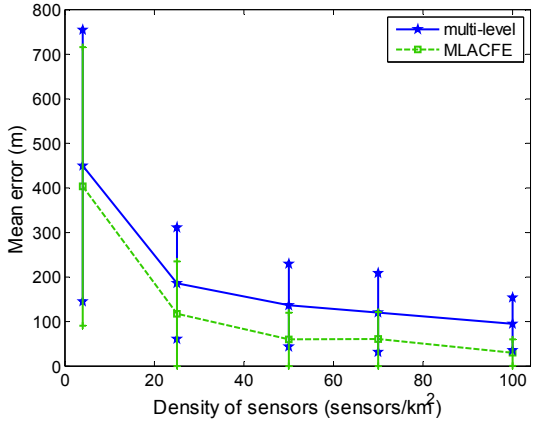


(a)

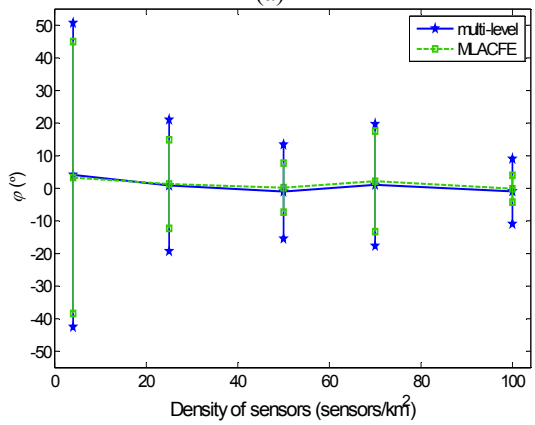


(b)

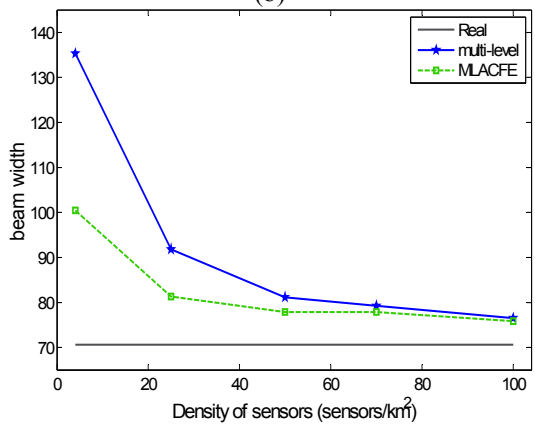


(c)

Figure 6.4: Mean error and standard deviation error in transmitter position estimation (a), and in antenna direction estimation (b), and estimated beam width (c) for different sensor densities, comparing multi-level methodology and MLACFE methodology, on scenario E.

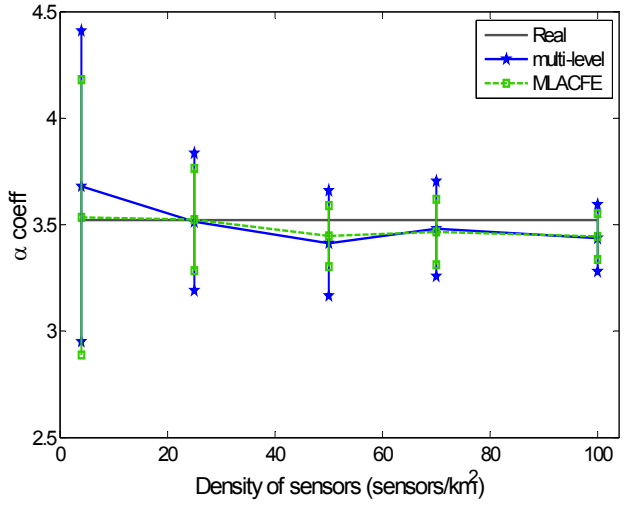


(a)

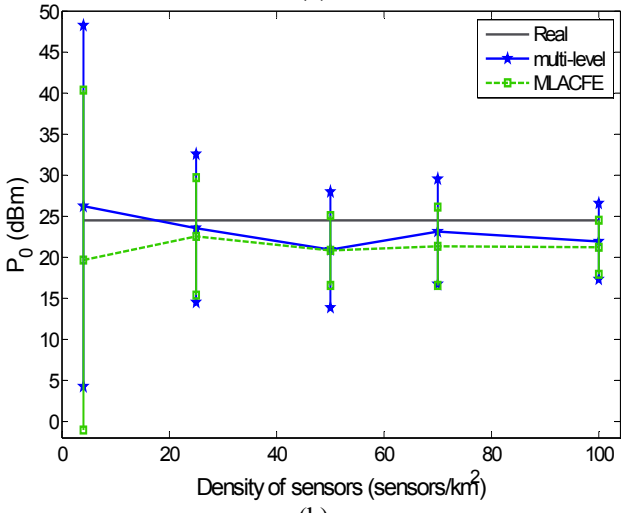


(b)

Figure 6.5: Estimated propagation factor $\alpha$ (a) and estimated $P_0$ (b) as a function of sensor density, comparing multi-level methodology and MLACFE methodology, on scenario E.

MLACFE algorithm reduces the standard deviation error.

The estimated radiation pattern of the primary transmitter antenna for the case $D$ = 50 sensors/km$^2$ is presented in Figure 6.6, comparing the MLACFE methodology (that provides exactly the same result as multi-level methodology) with the theoretical value. A very good estimation of the original radiation pattern is observed, especially in the main lobe.

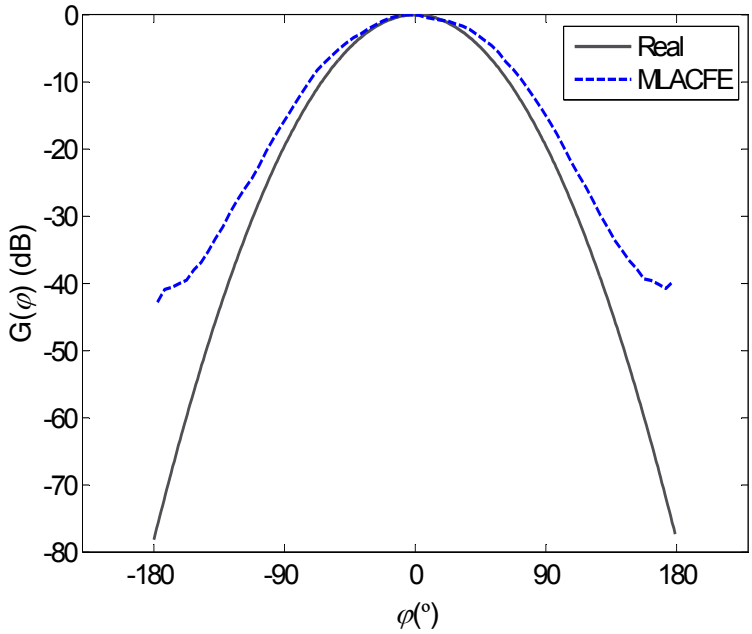


Figure 6.6: Horizontal radiation pattern estimation of Gaussian antenna for $D$ = 50 sensors/km$^2$, on scenario E.

Additional simulations ware made, where the shadowing standard deviation $\sigma$ had a range from 4 dB to 12 dB. As example, Figure 6.7 presents the mean error in transmitter position estimation of Gaussian antenna, on MLACFE methodology, for different values of sensor density $D$ and different values of shadowing standard deviation $\sigma$. The results revealed that the errors are lower as the shadowing standard deviation decreases and as sensor density grows. For the case $\sigma$ = 4 dB errors in the estimation are reduced down to 24 m which is very close to the pixel size (i.e., the resolution of the scenario).

### 6.3.2. Scenario with non-parameterized antenna pattern

The results in this subsection consider the non-parameterized antenna pattern shown in Figure 3.9. Figure 6.8 (a) shows the mean error and standard deviation error of the position estimation, for different values of sensor density $D$, for the multi-level methodology and the MLACFE methodology. Similarly, Figure 6.8 (b) shows the mean error and standard deviation error in the antenna direction estimation, revealing that there are very small differences between both

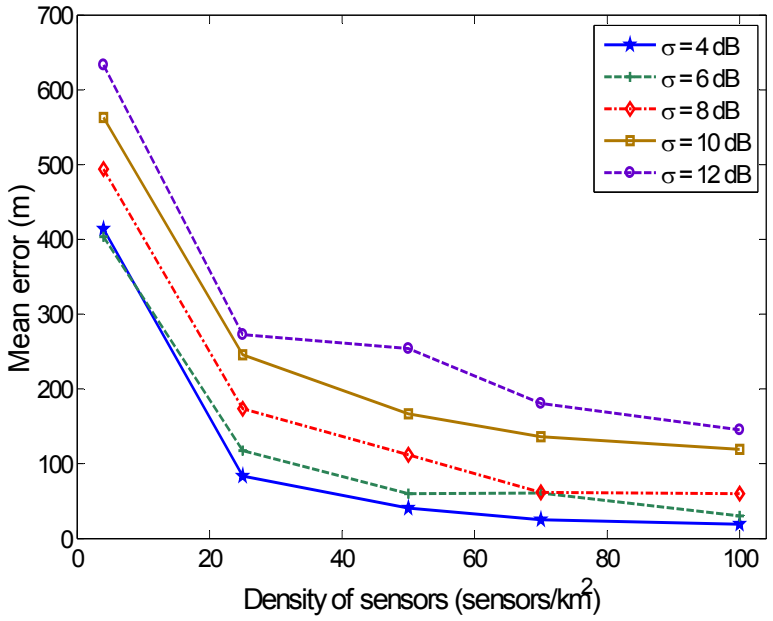


Figure 6.7: Mean error in transmitter position estimation for different sensor densities and for different shadowing standard deviation, MLACFE methodology, on scenario E.

approaches. Like in the previous subsection, results were averaged over 150 realizations for each sensor density.

For a low sensor density ($D$ = 4 sensors/km$^2$) the mean error as well as the standard deviation error are high for all parameters. As the sensor density increases, both position and direction errors decrease. MLACFE methodology achieves a lower error than the reference scheme for the case of the position, and at the same time a lower standard deviation error for both estimated parameters.

Figure 6.9 shows the estimated radiation pattern of the primary transmitter antenna for the case $D$ = 50 sensors/km$^2$. It is clear from the figure that the estimated radiation pattern follows the original radiation pattern, especially in the main lobe.

Figure 6.10 plots the mean error in transmitter position estimation of the non-parameterized antenna, using MLACFE methodology, for different values of sensor density $D$ and different values of shadowing standard deviation $\sigma$. Like with the Gaussian antenna, the results show that the errors are higher as the shadowing standard deviation increases and as sensor density decreases.

### 6.3.3. Comparison of MLACFE performance against ML estimation

In this subsection, the ML estimation algorithm proposed by Martin and Thomas in [69] is compared against the MLACFE methodology. In order for the comparison to be fair, only the Gaussian antenna pattern is considered, since this is

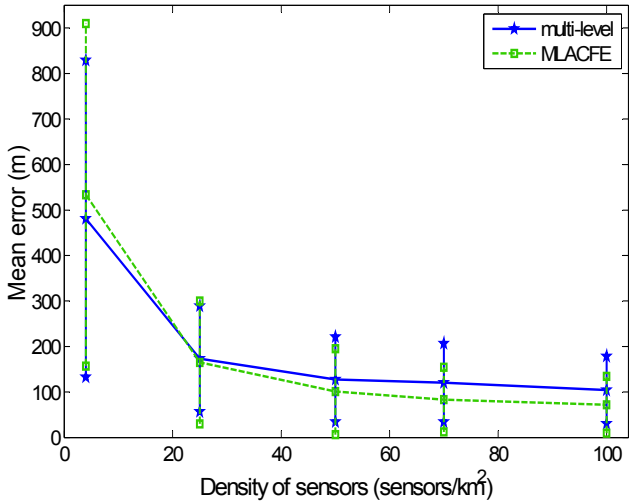


(a)

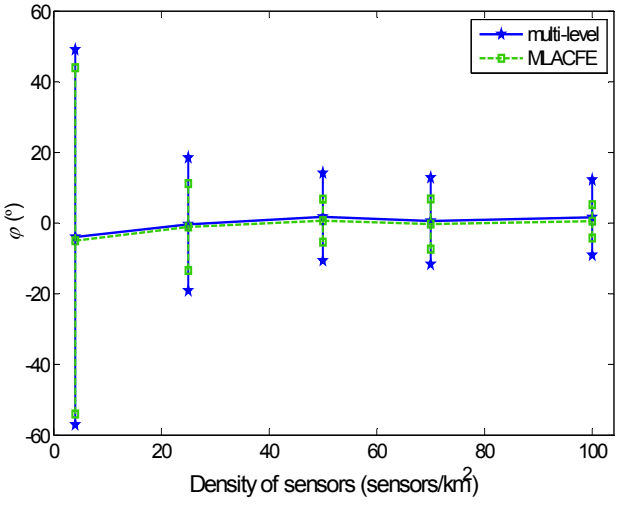


(b)

Figure 6.8: Mean error and standard deviation error in transmitter position estimation (a), and in antenna direction estimation (b) for different sensor densities, comparing multi-level methodology and MLACFE methodology, on scenario D.

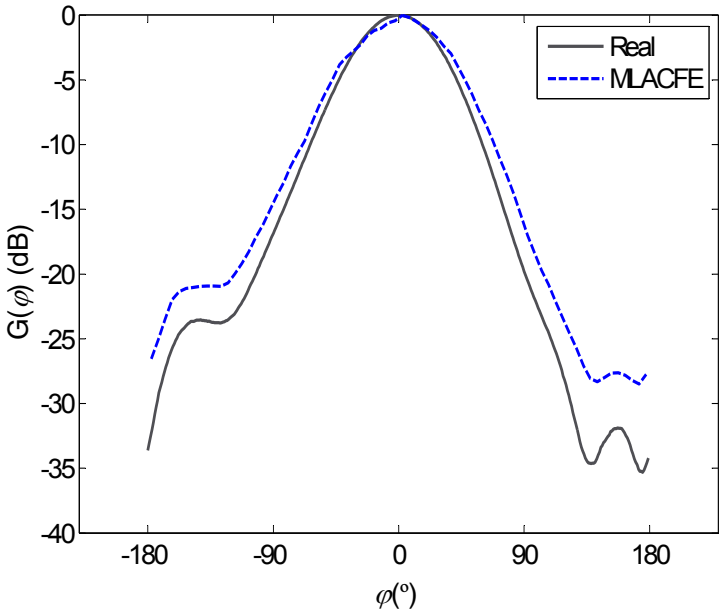


Figure 6.9: Horizontal radiation pattern estimation of non-parameterized antenna for $D$ = 50 sensors/km$^2$, on scenario D.

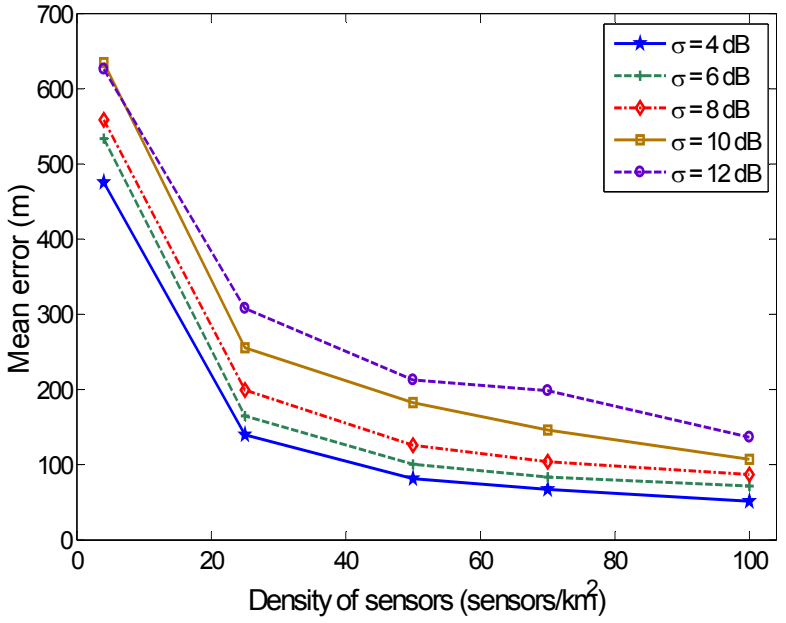


Figure 6.10: Mean error in transmitter position estimation for different sensor densities and for different shadowing standard deviation, MLACFE methodology, on scenario D.

the assumption of [69]. Given the extremely high computational complexity associated to the method in [69] when all parameters are unknown, the results are only presented for the sensor density of $D = 25$ sensors/km$^2$ and averaged with just 10 realizations of sensor distributions.

Table 6.1 presents the comparison between the proposed MLACFE methodology, the ML estimation algorithm ([69]) and the multi-level methodology described in Chapter 3, Chapter 4, and Chapter 5. The results present the mean estimated value for each parameter, its bias against the real value, and the standard deviation of the error.

In general, ML estimation algorithm offers better estimation of position transmitter than the proposed MLACFE methodology, while there are not many differences in the estimation of the antenna beam width and the propagation model parameters. When comparing MLACFE with multi-level similar conclusions as stated in subsection 6.3.1 are obtained. A lower standard deviation error is given by ML estimation algorithm, for all of the parameters. However, as illustrated in

Table 6.1: Comparison of MLACFE methodology against ML estimation algorithm and multi-level methodology for a sensor density $D = 25$ sensors/km$^2$, on scenario E.

| Variable | exact value | ML estimation algorithm [69] | | | multi-level methodology | | | MLACFE methodology | | |
|---|---|---|---|---|---|---|---|---|---|---|
| | | est. value | bias | std. dev | est. value | bias | std. dev | est. value | bias | std. dev |
| position error (m) | N/A | N/A | 37.26 | 18.74 | N/A | 181.80 | 88.56 | N/A | 82.71 | 81.35 |
| direction (º) | 0 | 0.6 | 0.6 | 1.35 | -2.60 | -2.60 | 17.51 | -0.1 | -0.1 | 10.98 |
| $\alpha$ | 3.52 | 3.48 | -0.04 | 0.12 | 3.51 | -0.01 | 0.31 | 3.52 | 0 | 0.21 |
| $P_0$ (dBm) | 24.5 | 22.71 | -1.79 | 3.69 | 23.54 | -0.96 | 8.94 | 22.86 | -1.64 | 5.47 |
| beam width (º) | 70.64 | 74.90 | 4.26 | 1.93 | 74.97 | 4.33 | 17.50 | 75.42 | 4.78 | 4.77 |

Figure 6.11, it is worth noticing this is at the expense of a much higher computational complexity.

This figure shows the average computation times observed in the simulations performed in the context of this study, based on Matlab running in a PC with an Intel Core2 Quad processor at 1.86 GHz. It can be observed how the proposed MLACFE methodology achieves a very significant reduction, about three orders of magnitude, with respect to the ML estimation algorithm.

At it was mentioned in subsection 6.1.1, ML estimation algorithm is looking into the entire 3D grid, analyzing every combination of ($x_k$, $y_k$, $\varphi_k$) to choose the best solution, leading to a slower process than the proposed algorithm. In turn, the multi-level methodology is much faster to run, having a lower computational time compared to both ML estimation algorithm and to MLACFE methodology. Still, as it had been previously stated, it provides worst performance in terms of position error estimation and standard deviation of the error for different parameters. Consequently, MLACFE methodology achieves a better trade-off between computational cost and obtained performance.

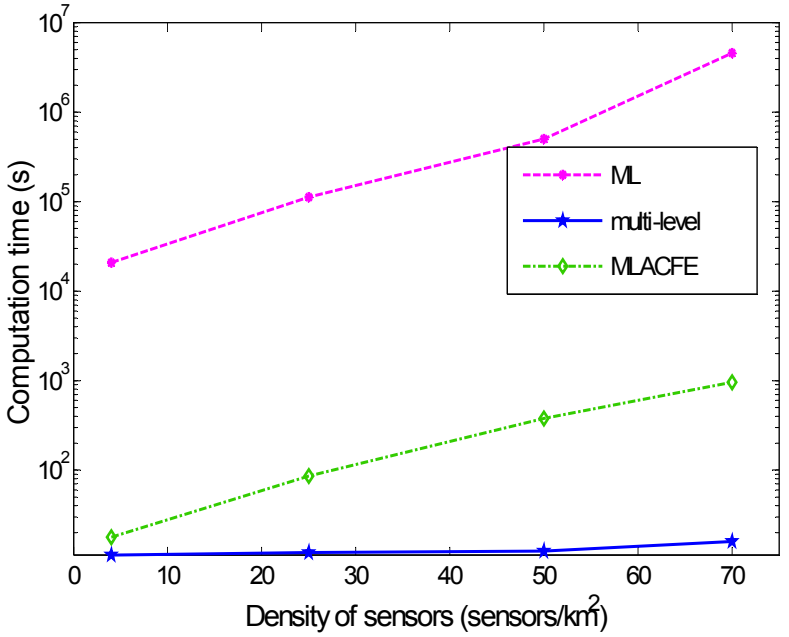


Figure 6.11: Computational complexity analysis of the ML estimation algorithm, multi-level methodology, and MLACFE methodology as function of sensor density, on scenario E.

## 6.4. Conclusions

This Chapter has proposed the MLACFE methodology for estimating different context features of a primary user network, namely the transmitters' positions, antenna pattern, antenna direction and propagation model parameters, by properly combining RSS measurements obtained by a number of secondary sensors randomly deployed in a given scenario. Like the previous proposed methods, this methodology neither assumes any prior knowledge about the characteristics of the primary network, nor requires any type of cooperation between primary and secondary networks, so it can be exploited to capture the relevant contextual elements that can guide the spectrum selection decisions of the secondary network. The proposed methodology combines an ML approach with image interpolation and processing techniques, which enables keeping at a great extent the benefits of the optimality of ML performance while at the same time reducing dramatically the overall computational complexity with respect to the ML approach.

The proposed MLACFE methodology had been compared against the ML estimation algorithm presented in [69], revealing that it can provide a quite similar performance in terms of average estimation errors while at the same time reducing the computation time in about three orders of magnitude, for the considered case study. In addition, the MLACFE methodology does not require any prior knowledge about the type of antenna patterns used by the primary transmitters. On the other hand, MLACFE methodology had also been compared against multi-level methodology, revealing a better performance in terms of position error estimation and standard deviation error for different parameters.

# 7. Conclusions and future work

This thesis has tackled the problem of characterizing the RF environment where CRNs are deployed with the scope of building REMs that can be easily used in the optimization of CR operation. In this aspect, different sensed samples at different geographical positions collected by secondary sensors are gathered in a CR central entity and are combined, using image processing techniques, for the purpose of estimating context features where CRNs are deployed. The acquired information is stored in a database, like REM, which can be further used by CRNs. Section 7.1 summarizes the main conclusions of this thesis, while Section 7.2 discusses possible work to be carried out in the future.

## 7.1. Conclusions

The context discovery was started with transmitter position estimation, for which the thesis has proposed two new algorithms: binary method and multi-level method, both of them based on image processing techniques. In the first method, from the measurements of the received power of specific frequencies, each sensor sends to CR central entity just one bit for each frequency detected. In turn, in the

multi-level method, the information collected by the sensors was being quantified to a set of $2^n - 1$ values and sent to CR central entity as a word of $n$ bits, for each frequency detected.

It is worth to remark the simplicity of the proposed binary method, which revealed error below 5% in the transmitter position estimation in a scenario with omnidirectional antennas placed homogeneously in a field. Instead, in a more complex scenario, with omnidirectional antennas irregularly distributed in a field, the errors were increasing till 25%. In this scenario, the multi-level method is more efficient, presenting error below 7% in the transmitter position estimation.

In case of a scenario with directive antennas, the results obtained with multi-level method revealed the utility and benefits of this algorithm, with errors below 150 m in the transmitter position estimation. By increasing the number of bits that are to be sent to CR central entity, which means also an increase of the complexity of the method, passing from binary to multi-level, the efficiency of the algorithm is increasing as well.

The following stage in the workflow of this dissertation has been to expand the context features estimation by adding new features like antenna pattern estimation, antenna orientation estimation, and propagation model estimation on multi-level method. The algorithm includes also a process to determine if the transmitter has an omnidirectional antenna or a directive antenna. The estimation of propagation model is made through a regression analysis of the received power at the available sensors. Moreover, this process allows also identifying which of the detected transmitters actually correspond to real transmitters and to discard spurious effects due to the shadowing.

It is worth pointing out the efficacy of the proposed algorithm that presented errors in the order of 12% in propagation model estimation for both omnidirectional antennas scenario and directive antennas scenario. Furthermore, in case of a scenario with directive antennas, the errors in antenna orientation estimation were close to zero while the estimated radiation pattern tracked satisfactorily the original radiation pattern.

With the objective of improving the characterization of RF environment, a comparative study of different interpolation techniques was introduced in the thesis, where the nearest neighbor interpolation used in multi-level method was compared with other three interpolation techniques: linear interpolation, natural neighbor interpolation, and kriging interpolation. These techniques were tested in a

scenario with directive antenna that included correlated or non-correlated shadowing losses in the environment, or no shadowing at all.

It is worth mentioned that all four interpolation techniques showed an acceptable accuracy in the estimation of context features (which means transmitter position estimation, antenna orientation estimation, antenna radiation pattern estimation, and propagation model estimation), presenting a similar behavior in a scenario without shadowing.

However, as it was expected, the errors grew in the presence of shadowing, either correlated or non-correlated. On the whole, in case that shadowing is presented in the scenario, kriging interpolation offered slightly better results than the rest of the interpolation techniques. In turn, nearest neighbor interpolation displayed a higher standard deviation error. The obtained results also demonstrated that in general the errors are reduced in case of spatial correlated shadowing, comparing with the case of non-correlated shadowing.

The last part of the thesis tackled the proposal of a new algorithm, namely MLACFE, which can be exploited to capture more accurately the relevant contextual elements that can guide the spectrum selection decisions of the secondary network. This new algorithm is the result of the combination of multi-level method with ML estimation method previously presented in [69], aimed on characterizing the RF environment where SUs are deployed. Unlike the work from [69], no prior information about antenna radiation pattern was needed by the proposed method.

The results obtained with MLACFE method were compared with the ones from multi-level method, in scenario either with a Gaussian shaped radiation antenna pattern or with a non-parameterized radiation antenna pattern. It was shown the advantage of the proposed MLACFE algorithm that displayed better error in transmitter position estimation, while reducing the standard deviation error for all the parameters.

By comparing MLACFE algorithm with ML approach, it was concluded that the performance of these two methods was similar in terms of average estimation errors, with slightly better results being obtained with ML. However, the proposed MLACFE method decreases dramatically the computational time in about three orders of magnitude.

## 7.2. Future research lines

During the implementation of this dissertation, several new research directions have emerged to be study in the future. In the following, some possible investigation lines are suggested to improve and develop the studies accomplished in this thesis.

The studies performed in this thesis have been considered in a centralized approach, where a CR central entity gathers information from specific number of sensors. However, distributed resource allocation algorithms are of significant interest. An important aspect to investigate in the future is to consider a distributed implementation of the frameworks proposed in this thesis. As investigated in [92] – [94], it is possible that the centralized algorithms can be precursors for distributed algorithms.

In the research investigated in this dissertation, only static PUs were considered. An ambitious goal for future work would be to study the mobile of PUs. This fact puts restrictions in terms of computational costs and performance achievements that should be investigated. Many questions will arise like the need to target properly when to sense, to know which sensors should be activated out of the $N$ deployed, to estimate the traffic load that the CRN has to manage as overhead, etc. Initially simulations should be extensively used trying to envisage feasibility of the methodology as well as to know the limits attained in terms of performance and computational cost. Certainly, prior to that, a simulation scenario with a number of primaries including different mobility patterns will have to be identified.

Another possible investigation line will be to devise a scenario that includes PUs of different types as well as a deployed secondary system. There are many possible combinations that will be necessary to bound to those that still can capture the major key ingredients including different featured contexts, and a particular deployment of a CRN based on the context knowledge acquired.

# Bibliography


[1] Brian X. Chen, "Q.&A.: Martin Cooper, father of the cellphone, on spectrum sharing," Bits blog, New York Time, May 2012.

[2] Federal Communications Commission (FCC), Spectrum Policy Task Force, "Report of the spectrum efficiency working group," Nov. 2002.

[3] J. Mitola, III and G. Q. Maguire, Jr., "Cognitive radio: making software radios more personal," IEEE Personal Communications Magazine, vol. 6, no. 4, pp. 13 – 18, Aug. 1999.

[4] Y. Zhao, L. Morales, J. Gaeddert, K. K. Bae, J.-S. Um, and J. H. Reed, "Applying radio environment maps to cognitive wireless regional area networks," in Proc. IEEE Dynamic Spectrum Access Networks (DySPAN), pp. 115 – 118, Apr. 2007.

[5] "The first phone call over a cognitive radio network." Available at: http://www.cwc.oulu.fi/home/newsitem.php?id=0043, June 2013.

[6] T.X. Brown, "An analysis of unlicensed device operation in licensed broadcast service bands," in Proc. IEEE Dynamic Spectrum Access Networks (DySPAN), pp. 11 – 29, Nov. 2005.

[7] Federal Communications Commission (FCC), "ET Docket no. 03-322: Notice of proposed rule making and order," Dec. 2003.

[8] I. Akyildiz, W.-Y. Lee, M. Vuran, and S. Mohanty, "Next generation/dynamic spectrum access/cognitive radio wireless networks: a survey," Computer Networks, vol. 50, no. 13, pp. 2127–2159, Sep. 2006.

[9] J. Mitola III, "Cognitive radio: an integrated agent architecture for software defined radio," Ph.D. dissertation, KTH Royal Institute of Technology, 2000.

[10] J. Mitola III, "Cognitive radio for flexible mobile multimedia communications," in Proc. IEEE International Workshop on Mobile Multimedia Communications (MoMuC), pp.3 – 10, Nov. 1999

[11] S. Haykin, "Cognitive radio: brain-empowered wireless communications," IEEE Journal on Selected Areas in Communications, vol. 23, no. 2, pp. 201 – 220, Feb. 2005.

[12] "Definitions of software defined radio (SDR) and cognitive radio system (CRS)," ITU-R Report SM 2152, 2009.

[13] V. Petty et at, "Feasibility of dynamic spectrum access in underutilized television bands," in Proc. IEEE Dynamic Spectrum Access Networks (DySPAN), pp. 331 – 339, Apr. 2007.

[14] I. Akyildiz, W.-Y. Lee, M. Vuran, and S. Mohanty, "A survey on spectrum management in cognitive radio networks," IEEE Communications Magazine, vol. 46, no. 4, pp. 40 – 48, Apr. 2008.

[15] M.M. Buddhikot, P. Kolody, S. Miller, K. Ryan, J. Evans, "Dimsumnet: new directions in wireless networking using coordinated dynamic spectrum access," in Proc. IEEE World of Wireless, Mobile, and Multimedia Networks (WoWMoM), pp. 78 – 85, June 2005.

[16] O. Ileri, D. Samardzija, and N. Mandayam, "Demand responsive pricing and competitive spectrum allocation via spectrum server," in Proc. IEEE Dynamic Spectrum Access Networks (DySPAN), pp. 194 – 202, Nov. 2005.

[17] S.A. Zekavat, X. Li, "User-central wireless system: ultimate dynamic channel allocation," in Proc. IEEE Dynamic Spectrum Access Networks (DySPAN), pp. 82 – 87, Nov. 2005.

[18] A. Ghasemi and E. S. Sousa, "Collaborative spectrum sensing for oppotunistic access in fading environments," in Proc. IEEE Dynamic Spectrum Access Networks (DySPAN), pp. 131 – 136, Nov. 2005.

[19] G. Ganesan and Y.G. LI, "Cooperative spectrum sensing in cognitive radio – part I: two user networks," IEEE Transactions on Wireless Communications, vol. 6, no. 6, pp. 2204 – 2213, June 2007.

[20] G. Ganesan and Y.G. LI, "Cooperative spectrum sensing in cognitive radio: part II: multiuser networks," IEEE Transactions on Wireless Communications, vol. 6, no. 6, pp. 2214 – 2222, June 2007.

[21] S.M. Mishra, A. Sahai, and R.W. Brodersen, "Cooperative sensing among cognitive radios," in Proc. IEEE International Conference on Communications (ICC), pp. 1658 – 1663, June 2006.

[22] Wei Zhang and Khaled Lataief, "Cooperative spectrum sensing with transmit and relay diversity in cognitive radio networks," IEEE Transactions on Wireless Communications, vol. 7, no. 12, pp. 4761 – 4766, Dec. 2008.

[23] Shengli Xie, Yi Liu, Yan Zhang, and Rong Yu, "A parallel cooperative spectrum sensing in cognitive radio networks," IEEE Transactions on Vehicular Technology, vol. 59, no. 8, pp. 4079 – 4092, Oct. 2010.

[24] S. Atapattu, C. Tellambura, and Hai Jiang, "Energy detection based cooperative spectrum sensing in cognitive radio networks," IEEE Transactions on Wireless Communications, vol. 10, no. 4, pp. 1232 – 1241, Apr. 2011.

[25] C. Raman, R.D. Yates, and N. B. Mandayam, "Scheduling variable rate links via a spectrum server," in Proc. IEEE Dynamic Spectrum Access Networks (DySPAN), pp. 110 – 118, Nov. 2005.

[26] O. Ileri, D. Samardzija, and N.B. Mandayam, "Demand responsive pricing and competitive spectrum allocation via a spectrum server," in Proc. IEEE Dynamic Spectrum Access Networks (DySPAN), pp. 194 – 202, Nov. 2005.

[27] V. Brik, E. Rozner, S. Banerjee, and P. Bahl, "DSAP: a protocol for coordinated spectrum access," in Proc. IEEE Dynamic Spectrum Access Networks (DySPAN), pp. 611 – 614, Nov. 2005.

[28] R. Etkin, A. Parekh, and D. Tse, "Spectrum sharing for unlicensed bands," IEEE Journal on Selected Areas in Communications, vol. 25, no. 3, pp. 517 – 528, Apr. 2007.

[29] J. Huang, R. A. Berry, and M. L. Honig, "Spectrum sharing with distributed interference compensation," in Proc. IEEE Dynamic Spectrum Access Networks (DySPAN), pp. 88 – 93, Nov. 2005.

[30] N. Clemens and C. Rose, "Intelligent power allocation strategies in an unlicensed spectrum," in Proc. IEEE Dynamic Spectrum Access Networks (DySPAN), pp. 37 – 42, Nov. 2005.

[31] W. Wang, L. Zhang, W. Zou, and Z. Zhou, "On the distributed cooperative spectrum sensing for cognitive radio," in Proc. IEEE International Symposium on Communications and Information Technologies (ISCIT), pp. 1496 – 1501, Oct. 2007.

[32] A. Sahai, N. Hoven, and R. Tandra, "Some fundamental limits in cognitive radio," in Proc. of Allerton Conference on Communication, Control and Computing, pp. 1662 – 1671, Oct. 2004.

[33] A. Fehske, J. Gaeddert, and J. Reed, "A new approach to signal classification using spectral correlation and neural networks," in Proc. IEEE Dynamic Spectrum Access Networks (DySPAN), pp. 144 – 150, Nov. 2005.

[34] Jun Ma; G.Y. Li, and Biing-Hwang Juang, "Signal processing in cognitive radio," in Proc. of the IEEE, vol. 97, no. 5, pp. 805 – 823, May 2009.

[35] D. Cabric, S.M. Mishra, and R.W. Brodersen, "Implementation issues in spectrum sensing for cognitive radios," in Proc. of Asilomar Conference on Signals, Systems and Computers, pp. 772 – 776, Nov. 2004.

[36] D. Cabric, A. Tkachenko, and R.W. Brodersen, "Spectrum sensing measurements of pilot, energy, and collaborative detection," in Proc. IEEE Military Communications Conference (MILCOM), pp. 1 – 7, Oct. 2006.

[37] B. Wild and K. Ramchandran, "Detecting primary receivers for cognitive radio applications," in Proc. IEEE Dynamic Spectrum Access Networks (DySPAN), pp. 124 – 130, Nov. 2005.

[38] M. Sharma, A. Sahoo, and K.D. Nayak, "Channel selection under interference temperature model in multi-hop cognitive mesh networks," in Proc. IEEE Dynamic Spectrum Access Networks (DySPAN), pp. 133 – 136, Apr. 2007.

[39] Y. Xing, C.N. Mathur, M.A. Haleem, R. Chandramouli, and K.P. Subbalakshmi, "Dynamic spectrum access with QoS and interference temperature constraints," IEEE Transactions on Mobile Computing , vol. 6, no. 4, pp. 423 – 433, Apr. 2007.

[40] Tsai-Wei Wu and Hung-Yun Hsieh, "An investigation of primary transmitter detection techniques in cognitive radio networks from network optimization perspective," in Proc. IEEE Wireless Communications and Networking Conference (WCNC), pp. 2753 – 2758, Apr. 2008.

[41] M.J. Marcus, "CR: cooperative radio or confrontational radio," in Proc. IEEE Dynamic Spectrum Access Networks (DySPAN), pp. 208 – 211, Apr. 2007.

[42] O. Sallent, J. Perez-Romero, R. Agusti, and P. Cordier, "Cognitive pilot channel enabling spectrum awareness," in Proc. IEEE International Conference on Communications Workshops, pp. 1 – 6, June 2009.

[43] J. Pérez-Romero, X. Gelabert, O. Sallent, and R. Agustí, "A novel framework for the characterization of dynamic spectrum access scenarios," in Proc. IEEE International Symposium on Personal, Indoor and Mobile Radio Communications (PIMRC), pp. 1 – 6, Sep. 2008.

[44] M. Filo, A. Hossain, A.R. Biswas, and R. Piesiewicz, "Cognitive pilot channel: enabler for radio systems coexistence," in Proc. on International Workshop on Cognitive Radio and Advanced Spectrum Management (CogART), pp. 17 – 23, May 2009.

[45] M. Shaat, "Resource management in multicarrier based cognitive radio systems," Ph.D. dissertation, Universitat Politècnica de Catalunya (UPC), Mar. 2012.

[46] J. M. Peha, "Emerging technology and spectrum policy reform," in Proc. on International Telecommunications Union (ITU) Workshop on Market Mechanisms for Spectrum Management, Jan. 2007.

[47] Y. Zhao, D. Raymond, da Silva, , C. R. C. M. da Silva, J. H. Reed, and S. F. Midkiff, "Performance evaluation of radio environment map-enabled cognitive spectrum-sharing networks," in Proc. IEEE Military Communications Conference (MILCOM), pp. 1 – 7, Oct. 2007.

[48] Federal Communications Commission (FCC), "Unlicensed Operation in the TV Broadcast Bands," ET Docket No. 04 -186, Sep. 2010.

[49] W. Krenik and A. Batra, "Cognitive radio techniques for wide area networks," in Proc. on Design Automation Conference, pp. 409 – 412, June 2005.

[50] W. Krenik and C. Panasik, "The potential for unlicensed wide area networks," Wireless Advanced Architectures Group, Texas Instruments White Paper, Nov. 2004.

[51] Flexible and spectrum-aware radio access through measurements and modelling in cognitive radio systems FARAMIR, "D2.1 Stade of the art review," Technical Report, Apr. 2010.

[52] Y. Zhao, J. H. Reed, S. Mao, and K. K. Bae, "Overhead analysis for radio environment mapenabled cognitive cadio networks," in Proc. IEEE Workshop on Networking Technologies for Software Defined Radio Networks, pp. 18 – 25, Sept. 2006.

[53] A. Vizziello and J. Pérez-Romero, "System architecture in cognitive radio networks using a radio environment map," in Proc. on International Conference on Cognitive Radio and Advanced Spectrum Management (CogART), no. 43, Oct. 2011.

[54] Cai Tao et al., "Design of layered radio environment maps for RAN optimization in heterogeneous LTE systems," in Proc. IEEE International Symposium on Personal, Indoor and Mobile Radio Communications (PIMRC), pp.172 – 176, Sept. 2011

[55] J. van de Beek et al., "How a layered rem architecture brings cognition to today's mobile networks," IEEE Wireless Communications, vol.19, no.4, pp.17 – 24, Aug. 2012.

[56] Flexible and spectrum-aware radio access through measurements and modelling in cognitive radio systems FARAMIR, "D4.1 Radio environmental maps: Information models and reference model," Technical Report, Apr. 2011.

[57] S. Faint, X.O. Üreten, and T. Willink, "Impact of the number of sensors on the network cost and accuracy of the radio environment map," in Proc. IEEE Canadian Conference on Electrical and Computer Engineering (CCECE), pp. 1 – 5, May 2010.

[58] D. Blatt and A.O. Hero, "Energy-based sensor network source localization via projection onto convex sets," IEEE Transactions on. Signal Processing., vol. 54, no. 9, pp. 3614 – 3619, Sep. 2006.

[59] M.G. Rabbat and R.D. Nowak, "Decentralized source localization and tracking," IEEE International Conference on Acoustics, Speech, and Signal Processing (ICASSP), vol. 3, pp. 921 – 924, May 2004.

[60] N. Patwari, A.O. Hero, M. Perkins, N.S. Correal, and R.J. O'Dea , "Relative Location Estimation in Wireless Sensor Networks," IEEE Transactions on. Signal Processing, vol. 51, no. 8, pp. 2137 – 2148, Aug. 2003.

[61] A.J. Weiss, "On The Accuracy of a Cellular Location System Based on RSS Measurements," IEEE Transactions on Vehicular Technology, vol. 52, no. 6, pp. 1508 – 1518, Nov. 2003.

[62] S. Grimoud, B. Sayrac, S. Ben Jemaa, and E. Moulines, "An algorithm for fast REM construction," in Proc. on International Conference on Cognitive Radio Oriented Wireless Networks and Communications (CROWNCOM), pp. 251 – 255, June 2011.

[63] V. Atanasovski et al., "Constructing radio environment maps with heterogeneous spectrum sensors," in Proc. IEEE Symposium on New Frontiers in Dynamic Spectrum Access Networks (DySPAN), pp. 660 – 661, May 2011.

[64] H.B. Yilmaz and T. Tugcu, "Location Estimation-based Radio Environment Map Construction in Fading Channels," Wireless Communications and Mobile Computing, doi: 10.1002/wcm.2367, Mar. 2013.

[65] Li Husheng, "Reconstructing geographical-spectral pattern in cognitive radio networks," in Proc. on International Conference on Cognitive Radio Oriented Wireless Networks and Communications (CROWNCOM), pp. 1 – 5, June 2010.

[66] A.A. Honoré, R.W. Thomas, R.K. Martin, and S.H. Kurkowski, "Implementation of collaborative rf localization using a software-defined radio network," in Proc. IEEE Military Communications Conference (MILCOM), pp. 1 – 7, Oct. 2009.

[67] M. Zafer, Bong Jung Ko, and I.W.-H. Ho, "Transmit power estimation using spatially diverse measurements under wireless fading," IEEE/ACM Transactions on Networking, vol. 18, no. 4, pp. 1171 – 1180, Aug. 2010.

[68] R. K. Martin, "Wireless network discovery via RSS-based estimation of multi-transmitter RF footprint," in Proc. IEEE International Workshop on Computational Advances in Multi-Sensor Adaptive Processing (CAMSAP), pp. 336 – 339, Dec. 2009.

[69] R.K. Martin and R.W. Thomas, "Algorithms and bounds for estimating location, directionality, and environmental parameters of primary spectrum users," IEEE Transactions on Wireless Communications, vol. 8, no. 11, pp. 5692 – 5701, Nov. 2009.

[70] B. Mercier et al., "Sensor networks for cognitive radio: theory and system design," ICT Mobile Summit, June, 2008.

[71] T.S. Rappaport, "Wireless Communications: Principles and Practice," Englewood Cliffs, NJ: Prentice Hall, 1996.

[72] J. Pérez-Romero, O. Sallent, R. Agustí, "On the applicability of image processing techniques in the radio environment characterization," IEEE Vehicular Technology Conference (VTC Spring), pp. 1 – 5, Apr. 2009.

[73] "Morphological operations on binary images," Image Processing Toolbox, The Mathworks. Available at: http://www.mathworks.es/es/help/images/ref/bwmorph.html, June 2013.

[74] R. Fisher, S. Perkins, A. Walker, and E. Wolfart (2003), "Connected Component Labeling," Available at: http://homepages.inf.ed.ac.uk/rbf/HIPR2/label.htm#1, June 2013.

[75] T. Hill and P. Lewicki, "Statistics methods and applications," Tulsa, StatSoft, 2007.

[76] V. Fodor, I. Glaropoulos, L. Pescosolido, "Detecting low-power primary signals via distributed sensing to support opportunistic spectrum access", in Proc. IEEE International Conference on Communiation (ICC), pp. 1 – 6, June 2009.

[77] M. Sambridge, J. Braun, and H. McQueen, "Geophysical parameterization and interpolation of irregular data using natural neighbours," Geophysical Journal International, 122, pp. 837 – 857, 1995.

[78] I. Amidror, "Scattered data interpolation methods for electronic imaging systems: a survey," Jurnal of Electronic Imaging, 11(2), pp. 157 – 176, 2002.

[79] H. Gouraud, "Continuous shading of curved surfaces," IEEE Transactions on Computers, vol. C-20, no. 6, pp. 623 – 629, June 1971.

[80] E. Walia and C. Singh, "An analysis of linear and non-linear interpolation techniques for three-dimensional rendering," Geometric Modeling and Imaging--New Trends, pp.69 – 76, Aug. 1993

[81] R. Sibson, "A vector identity for the dirichlet tesselation," In Mathematical Proceedings of the Cambridge Philosophical Society, 87, pp. 151 – 155, 1980.

[82] R. Sibson, "A brief description of natural neighbor interpolation," Chapter 2 In V. Barnett, editor, Interpreting Multivariate Data, pp. 21 – 36, 1981.

[83] D.G. Krige, "A statistical approch to some basic mine valuation problems on the Witwatersrand," Journal of the Chemistry, Metal and Mining Society of South Africa, vol. 52, pp. 119 – 139, Dec. 1951.

[84] P.A. Burrough and R.A. McDonnell, "Principles of geographical information systems," Oxford: Oxford University Press, Apr. 1998.

[85] A. Ben Hadj Alaya-Feki, S. Ben Jemaa, B. Sayrac, P. .Houze , and E. Moulines, "Informed spectrum usage in cognitive radio networks: Interference Cartography," in Proc. IEEE International Symposium on Personal, Indoor and Mobile Radio Communications (PIMRC), pp. 1 – 5, Sep. 2008.

[86] A. Ben Hadj Alaya-Feki, B. Sayrac, S. Ben Jemaa, and E. Moulines, "Interference cartography for hierarchical dynamic spectrum access," in Proc. IEEE Dynamic Spectrum Access Networks (DySPAN), pp. 1 – 5, Oct. 2008.

[87] R.Sidler, "Kriging and conditional geostatistical simulation based on scale-invariant covariance models," Diploma thesis, Institute of geophysics, Department of Earth Science, Oct. 2003.

[88] T. Von Karman, "Progress in the statistican theory of turbulence," Journal of Maritime Researches, vol. 7, pp. 252 – 264, 1948.

[89] P. K. Kitanidis, "Introduction to geostatistics: applications to hydrogeology," Cambridge University Press, 1997.

[90] J. J. Lehtomaki, M. Juntti, H. Saarnisaari, and S. Koivu, "Threshold setting strategies for a quantized total power radiometer," IEEE Signal Processing Letters, vol. 12, no. 11, pp. 796 – 799, Nov. 2005.

[91] R. Fraile, J. Gozálvez, O. Lázaro, J. Monserrat, and N. Cardona "Effect of a two dimensional shadowing model on system level performance evaluation", in Proc. on Wireless Personal Multimedia Communications (WPMC), vol. 2, pp. 149 – 153, Sept. 2004.

[92] P. Cheng, Z. Zhang, H.H. Chen, and P. Qiu, "Optimal distributed joint frequency, rate and power allocation in cognitive OFDMA systems," IET Communications, vol. 2, no. 6, pp. 815 – 826, July 2008.

[93] Duy Trong Ngo and Tho Le-Ngoc, "Distributed resource allocation for cognitive radio networks with spectrum-sharing constraints," IEEE Transactions on Vehicular Technology, vol. 60, no. 7, pp. 3436 – 3449, Sept. 2011.

[94] Y. Zhang and C. Leung, "A distributed algorithm for resource allocation in OFDM cognitive radio systems," IEEE Transactions on Vehicular Technology, vol. 60, no. 2, pp. 546 – 554, Feb. 2011.